UNIVERSITY OF CALIFORNIA

Los Angeles

The Role of Spire and Cofilin in Actin Dynamics

A dissertation submitted in partial satisfaction of the

requirements for the degree Doctor of Philosophy

in Biochemistry and Molecular Biology

by

Christine Kwuan-Ye Chen

2012

ABSTRACT OF THE DISSERTATION

The Role of Spire and Cofilin in Actin Dynamics

by

Christine Kwuan-Ye Chen

Doctor of Philosophy in Biochemistry and Molecular Biology

University of California, Los Angeles, 2012

Professor Emil Reisler, Chair

Rapid remodeling of the actin cytoskeleton is essential for many cellular processes including cell growth, differentiation, division, and motility. Actin dynamics is expedited by various actin-binding proteins, with Spire and cofilin being prominent among them. *In vitro*, Spire and cofilin are able to sever, nucleate, and depolymerize filaments, albeit by different methods. This dissertation focuses on characterizing the mechanisms of Spire and cofilin interactions with actin and studying their roles in actin dynamics.

We first study the complex role of Spire in actin dynamics. We observe that the severing activity of Spir is weak and conclude that rapid actin depolymerization is mainly due to the sequestering activity of Spir. Polymerization assays show that Spir and actin form complexes that accelerate polymerization, when present at low stoichiometries, but suggest their heterogeneity. Notably, Spir does not bind readily four actin monomers in a stable complex. Similarly, depolymerization of actin by Spir leads to the formation of several types of their

complexes. Strikingly, as detected by cross-linking experiments, Spir induces the formation of lateral actin-actin complexes in addition to the expected longitudinal complexes. The formation of these structures is not affected by the presence of Cappuccino. Finally, using yeast actin mutants labeled with fluorescent probes, we detected different affinities of Spir domains for actin protomers. Together, our data suggest that Spir-actin interactions are more complex than originally believed.

Next, we examined the effects of cofilin isoforms on the dynamics of actin isoforms. First, we studied the change in the persistence length of both vertebrate and yeast F-actin upon binding of human and yeast cofilin. We observe that human cofilin-1 (hCof1) binds to yeast actin filaments but neither increases their flexibility nor severs them. In contrast to that, yeast cofilin increases the flexibility of skeletal and yeast actin filaments and severs them efficiently, confirming the correlation of severing activity with changes in filament flexibility. We further observe that although yeast cofilin is an effective severer of yeast actin at low ratios of cofilin to actin, hCof1 severs yeast actin only when added in excess, despite changing their twist similarly to yeast cofilin. This contradicts previous observations that severing occurs only, or mainly, under subsaturating conditions. Our results raise questions about the role of actin isoforms in their severing by cofilin and the specific actin-cofilin contacts that contribute to this activity. Lastly, actin cross-linkings with benzophenone-4-maleimide (BPM) reveal two types of structural transitions: one associated with actin polymerization into filaments, and the other coupled to coflin binding to F-actin. We map the intramolecular cross-link in F-actin to Cys374 and Asp11 and the intermolecular one, due to cofilin binding, to Cys374 and Met44. We also report differences in dissociation rates of cofilin from cross-linked and uncross-linked F-actin,

showing the role of filament flexibility in cofilin dissociation. Cofilin-induced changes may help elucidate the local and global changes in F-actin that destabilize specific interprotomer contacts.

Together, our work on Spir and cofilin provides insight into the mechanisms of their interactions with actin and the roles they play in actin dynamics.

The dissertation of Christine Kwuan-Ye Chen is approved.

Frank A. Laski

Joseph A. Loo

Margot E. Quinlan

Emil Reisler, Committee Chair

University of California, Los Angeles

2012

Dedicated to FP

TABLE OF CONTENTS

List of Figures viii

List of Tables x

Acknowledgements xi

Vita xiv

Publications and Presentations xv

Chapter 1 Introduction 1

References 22

Chapter 2 Multiple forms of Spir-actin complexes and their functional consequences 26

References 34

Supplementary Information 36

Chapter 3 Additional aspects of the multiple forms of Spir-actin complexes 45

References 67

Chapter 4 Cofilin-linked changes in actin flexibility promote severing 70

References 78

Supplemental Information 80

Chapter 5 Cofilin induced changes in F-actin mapped by cross-linking with benzophenone-4-maleimide 95

References 115

Chapter 6 Conclusions 118

References 123

LIST OF FIGURES

1.1 Structure of monomeric actin with its important elements highlighted....4

1.2 Schematic representation of actin treadmilling at steady-state....6

1.3 Structural representation of F-actin 7

1.4 Domain organization of *Drosophila* Spir 10

1.5 Model of cofilin decorated F-actin 14

1.6 Alignment of yeast and human cofilin structures 17

2.1 Rapid actin filament depolymerization by Spir 29

2.2 Spir severs weakly in bulk assays 29

2.3 Spir severs and depolymerizes actin filaments from the barbed end 30

2.4 Spir-ABCD and Spir-CD seeds enhance actin polymerization 31

2.5 Longitudinal and lateral actin contacts induced by Spir 32

2.6 Crystal structure of Spir-D (magenta) with ECP-cleaved actin (cyan) forming an anti-parallel dimer 33

2.S1 Actin filament depolymerization by Spir-CD is dose-dependent 41

2.S2 Spir severs and depolymerizes from the barbed end of F-actin 42

2.S3 Actin monomer inhibits Spir severing activity 43

2.S4 Results from sedimentation velocity experiments with actin and Spir-ABCD 44

3.1 Spir-actin complexes detected after Spir induced depolymerization of F-actin 55

3.2 Capu has no effect on Spir induced depolymerization and cross-linking of actin 57

3.3 Spir-actin seeds do not polymerize....58

3.4 Binding of Spir to labeled actin causes a bimodal change in fluorescence 60

3.5 Overlay of crystal structures for Spir-CD with Acanthamoeba actin and ECP-

cleaved actin 62

4.1 Bending flexibility of yeast and vertebrate cofilactin filaments 74

4.2 Real-time actin filament severing by cofilin 75

4.3 Dependence of average actin filament length on cofilin binding density 75

4.4 Modulation of the critical actin filament severing angle by cofilin 76

4.5 Calculated applied shear force from bending of actin and cofilactin filaments 77

4.6 Model for cofilin-dependent actin filament severing.....78

4.S1 Severing rates of skeletal and yeast actin by yeast cofilin and human cofilin1 (hCof1).....85

4.S2 The average length of yeast actin filaments shortens at high concentrations of hCof1.....86

4.S3 Filament length distributions for yeast actin incubated at different concentrations with either yeast cofilin or human cofilin1 (hCof1) 88

4.S4 Filament length distributions for skeletal actin and the N-terminal acidic yeast actin mutant (4Ac-actin) incubated with increasing amounts of human cofilin1 (hCof1)...89

4.S5 Comparison of F-actin twist in the presence of either yeast cofilin or human cofilin-1 90

5.1 Cofilin causes a switch from intramolecular to intermolecular cross-linking by BPM (benzophenone maleimide) in F-actin.....104

5.2 EM images of F-actin formed from BPM cross-linked dimers are similar to those of uncross-linked actin 105

5.3 Mapping actin sites involved in intermolecular and intramolecular cross-linking by BPM.....107

5.4 MS sequencing of the BP cross-linked actin to actin peptides 108

5.5 Cofilin remains associated with cross-linked actin at high salt concentrations 110

LIST OF TABLES

2.1 Comparison of observed and theoretical sedimentation coefficients (in Svedbergs) of Spir constructs incubated with actin at stoichiometric ratios under polymerizing and nonpolymerizing conditions 33

2.S1 Data collection and refinement statistics 40

3.1 Data collection and refinement statistics 63

4.1 Summary of actin and cofilactin filament bending parameters 75

ACKNOWLEDGEMENTS

I would first like to acknowledge my advisor and committee chair, Dr. Emil Reisler, for accepting me into his lab and exposing me to the wonderful world of actin. Under his mentorship, I have grown as a researcher. I will always remember him for his undying patience, kindness, and selflessness. I am thankful for the wealth of knowledge that he has been willing to impart onto me and the support that he has provided me throughout my graduate career.

I would also like to acknowledge the rest of my committee: Dr. Margot Quinlan, Dr. Frank Laski, and Dr. Joseph Loo. Dr. Margot Quinlan has been especially helpful in my graduate career as a wonderful collaborator. I am very thankful for her support and guidance throughout the Spir project.

My lab has also been an excellent support system and I would like to thank all current and past members for engaging scientific discussions as well as the gossip that kept my personal life amusing. Thank you to Dr. Elena Grintsevich, for her help with cofilin-related and general biochemical tasks. She was also a great initial mentor during my rotation. I would also like to thank Mona Mikati, for not only being a fun and benevolent labmate but also a confidante and friend. Many thanks to Pamchal Faroghi for her help with daily tasks and entertaining talks at lunch. Thank you to my undergraduate researcher, Sanjali Kumar, for her help with my projects. She has taught me how to be a better mentor. I would also like to thank Dr. Sabrina Benchaar, who initially helped me through my first year in the lab and then later again with the cofilin project. She has also been a great confidante and friend.

Many thanks to the Quinlan lab who have also been very supportive and helpful with all things Spir- and TIRF-related, as well as including me in March Madness or Indian food outings.

I would like to especially thank Dr. Christina Vizcarra for her help with many difficult scientific problems.

I would like to thank Dr. Martin Phillips for his help with the many instruments in the Biochemistry facility. I would also like to thank Dr. Michael Sawaya for his help with x-ray crystallography.

I would like to thank all of the friends that I have made at UCLA, especially Ron Lin. He has been a great friend and fellow scientist that initially pushed me into doing TIRF microscopy. His humor has kept me laughing and entertained through grad school.

Many thanks to all my previous mentors and labmates at both UNC and Scripps. I would like to especially thank Dr. Brian Hogan who gave me the initial push into research. He has been a wonderful role model and friend.

Lastly, I would like to thank my entire family. Thank you, mom and dad, for bringing me into this world. Thank you for your support and encouragement. I would also like to give a special thanks to my brother, Benson, who initially pushed me into pursuing a PhD. He has been a second father to me and my role model. My sister-in-law, Aly, has also been very supportive and I am very thankful that I have both of them in my life. Last but not least, I would like to thank the newest addition to my family, Rob. My life would not be the same without him. He has provided me with much love and happiness throughout my graduate career. Scrumps for life.

I would also like to acknowledge the Journal of Biological Chemistry for allowing me to reprint my published work in Chapter 2:

Chen CK, Sawaya MR, Phillips ML, Reisler E, Quinlan ME. “Multiple forms of Spir-actin complexes and their functional consequences,” *J. Biol. Chem.* **2012**, 287(13): 10684-92.

Chapter 4 was reprinted with permission from the Biophysical Journal. I would also like to thank Dr. Edward Egelman and Vitold Galkin for supplying EM data in Supplemental Information.

McCullough BR, Grintsevich EE, Chen CK, Kang H, Hutchison AL, Henn A, Cao W, Suarez C, Martiel JL, Blanchoin L, Reisler E, De La Cruz EM. "Cofilin-linked changes in actin filament flexibility promote severing," *Biophys. J.* **2011**, 101(1): 151-9.

Chapter 5 is a version of a manuscript. I would like to thank those who contributed to it: Sabrina Benchaar, Mai Phan, Rachel Loo, and Joseph Loo.

This work was supported by the U.S. Public Health Service grant to Emil Reisler.

VITA

December 15, 1981	Born, Huntsville, Alabama
2002-2004	Undergraduate Researcher Department of Chemistry University of North Carolina, Chapel Hill
2003-2004	Teaching Assistant Department of Chemistry University of North Carolina, Chapel Hill
2004	B.S., Chemistry University of North Carolina, Chapel Hill
2004-2005	Research Technician Department of Chemistry University of North Carolina, Chapel Hill
2005-2006	Research Assistant Scripps Research Institute, La Jolla, California
2007	Teaching Assistant Department of Chemistry and Biochemistry University of California, Los Angeles
2008	Teaching Assistant Coordinator University of California, Los Angeles
2010-2011	Teaching Assistant Department of Chemistry and Biochemistry University of California, Los Angeles

PUBLICATIONS AND PRESENTATIONS

McCullough BR, Grintsevich EE, Chen CK, Kang H, Hutchison AL, Henn A, Cao W, Suarez C, Martiel JL, Blanchoin L, Reisler E, De La Cruz EM. "Cofilin-linked changes in actin filament flexibility promote severing," *Biophys. J.* **2011**, 101(1): 151-9.

Chen CK, Sawaya MR, Phillips ML, Reisler E, Quinlan ME, "Different modes of Spir-actin interaction," American Society for Cell Biology, 2011, Abstract #106.

Chen CK, Sawaya MR, Phillips ML, Reisler E, Quinlan ME. "Multiple forms of Spir-actin complexes and their functional consequences," *J. Biol. Chem.* **2012**, 287(13): 10684-92.

Chapter 1

Introduction

Actin Cytoskeleton

Actin is a 42-kDa globular protein most notable for forming microfilaments in the cytoskeleton of non-muscle cells and the thin filaments in myofibrils. Actin is one of the most abundant proteins and is essential for many cellular processes including cell growth, differentiation, division, membrane organization, and motility. It is one of the most highly conserved proteins in eukaryotes, with ~95% sequence homology across various species. Actin is a ubiquitous protein that exists in many areas of the cell. The main actin isoform in muscle cells, α-actin, plays along with myosin as a major role in force generation and muscle contraction. The two main isoforms in non-muscle cells are β-actin and γ-actin. Although actin isoforms possess very similar amino acid sequences, actin isoforms localize to different subcellular regions of a cell to perform distinct functions. Muscle and cytoplasmic actin isoforms can interact with different actin binding proteins that are able to distinguish between these isoforms.

The actin cytoskeleton provides shape and structure to cells. Actin networks can be used for cell motility and intracellular transport. Motor proteins can exploit these actin networks to transport cargo within the cell. Polymerization of actin into filaments allows for force generation to drive the crawling locomotion of eukaryotic cells, as seen with amoebas. Several different actin-binding proteins are involved in the assembly and disassembly of actin filaments and can affect actin organization in the cell. Its interaction with various proteins in different pathways makes actin an attractive target for investigating cell motility.

Structure and dynamics of actin

Actin is a dynamic molecule that is involved in maintaining cell shape and cytoskeletal integrity. The first crystal structure of an actin monomer (G-actin) in complex with DNaseI was solved in 1990 (1). Actin is composed of four subdomains (Figure 1), each containing important regions for either filament stabilization or protein interactions. The DNaseI binding loop (D-loop) is located in subdomain 2 of actin (residues 38-51). This flexible loop is disordered in many crystal structures but is predicted to have a beta sheet conformation. Most recently, a crystal structure depicting an alpha helix conformation of the D-loop prompted questions of whether the helix was an artifact of crystal packing or an inherent part of the actin structure (2). The W-loop (residues 165-172) is an important region that interacts with Wasp (Wiskott-Aldrich syndrome protein) homology 2 (WH2)-containing proteins. The hydrophobic loop (residues 262-274) is an important region for filament stabilization and assembly. The region between subdomains 2 and 4 contains an ATP binding cleft (Figure 1) that was proposed to open and close during ATP hydrolysis.

The hydrolysis of ATP occurs during actin polymerization. Actin polymerization can be divided into four steps: activation, nucleation, elongation, and annealing. Activation involves the binding of salts (usually a combination of monovalent and divalent cations) that results in a conformational change in G-actin (3). G-actin can then polymerize into a double-stranded helical filament (F-actin). Nucleation refers to the formation of oligomers more likely to grow into a filament than to decompose into monomers. It is often referred to as the rate-limiting step in the formation of unstable intermediates, actin dimers and trimers. The nucleus, once formed, has both a longitudinal monomer and lateral monomer in place to seed polymerization. This step is usually overcome by various actin-binding proteins that can provide a template for nucleation.

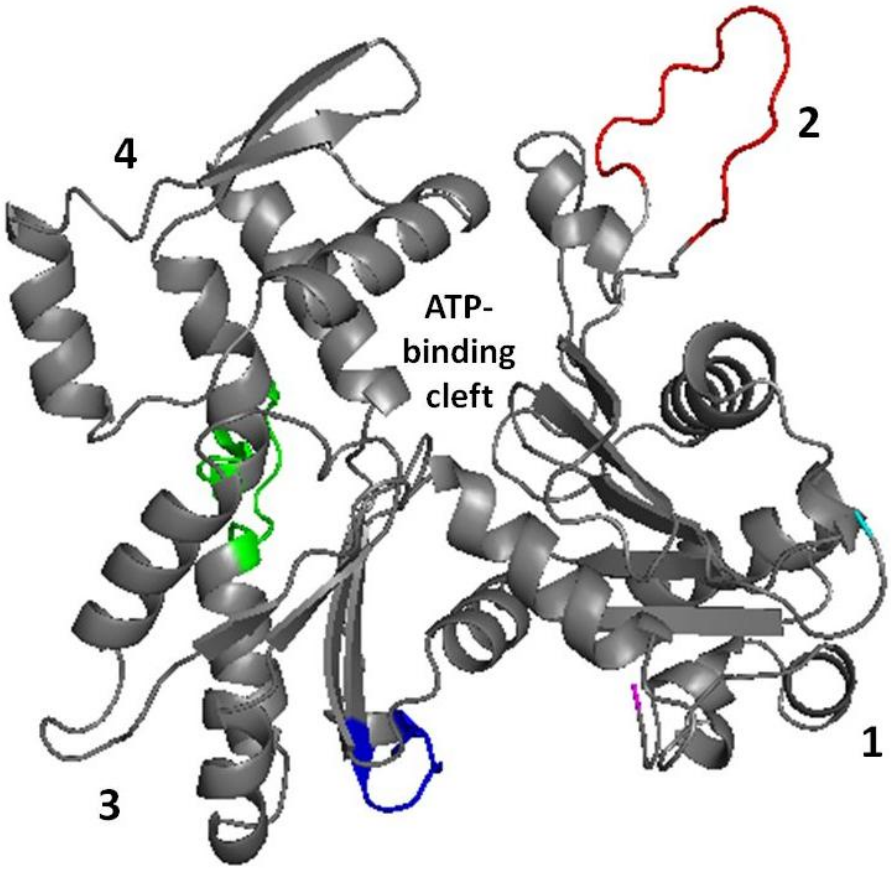

Figure 1. Structure of monomeric actin with its important elements highlighted. Numbers 1-4 refer to the subdomains of G-actin. Residues 38-51 (red) correspond to the DNaseI binding loop. Residues 165-172 (blue) represent the W-loop. Residues 262-274 (green) represent the hydrophobic loop. The N-terminus (cyan) and the C-terminus (magenta) are also highlighted. The structure of G-actin is shown using Pymol and PDB code 3MFP.

Elongation of the filament proceeds after nucleation and refers to the bidirectional growth of the filament. Annealing can then occur, which is the end-to-end joining of two filaments. The time-course for spontaneous actin polymerization, as measured in pyrene-fluorescence and light scattering assays, is sigmoidal with a lag phase due to the rate-limiting nucleation step (4).

Actin filaments are polar because the subunits point in the same direction. Treadmilling of actin (Figure 2) involves the net addition of monomers to the barbed (+) end of filaments (fast-growing end) and the net loss of monomers from the pointed (-) end (slow-growing end). After polymerization is complete, the F-actin concentration remains in equilibrium with the G-actin concentration, known as the critical concentration. Critical concentrations can vary amongst different actin isoforms and can be affected by the various actin-binding proteins involved in a given system. The critical concentration for skeletal actin is ~0.6 μM at the pointed end and ~0.08 μM at the barbed end (5). Over time, hydrolysis of ATP causes F-actin to 'age,' thus causing a varied distribution of ATP-bound, ADP-P_i-bound, or ADP-bound actin in the filament. ATP-actin resides at the barbed-end of F-actin with ADP-bound actin located towards the pointed end of F-actin. Different actin-binding proteins have different affinities for the three nucleotide states of actin and can therefore affect its treadmilling.

The assembly of actin filaments is essential for many processes including cell migration, endo and exocytosis, phagocytosis, cytokinesis, morphogenesis of the embryo, and apoptosis. For example, in epithelial cells, the rapid reorganization of the cytoskeleton and the assembly of actin filaments lead to the growth of the lamellipodia and subsequent force generation for migration of the cell. The rate of filament elongation is directly proportional to the concentration of monomeric actin. Because subunit dissociation from the pointed end is slow (~0.3 s^{-1}), the rate

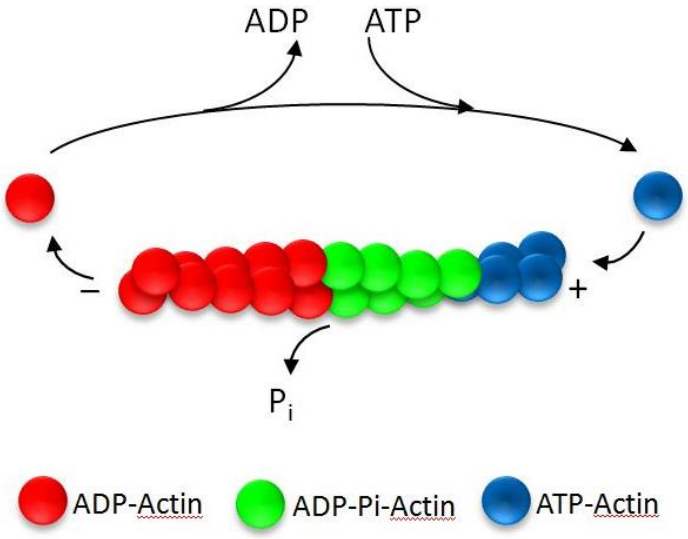

Figure 2. Schematic representation of actin treadmilling at steady-state. Dissociation of ADP-actin occurs at the pointed-end (–) of F-actin with the concomitant addition of ATP-actin onto the barbed end (+). As ATP hydrolyzes, the filament "ages" and contains a mixture of ATP-actin, ADP-P_i actin, and ADP-actin. Because subunit dissociation from the pointed end is slow, the rate for actin treadmilling is also slow in the absence of regulatory proteins.

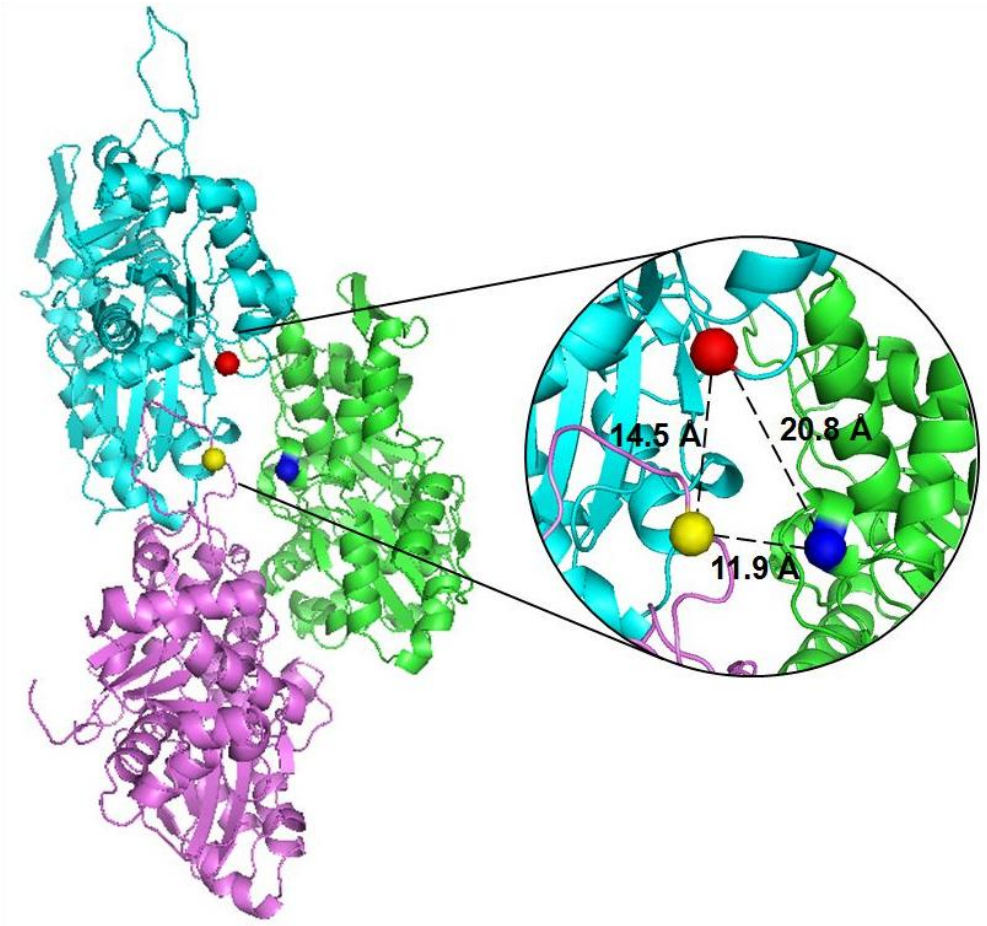

Figure 3. Structural representation of F-actin. Three actin protomers are shown (cyan, green, purple). Residues Gln41 (yellow), Ser265 (blue), and Cys374 reside in the D-loop, the hydrophobic loop, and the C-terminus, respectively. When these residues are labeled with pyrene, lateral (Ser265-Cys374) and longitudinal (Gln41-Cys374) F-actin proximities can be probed by pyrene excimer fluorescence. The F-actin model (PDB code 3MFP) is presented using Pymol. Enlarged view of the interprotomer space and the model distances between Gln41, Ser265 and Cys374 are shown on the right side.

of actin treadmilling is also slow. Actin-binding proteins are then needed to expedite this process in order to meet the required rates of >7 s^{-1} for the rapid turnover of actin filaments in lamellipods (6). Depolymerizing factors, like cofilin, aid in replenishing the monomeric pool to increase subunit turnover. Severing proteins break filaments apart and can provide seeds for more filament growth. Sequestering proteins, like profilin, help to maintain the available monomeric pool of actin. Branching proteins such as Arp2/3 create new filaments from existing filaments and these branched networks can be seen at the leading edge of moving lamellipodia. Capping proteins bind to filament ends to prevent elongation. Cross-linking proteins, like fascin, help to form and stabilize actin bundles.

Spire

Actin nucleators are factors that initiate the formation of new filaments. Because spontaneous nucleation is highly inefficient, actin nucleators use different mechanisms to overcome this barrier. To date, three classes of nucleators have been identified: the Arp2/3 complex (which forms new filaments from the side of pre-existing filaments), the formins (which stabilize actin dimers and move processively along the barbed-end for further monomer additions), and Wasp homology 2 (WH2)-nucleators. As the name implies, the third class uses actin-monomer-binding WH2 domains to nucleate filaments. The WH2 domains range from 20-50 amino acids in length and contain a consensus sequence for an actin-binding motif of Leu-Lys-Lys-Thr (LKKT). They are unstructured in the free state, but become structured once bound to actin. Spire (Spir), JMY, Cordon bleu (Cobl), Leimodin (Lmod) and the bacterial proteins VopF/L/N are grouped together in this class of nucleators although they are likely to act by distinct mechanisms (7-13).

Spir, which contains four tandem WH2 domains, is believed to regulate actin dynamics in developmental processes such as cell shape determination, intracellular transport, and division (7). Spir protein orthologs share a common structural array: a kinase non-catalytic C-lobe domain (KIND) at the N-terminus, a cluster of four conserved WH2 domains in the central region, and a Spir-Box and a FYVE (Fab1p, YOTB, Vac1p, and EEA1) zinc-finger membrane-binding domain at the C-terminus (Figure 4). Constructs containing all four WH2 domains (the N-terminal half of Spir (Spir-NT) or just the cluster of WH2 domains (Spir-ABCD)) have equivalent, maximal nucleation activity. A construct which contains only the two C-terminal WH2 domains (Spir-CD) is sufficient to nucleate albeit at a slower rate (7). The KIND domain of *Drosophila* Spir binds tightly to the formin homology 2 (FH2) domain of Cappuccino (Capu). The KIND domain competes for Capu's microtubule and F-actin binding activity and inhibits its ability to nucleate actin. In contrast, nucleation by Spir is enhanced by binding to the C-terminal half of Capu. Thus, the interaction of the two proteins results in the exclusive use of Capu to boost Spir's nucleation ability (14). In genetic studies of *Drosophila* oogenesis, loss of the actin network by *cappuccino* mutants cannot be rescued by overexpression of Spir, but loss of the network due to *spire* mutants can be partially rescued by expression of Capu (15). Little is known about the C-terminus of Spir due to difficulties in purification, but it may be involved in intracellular trafficking. The Spir-Box is a potential binding site for Rab GTPases. The FYVE domain may help direct Spir to the Gogli apparatus, post-Golgi vesicles, and endosomes (16).

Spir plays a role in early development of metazoans (17, 18). Mammals have two isoforms of this protein. Spir-1 and Spir-2 are expressed in the nervous system, but Spir-2 is also

Figure 4. Domain organization of *Drosophila* Spir. The major domains of Spir shown here include the N-terminal KIND domain, believed to interact with Cappuccino, four tandem WH2 domains that bind actin monomers, and a C-terminal Spir-Box and mFYVE domain believed to aid in membrane trafficking and binding.

present in the digestive tract, liver, and testis (19). The *spir* locus was first identified as a *Drosophila* maternal effect gene essential to establishment of both the anterior/posterior and dorsal/ventral body axes in developing oocytes and embryos (17). Mutations in *spir* result in premature microtubule-based cytoplasmic streaming in developing oocytes. An actin mesh which traverses the *Drosophila* ooctye is absent when the *spir* gene is mutated. The presence of an actin mesh may repress the onset of premature cytoplasmic streaming. A similar mesh is absent in mouse ooctyes in which both Spir1 and Spir2 are knocked down by RNAi (18, 20). These data demonstrate that Spir plays a role in building this mesh, suggesting its *in vivo* role as a nucleator.

Models of the nucleation mechanism by Spir vary in detail. Quinlan et al. (7) first proposed a model for actin nucleation by Spir. They proposed that the closely spaced WH2 domains bind actin monomers in an elongated longitudinal structure, acting as a template for monomer additions. As observed by electron microscopy and detected by analytical ultracentrifugation, each WH2 domain binds up to four monomers (7, 21). However, the orientation and rigidity of adjacent monomers with respect to each other before their elongation into filaments remains unclear. Bosch et al. (21) report that the N-terminal half of human Spir1 (hSpir1) binds actin cooperatively, forming a stable complex with four actin monomers (SA_4). They conclude that the SA_4 complex is a sequesteration complex rather than a nucleus. Rebowski et al. (22) crystallized a structure of longitudinal actin dimers bound to artificially tethered N-Wasp WH2 domains, and observed that the actin monomers are rotated ~60° more than adjacent monomers in unbound F-actin. They interpret this structure as a weak nucleation complex and question the function of Spir as a nucleator. However, the nucleation activity of Spir is sequence specific. The sequence between WH2 domains, especially linker 3 between

Spir-C and Spir-D, as well as the specific order of WH2 domains in Spir contribute significantly to the nucleation activity (7, 12) making it unclear how relevant this crystal structure is to understanding Spir. Ducka et al. (23) co-crystalized Spir with actin, and resolved only the last WH2 domain (Spir-D) bound to actin. Important information regarding the other WH2 domains was missing and the linkers were disordered in their structures. Their model also proposes an elongated longitudinal configuration of actin monomers, but the lack of atomic information for the linkers and the corresponding WH2 domains leaves room for speculations regarding the orientation of actins bound to adjacent WH2 domains. Thus, more work is required to understand how Spir associates with actin monomers and nucleates filaments.

In addition to nucleating filaments and possibly sequestering monomers, Spir was also found to sever filaments *in vitro* (21). Spir was proposed to bind to the barbed-end of filaments, which conflicts with previous results of pointed-end binding (24). The additional functions are not implausible since two other proteins, cofilin and gelsolin, can both sever and nucleate actin filaments, at least *in vitro* (25). Cobl, another tandem WH2-containing actin nucleator, is also proposed to have similar multifunctional characteristics (26). It remains to be determined which of these activities are dominant *in vivo* and/or when the different activities are physiologically relevant for Spir.

ADF/cofilin

Cofilin belongs to a family of Actin Depolymerizing Factors (ADF) and is found in all eukaryotic cells. It is a small 16 kDa protein that binds to ADP-actin with high affinity, inhibiting nucleotide exchange and regulating the recycling of the ATP-actin monomer pool. It can also bind to F-actin allowing it to be involved in a range of activities. Because cofilin has a

greater affinity for ADP-actin than ATP-actin, cofilin is generally restricted to the older parts of aging filaments and accelerates the release of subunits from the pointed-end through depolymerization and severing. Severing can both increase the number of free barbed-ends (+) for polymerization and increase the rate of actin depolymerization, but filament growth or shrinkage would depend on the available actin subunits within a particular cell. Binding of cofilin to actin is pH dependent and is inhibited by the phosphorylation of Ser3 at the N-terminus. Cofilin is activated by two phosphatases, chronophin and slingshot 1L. Cofilin has been implicated in various diseases including cancer metastasis and Alzheimer's disease (27, 28). Activation of cofilin through dephosphorylation, PIP2 hydrolysis, and increasing pH could potentially initiate tumor cell motility and invasion. For example, local activation of cofilin in mammary tumor cells produces free F-actin barbed ends initiating actin polymerization, inducing protrusion of the cell membrane, and determining the direction of cell migration (29).

The mechanism of depolymerization and severing by cofilin has been studied extensively. Using cryo-electron microscopy and image reconstructions, McGough et al. (30) showed that ADF/cofilin decreases the filament twist by 5° (from 167° per subunit in undecorated F-actin) and reduces torsional rigidity upon binding to F-actin. This change increases the number of actin filament crossovers (Figure 5) and modifies the interprotomer contacts. In unbound F-actin, the crossovers are ~365 Å in length whereas upon cofilin binding, the crossovers are reduced to ~270 Å in length (30). They conclude that cofilin stabilizes a twisted form of the filament, thereby inducing severing and increasing subunit loss. Binding of other actin binding proteins can be affected by the interprotomer modifications induced by cofilin binding. For example, phalloidin, an actin phallotoxin that stabilizes F-actin contacts, competes for binding with cofilin (31).

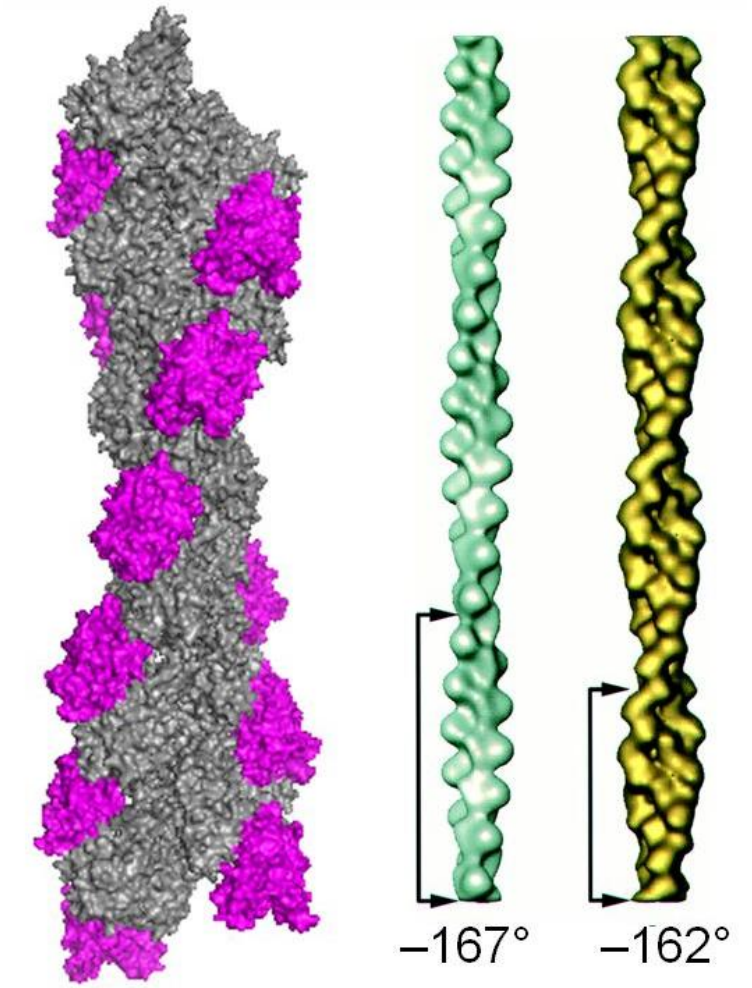

Figure 5. Model of cofilin decorated F-actin. Cofilin (magenta) binds F-actin (gray) and decreases its twist by 5°, from -167° to -162° (shown on the right side). The reconstruction is shown from PDB code 3J0S.

Cofilin is also known to be an effective nucleator of assembly. How can a protein both destabilize F-actin through severing but also stabilize a filament nuclei? One line of evidence to address this question is that cofilin is able to rescue polymerization of polymerization-incompetent yeast actin mutant T203S/C374S and tetramethylrhodamine (TMR)-labeled actin at Cys374. Kudryashov et al. (32) proposed that cofilin is able to rescue polymerization by stabilizing a new interface between subdomains 1 and 3 of the upper protomer to subdomain 2 of the lower protomer, thus reversing the destabilizing effects from mutations/modifications lethal to actin. This hypothesis was further reinforced through chemical cross-linking, fluorescent probes, and differential scanning calorimetry experiments. Pavlov et al. (33) concluded that cofilin destabilizes actin allosterically and cooperatively in bare F-actin but stabilizes bound regions sterically and non-cooperatively. Thus, severing would occur in bare regions that have been destabilized by an attached cofilin nearby, and would be more efficient under sub-saturating conditions. Under saturating conditions, cofilin would stabilize the filament rather than destabilize. The current model for severing is that filaments partially decorated with cofilin accumulate stress that is propogated along the helix (>100 protomers) in a cooperative manner. Severing would then release the stress. This severing model predicts that changes in actin filament compliance due to cofilin binding affect severing activity.

Prior to the most recent ~9 Å resolution model of cofilin bound to F-actin (34), several groups have mapped the binding sites of cofilin onto both G and F-actin via mutagenesis, fluorescence probing, and chemical cross-linking in an effort to understand cofilin's functions (35-39). Grintsevich et al. (35) concluded that cofilin binds to the hydrophobic cleft between subdomains 1 and 3 on G-actin, which coincides with previous models. The atomic structure of the C-terminal ADF homology domain of twinfilin in complex with G-actin also supports

binding between subdomains 1 and 3 of G-actin. The ADF homology domain inserts an alpha-helix into the hydrophobic cleft in a similar manner to gelsolin and WH2 domains (40). The structure provides insight into the mechanism for ADF depolymerization through weakening intrafilament interactions. EM reconstructions, chemical cross-linking, and molecular dynamic (MD) simulations also reveal a model for the cofilin/F-actin complex. Galkin et al. (34) showed that cofilin binding displaces substantially the subdomain 2 of actin and results in its disordering, thus disrupting interprotomer contacts. The disordering of subdomain 2 caused by cofilin binding leads to a four-fold increase in F-actin flexibility (41). It should be noted that these reconstructions and simulations were accomplished with human cofilin. The activities of yeast cofilin and human cofilin are very similar, but based on structural alignments of human cofilin and yeast cofilin, human cofilin has two additional loop insertions in the N-terminal portion of the protein (Figure 6) leading to ambiguities in the interpretation of mutations and binding sites. Nevertheless, a sequence alignment of the two species can act as a guide to understanding cofilin's structure and function.

Overview of the Dissertation

This dissertation focuses on the effect of two specific actin binding proteins on actin structure and dynamics. We are interested in these two proteins because of their multifunctionality. Both Spir and cofilin were found to possess nucleation activity albeit by different methods. Both also were believed to possess severing capabilities and in more recent findings, depolymerization. Spir is part of an emerging class of actin nucleators, but its nucleation ability has been questioned by some studies (21, 22). Much more evidence is needed to understand fully Spir's effects *in vivo* and *in vitro*. Cofilin is a well studied factor predicted to

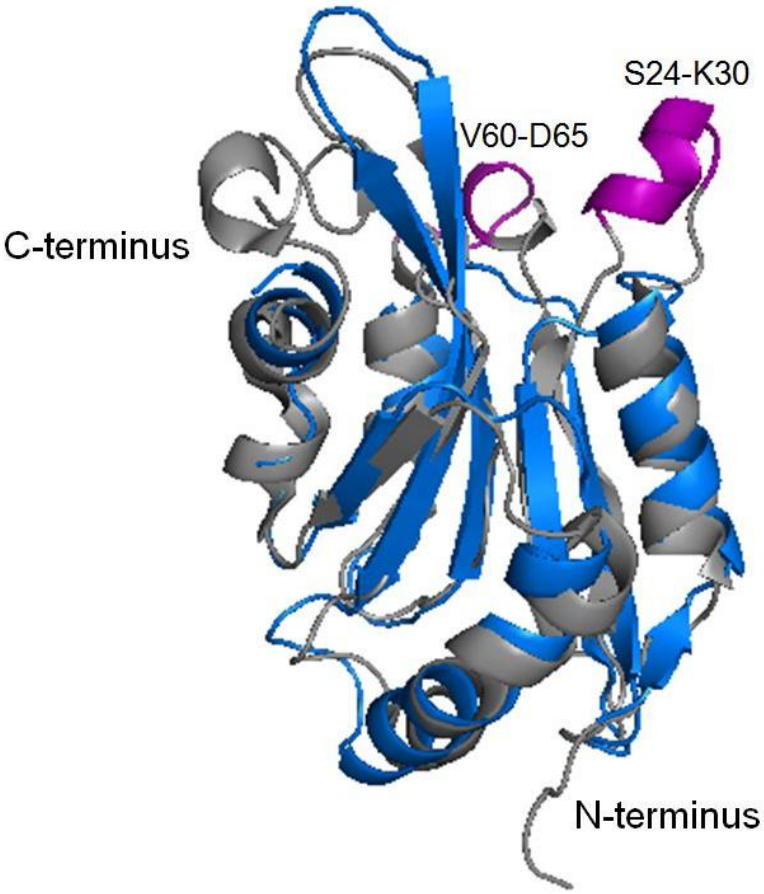

Figure 6. Alignment of yeast and human cofilin structures. Yeast cofilin (PDB code 1CFY) shown in blue and human cofilin (PDB code 1Q8G) shown in gray align with an RMSD=1.59. The loops highlighted in purple are absent in yeast cofilin and represent the main structural difference between human cofilin and yeast cofilin.

be involved in various human diseases. Many of the same techniques used to study cofilin could be applied to Spir due to the similarities in their behaviors.

Chapter 2 focuses on characterization of the interaction between Spir and actin. Current models of Spir's interaction with actin contradict each other (7, 21, 22). The most recent crystal structure of Spir in complex with actin is missing high-resolution data of major interacting components (23). Thus, more work is required to understand how Spir associates with actin monomers and nucleates filaments. Some of the major techniques that we used to study Spir's behavior were total internal fluorescence (TIRF) microscopy, x-ray crystallography, electron microscopy (EM), analytical ultracentrifugation, cross-linking, co-sedimentation, and pyrene fluorescence assays. In this chapter, we found that Spir is able to nucleate, sever, and depolymerize actin filaments. We found that the severing activity of Spir is weak and conclude that rapid depolymerization is largely due to the sequestering activity of Spir. Polymerization assays show that Spir binds actin in structures that accelerate polymerization but suggest their heterogeneity. Notably, velocity sedimentation data show that *Drosophila* Spir does not bind readily four actin monomers in a stable complex as described for hSpir1 (21) and confirm that Spir-actin solutions contain several structures. Finally, our data demonstrate differences between Spir-ABCD-actin and Spir-CD-actin complexes, providing evidence for Spir-dependent lateral actin interactions in addition to the expected longitudinal structures. Together, our data suggest that Spir-actin interactions are more complex than originally believed.

Chapter 3 is a continuation of the study of the interaction between Spir and actin. We further examined the types of species left after depolymerization by Spir on F-actin using analytical ultracentrifugation. Since Spir was found to possibly interact with Capu *in vivo*, we tested S265C cross-linking in the combined presence of Spir and Capu. We also looked at the

ability of pre-nuclei to nucleate the formation of F-actin. We analyzed the effect of Spir on yeast actin mutant fluorescence labeled at sites F169C and A167C. A bimodal change in the fluorescence attests to different affinities of Spir domains for actin protomers. Finally, the structure of Spir-D in complex with unmodified Acanthamoeba actin is overlaid with the previous structure in Chapter 2. Together, these data help to further characterize Spir's ability to act on both G and F-actin.

Chapter 4 studies the effect of different cofilin isoforms on actin filament dynamics. The mechanism of severing is further examined in this chapter. As previously stated, cofilin alters the helical structure of filaments by inducing a twist of 5° per subunit (30). Upon cofilin binding, the amount of bending increases due to the conformational dynamics of individual subunits (42, 43). The twisting and bending are two factors that may contribute to filament fragmentation. We proposed that a local asymmetry in actin filaments localizes stress at the boundaries of occupied unoccupied segments and promotes severing. We examined the change in persistence length of both vertebrate and yeast F-actin upon binding of vertebrate and yeast cofilin. Although yeast actin filaments are more compliant in bending than vertebrate actin filaments, we observed that human cofilin 1 (hCof1) binds to yeast actin filaments but neither increases filament flexibility nor severs them. In contrast, yeast cofilin is able to increase filament flexibility of both skeletal and yeast actin while efficiently severing them, thereby allowing us to correlate severing activity with changes in filament flexibility. Consistent with previous models, cofilin severing is maximal under subsaturating conditions (33, 44) and scales with the density of boundaries between bare and cofilin-decorated segments (45, 46). Imaging of filament thermal fluctuations reveals that severing events are associated with local bending and fragmentation when deformations attain a critical angle. These measurements support a cofilin-severing mechanism

in which mechanical asymmetry promotes local stress accumulation and fragmentation at boundaries of bare and cofilin-decorated segments.

Using TIRF microscopy, we also examined further the effects of severing on different actin isoforms by different cofilin isoforms in an effort to understand the differences in severing activities. Yeast cofilin is an effective severer of yeast actin at low ratios of cofilin to actin and continues to sever even at high ratios. In contrast, hCof1 is not an effective severer of yeast actin at low ratios but is able to sever filaments when added in excess, contradicting previous observations that severing occurs only, or mainly, under subsaturating conditions. Through EM reconstructions of yeast F-actin decorated with hCof1, we observe a twist of ~162° relative to adjacent subunits, which is the same as the twist induced by yeast cofilin. Severing is also enhanced, although to a lesser extent than with yeast cofilin, when hCof1 is incubated with skeletal actin, which raises questions of whether severing is cofilin-isoform dependent or actin-isoform dependent.

Chapter 5 reports on the structural dynamics of actin in the presence of cofilin. We provide experimental evidence derived from actin cross-linking by benzophenone-4-maleimide (BPM) for two types of structural transitions in actin: one associated with actin polymerization into filaments, and the other coupled to cofilin binding to F-actin. Although cross-linking captures changes that normally reflect contact-induced modification of specific sites, it is believed that actin polymerization prompts intramolecular changes as well.

Previous studies have shown little or no cross-linking in G-actin after Cys374 labeling with BPM. However, intramolecular BPM cross-linking was detected in F-actin after photoactivation of BPM. We confirm here this observation and map the intramolecular cross-link in F-actin to Cys374 and Asp11. Binding of cofilin to F-actin replaces this intramolecular cross-

linking with an intermolecular cross-linking from Cys374 to Met44. We also report differences in dissociation of cofilin from cross-linked and uncross-linked F-actin indicative of the need for filament flexibility in cofilin dissociation. Cofilin induced conformational changes may help elucidate the local and global changes that occur in F-actin and destabilize certain interprotomer contacts.

REFERENCES

1. Kabsch, W.; Mannherz, H. G.; Suck, D.; Pai, E. F.; Holmes, K. C., *Nature* **1990,** 347, (6288), 37-44.
2. Otterbein L.R.; Graceffa, P.; Dominguez R., *Science* **2001,** 293, (5530), 708-11.
3. Rouayrenc, J.F.; Travers, F., *European Journal of Biochemistry* **1981,** 116, (1), 73-77.
4. Pollard T.D.; Cooper. J.A., *Annual Reviews in Biochemestry* **1986,** 55, 987-1035.
5. Bonder, E. M.; Fishkind, D. J.; Mooseker, M. S., *Cell* **1983,** 34, (2), 491-501.
6. Zigmond, S.H., *Cell Motility and the Cytoskeleton* **1993,** 25, (4), 309-316.
7. Quinlan, M. E.; Heuser, J. E.; Kerkhoff, E.; Dyche Mullins, R., *Nature* **2005,** 433, (7024), 382-388.
8. Ahuja, R.; Pinyol, R.; Reichenbach, N.; Custer, L.; Klingensmith, J.; Kessels, M. M.; Qualmann, B., *Cell* **2007,** 131, (2), 337-350.
9. Liverman, A.; Cheng, H. C.; Trosky, J. E.; Leung, D. W.; Yarbrough, M. L.; Burdette, D. L.; Rosen, M. K.; Orth, K., *Proceedings of the National Academy of Sciences* **2007,** 104, (43), 17117-17122.
10. Tam, V. C.; Serruto, D.; Dziejman, M.; Brieher, W.; Mekalanos, J. J., *Cell Host & Microbe* **2007,** 1, (2), 95-107.
11. Chereau, D.; Boczkowska, M.; Skwarek-Maruszewska, A.; Fujiwara, I.; Hayes, D. B.; Rebowski, G.; Lappalainen, P.; Pollard, T. D.; Dominguez, R., *Science* **2008,** 320, (5873), 239-243.
12. Zuchero, J. B.; Coutts, A. S.; Quinlan, M. E.; Thangue, N. B. L.; Mullins, R. D., *Nat Cell Biol* **2009,** 11, (4), 451-459.

13. Tam, V. C.; Suzuki, M.; Coughlin, M.; Saslowsky, D.; Biswas, K.; Lencer, W. I.; Faruque, S. M.; Mekalanos, J. J., *mBio* 1, (5),

14. Quinlan, M. E.; Hilgert, S.; Bedrossian, A.; Mullins, R. D.; Kerkhoff, E., *The Journal of Cell Biology* **2007,** 179, (1), 117-128.

15. Rosales-Nieves, A. E.; Johndrow, J. E.; Keller, L. C.; Magie, C. R.; Pinto-Santini, D. M.; Parkhurst, S. M., *Nat Cell Biol* **2006,** 8, (4), 367-376.

16. Kerkhoff, E.; Simpson, J. C.; Leberfinger, C. B.; Otto, I. M.; Doerks, T.; Bork, P.; Rapp, U. R.; Raabe, T.; Pepperkok, R., *Current biology : CB* **2001,** 11, (24), 1963-1968.

17. Manseau, L. J.; Schupbach, T., *Genes & Development* **1989,** 3, (9), 1437-1452.

18. Pfender, S.; Kuznetsov, V.; Pleiser, S.; Kerkhoff, E.; Schuh, M., *Current biology : CB* **2011,** 21, (11), 955-960.

19. Schumacher, N.; Borawski, J. M.; Leberfinger, C. B.; Gessler, M.; Kerkhoff, E., *Gene Expression Patterns* **2004,** 4, (3), 249-255.

20. Dahlgaard, K.; Raposo, A. A. S. F.; Niccoli, T.; St Johnston, D., *Developmental Cell* **2007,** 13, (4), 539-553.

21. Bosch, M.; Le, K. H. D.; Bugyi, B.; Correia, J. J.; Renault, L.; Carlier, M.-F., *Molecular Cell* **2007,** 28, (4), 555-568.

22. Rebowski, G.; Boczkowska, M.; Hayes, D. B.; Guo, L.; Irving, T. C.; Dominguez, R., *Proceedings of the National Academy of Sciences* **2008,** 105, (31), 10785-10790.

23. Ducka, A. M.; Joel, P.; Popowicz, G. M.; Trybus, K. M.; Schleicher, M.; Noegel, A. A.; Huber, R.; Holak, T. A.; Sitar, T., *Proceedings of the National Academy of Sciences* **2010,** 107, (26), 11757-11762.

24. Ito, T.; Narita, A.; Hirayama, T.; Taki, M.; Iyoshi, S.; Yamamoto, Y.; MaÃ©da, Y.; Oda, T., *Journal of Molecular Biology* **2011,** 408, (1), 18-25.

25. Bamburg, J. R., *Annual Review of Cell and Developmental Biology* **1999,** 15, (1), 185-230.

26. Husson, C.; Renault, L.; Didry, D.; Pantaloni, D.; Carlier, M.-F., *Molecular Cell* **2011,** 43, (3), 464-477.

27. Maloney, M.T.; B. J., *Mol Neurobiol* **2007,** 35, (1), 21-44.

28. Bamburg, J. R.; Wiggan, O. N. P., *Trends in Cell Biology* **2002,** 12, (12), 598-605.

29. Wang, W.; Eddy, R.; Condeelis, J., *Nat Rev Cancer* **2007,** 7, (6), 429-440.

30. McGough, A.; Pope, B.; Chiu, W.; Weeds, A., *The Journal of Cell Biology* **1997,** 138, (4), 771-781.

31. Bamburg, J. R.; McGough, A.; Ono, S., *Trends in Cell Biology* **1999,** 9, (9), 364-370.

32. Kudryashov, D. S.; Galkin, V. E.; Orlova, A.; Phan, M.; Egelman, E. H.; Reisler, E., *Journal of Molecular Biology* **2006,** 358, (3), 785-797.

33. Pavlov, D.; Muhlrad, A.; Cooper, J.; Wear, M.; Reisler, E., *Journal of Molecular Biology* **2007,** 365, (5), 1350-1358.

34. Galkin, V. E.; Orlova, A.; Kudryashov, D. S.; Solodukhin, A.; Reisler, E.; Schroder, G. F.; Egelman, E. H., *Proceedings of the National Academy of Sciences* **2011,** 108, (51), 20568-20572.

35. Grintsevich, E. E.; Benchaar, S. A.; Warshaviak, D.; Boontheung, P.; Halgand, F. d. r.; Whitelegge, J. P.; Faull, K. F.; Ogorzalek Loo, R. R.; Sept, D.; Loo, J. A.; Reisler, E., *Journal of Molecular Biology* **2008,** 377, (2), 395-409.

36. Benchaar, S. A.; Xie, Y.; Phillips, M.; Loo, R. R. O.; Galkin, V. E.; Orlova, A.; Thevis, M.; Muhlrad, A.; Almo, S. C.; Loo, J. A.; Egelman, E. H.; Reisler, E., *Biochemistry* **2006,** 46, (1), 225-233.

37. Mannherz, H. G.; Ballweber, E.; Galla, M.; Villard, S.; Granier, C.; Steegborn, C.; Schmidtmann, A.; Jaquet, K.; Pope, B.; Weeds, A. G., *Journal of Molecular Biology* **2007,** 366, (3), 745-755.

38. Lappalainen, P.; Fedorov, E. V.; Fedorov, A. A.; Almo, S. C.; Drubin, D. G., *EMBO J* **1997,** 16, (18), 5520-5530.

39. Pope, B. J.; Zierler-Gould, K. M.; KÃ¼hne, R.; Weeds, A. G.; Ball, L. J., *Journal of Biological Chemistry* **2004,** 279, (6), 4840-4848.

40. Paavilainen, V. O.; Oksanen, E.; Goldman, A.; Lappalainen, P., *The Journal of Cell Biology* **2008,** 182, (1), 51-59.

41. Galkin, V. E.; Orlova, A.; VanLoock, M. S.; Shvetsov, A.; Reisler, E.; Egelman, E. H., *The Journal of Cell Biology* **2003,** 163, (5), 1057-1066.

42. McCullough, B. R.; Blanchoin, L.; Martiel, J.-L.; De La Cruz, E. M., *Journal of Molecular Biology* **2008,** 381, (3), 550-558.

43. Prochniewicz, E.; Janson, N.; Thomas, D. D.; De La Cruz, E. M., *Journal of Molecular Biology* **2005,** 353, (5), 990-1000.

44. Andrianantoandro, E.; Pollard, T. D., *Molecular Cell* **2006,** 24, (1), 13-23.

45. De La Cruz, E. M., *Biophysical Review* **2009,** 1, (2), 51-59.

46. Bobkov, A. A.; Muhlrad, A.; Pavlov, D. A.; Kokabi, K.; Yilmaz, A.; Reisler, E., *Journal of Molecular Biology* **2006,** 356, (2), 325-334.

Chapter 2

Multiple forms of Spire-actin complexes and their functional consequences

THE JOURNAL OF BIOLOGICAL CHEMISTRY VOL. 287, NO. 13, pp. 10684–10692, March 23, 2012

Multiple Forms of Spire-Actin Complexes and their Functional Consequences*[S]

Received for publication, October 29, 2011, and in revised form, February 6, 2012 Published, JBC Papers in Press, February 8, 2012, DOI 10.1074/jbc.M111.317792

Christine K. Chen[‡], Michael R. Sawaya[‡], Martin L. Phillips[‡], Emil Reisler[‡§], and Margot E. Quinlan[‡§1]

From the [‡]Department of Chemistry and Biochemistry and the [§]Molecular Biology Institute, University of California Los Angeles, Los Angeles, California 90095

Background: Spire is a WH2 domain-containing protein implicated in actin nucleation and critical to oogenesis.
Results: Spire rapidly depolymerizes actin filaments by combining monomer sequestration with weak filament severing, and it nucleates new filaments.
Conclusion: This shows functional and structural variations among actin complexes with Spire.
Significance: Spire-actin structures and actin remodeling by Spir are more complex than originally imagined.

Spire is a WH2 domain-containing actin nucleator essential for establishing an actin mesh during oogenesis. *In vitro*, in addition to nucleating filaments, Spire can sever them and sequester actin monomers. Understanding how Spire is capable of these disparate functions and which are physiologically relevant is an important goal. To study severing, we examined the effect of *Drosophila* Spire on preformed filaments in bulk and single filament assays. We observed rapid depolymerization of actin filaments by Spire, which we conclude is largely due to its sequestration activity and enhanced by its weak severing activity. We also studied the solution and crystal structures of Spire-actin complexes. We find structural and functional differences between constructs containing four WH2 domains (Spir-ABCD) and two WH2 domains (Spir-CD) that may provide insight into the mechanisms of nucleation and sequestration. Intriguingly, we observed lateral interactions between actin monomers associated with Spir-ABCD, suggesting that the structures built by these four tandem WH2 domains are more complex than originally imagined. Finally, we propose that Spire-actin mixtures contain both nuclei and sequestration structures.

Rapid remodeling of the actin cytoskeleton, involving regulation of its formation and depolymerization, is essential for many cellular processes including motility, cytokinesis, and endocytosis. Actin nucleators are factors that initiate formation of new filaments. To date, three classes of nucleators have been identified: the Arp2/3 complex, the formins, and Wasp homology 2 (WH2)[2] nucleators. As the name implies, the third class uses actin-monomer-binding WH2 domains to nucleate. Spire (Spir), JMY, Cordon bleu (Cobl), Leimodin (Lmod), and the bacterial proteins VopF/L/N are grouped together in this class of nucleators, although they are likely to act by distinct mechanisms (1–7). At least two of these proteins, Spir and Cobl, were found to sever filaments and sequester monomers in addition to nucleating new filaments (8, 9). This is not implausible because two other proteins, cofilin and gelsolin, can both sever and nucleate, at least *in vitro* (10). For Spir and Cobl, it remains to be determined which of these activities are dominant *in vivo* and/or when the different activities are physiologically relevant. Here we focus on Spir in an effort to better understand how it modulates the actin cytoskeleton.

Spir plays a role in early development of metazoans (11–13). The *spir* locus was first identified as a *Drosophila* maternal effect gene essential to establishment of both the anterior/posterior and dorsal/ventral body axes in developing oocytes and embryos (11). Recently a role for the mammalian orthologs, Spir1 and Spir2, in oogenesis was also described (13). An actin mesh that traverses the *Drosophila* ooctye is absent when the *spir* gene is mutated; a similar mesh is absent in mouse ooctyes in which both Spir1 and Spir2 are knocked down by RNAi (13–15). These data demonstrate that Spir plays a role in building this mesh, suggesting its *in vivo* role as a nucleator. In principle, Spir could also enhance polymerization by severing filaments, thereby increasing the concentration of barbed ends available to elongate.

Spir has four tandem WH2 domains. Constructs containing all four of these domains (the N-terminal half of Spir (Spir-NT) or just the cluster of WH2 domains (Spir-ABCD)) have equivalent, maximal nucleation activity. A construct that contains only the two C-terminal WH2 domains (Spir-CD) is sufficient to nucleate, although at a slower rate (1). Models of the nucleation mechanism vary in detail. A common theme is the idea that the closely spaced WH2 domains bind actin monomers in an elongated structure, as observed by electron microscopy and detected by analytical ultracentrifugation (1, 8). However, the

* This work was supported, in whole or in part, by National Institutes of Health Grant R01 GM096133, a Burroughs-Wellcome Fund Career Award in the Biomedical Sciences, and a March of Dimes Foundation, Basil O'Connor Starter Scholar Award (#5-FY10-81) (to M. E. Q). This work was also supported by U.S. Public Health Service Grant GM077190 (to E. R.).

[S] This article contains supplemental text, references, Table S1, and Figs. S1–S4.

The atomic coordinates and structure factors (code 3UE5) have been deposited in the Protein Data Bank, Research Collaboratory for Structural Bioinformatics, Rutgers University, New Brunswick, NJ (http://www.rcsb.org/).

[1] To whom correspondence should be addressed: Dept. of Chemistry and Biochemistry, 611 Charles E. Young Dr., East, University of California Los Angeles, CA 90095. Tel.: 310-206-8064; E-mail: margot@chem.ucla.edu.

[2] The abbreviations used are: WH2, Wasp homology 2; Dm, *D. melanogaster*; TIRF, total internal reflection fluorescence; LatA, latrunculin A.

orientation and rigidity of adjacent monomers with respect to each other before elongation begins is an open question. Bosch *et al.* (8) report that the N-terminal half of human Spir1 (hSpir1) binds actin cooperatively, forming a stable complex with four actin monomers (SA_4). They conclude that this structure is not a nucleus of actin filaments; instead it may be a sequesteration complex. Ducka *et al.* (16) co-crystallized Spir with actin. They observed that the last WH2 domain (Spir-D) binds actin in a conformation that closely resembles other WH2 domains (17), but information about the other WH2 domains and the linkers is absent in their structures. Because of the absence of linkers and the lack of correspondence between WH2 domains and actin monomers in the unit cells, information from these structures about the orientation of actins bound to adjacent WH2 domains is speculative at best. In a crystal of longitudinal actin dimers bound to tethered N-Wasp WH2 domains, the actin monomers are rotated, with respect to each other, ~30° more than adjacent monomers in a filament (18). Rebowski *et al.* (18) interpret this structure as an explanation for weak nucleation activity by Spir. Although this may be true, it must be noted that the sequence between WH2 domains, as well as the specific WH2 domains in Spir, contribute significantly to the nucleation activity (1, 6), making it unclear how relevant this crystal structure is to understanding Spir. Thus, more work is required to understand how Spir associates with actin monomers and nucleates filaments.

To study nucleation and severing by Spir, we analyzed the effects of *Drosophila melanogaster* (Dm) Spir on actin monomers and preformed filaments. We found that Dm Spir induces rapid depolymerization of actin filaments. We confirmed that Spir severs filaments, as reported for hSpir1 (8). However, we found that the severing activity of Spir is weak and conclude that rapid depolymerization is largely due to the sequestering activity of Spir. Polymerization assays show that Spir binds actin in structures that accelerate polymerization but suggest that the mixture is heterogeneous. Notably, velocity sedimentation data show that Dm Spir does not bind readily four actin monomers in a stable complex as described for hSpir1 (8) and confirm that Spir-actin solutions contain a mix of structures. Finally, our data demonstrate differences between Spir-ABCD-actin and Spir-CD-actin complexes, including evidence for Spir-dependent lateral actin interactions in addition to the expected longitudinal structures. Together our data suggest that Spir-actin interactions are more complex than originally believed.

EXPERIMENTAL PROCEDURES

Proteins—All proteins were purified and labeled according to standard published procedures. Details and minor modifications are given in the supplemental methods.

Fluorescence Measurements—Pyrene-actin polymerization and depolymerization assays were performed at 20 °C, using 5 μM actin (2.5% labeled) in 50 mM KCl, 1 mM $MgCl_2$, 1 mM EGTA, 10 mM Hepes, pH 7.0, 0.2 mM ATP unless otherwise noted. Pyrene excimer emission was measured with 5 μM G-actin in the presence of stoichiometric concentrations of Spir. Salts (50 mM KCl and 2 mM $MgCl_2$) were then added to the cuvette and incubated for 15 min before measuring maximum emission under F-actin conditions. Further details are given in the text and the supplemental methods.

Total Internal Reflection Fluorescence Microscopy—Direct visualization of filaments was performed as previously described, with some modifications (19, 20). All proteins were diluted in total internal reflection fluorescence (TIRF) buffer: 50 mM KCl, 1 mM $MgCl_2$, 1 mM EGTA, 10 mM Hepes, pH 7.0, 0.2 mM ATP, 100 mM DTT, 15 mM glucose, 20 μg/ml catalase, and 100 μg/ml glucose oxidase. Either a G-actin mixture or F-actin was labeled with 20% Cy3b-maleimide and 1% biotin-maleimide unless otherwise noted. Filaments were immobilized with streptavidin cross-links to biotin-PEG. See the supplemental methods for further detail.

Crystallization and Structure Determination—Actin was treated with the protease ECP32/grimelysin (ECP) at a 6:1 molar ratio to prevent polymerization. Cleaved actin was mixed with Spir-CD at a 1:1 molar ratio. Crystallography conditions are in the supplemental methods. Data collection and refinement statistics are reported in supplemental Table S1. The coordinates of the final model and the merged structure factors have been deposited in the Protein Data Bank under code 3UE5.

RESULTS

Spir Induces Rapid Depolymerization of Actin Filaments—In this paper we use two constructs of Dm Spir: Spir-ABCD, which has four WH2 domains, and Spir-CD, which has two. Throughout the paper we consider ratios of Spir to actin in terms of the number of WH2 domains in the construct. Thus, we refer to 1 mol of Spir-ABCD:4 mol of actin and 1 mol of Spir-CD:2 mol of actin as stoichiometric concentrations. Other ratios are defined when used.

We first observed Spir-induced loss of actin filaments in co-sedimentation assays. We added stoichiometric Spir-CD to actin filaments, centrifuged the solution, and analyzed the supernatant and pellet by SDS-PAGE. All of the Spir and actin was in the supernatant (Fig. 1*A*). We then measured the time-dependent effect of adding a range of concentrations of Spir-ABCD or Spir-CD to freshly polymerized actin in pyrene-actin assembly assays. At stoichiometric ratios, both Spir-ABCD and Spir-CD depolymerized over 50% of the filaments within 20 s (Fig. 1*B* and supplemental Fig. S1*A*). As expected from the loss of pyrene fluorescence, very few filaments could be detected after 15 min when visualized by EM (Fig. 1*A*). We compared the effect of Spir on F-actin with that of latrunculin A (LatA), a known sequestering agent. At a 10:1 molar ratio to actin, LatA induced depolymerization of F-actin but at a slower rate than Spir (Fig. 1*B* and supplemental Fig. S1*A*), suggesting that Spir may be acting by a distinct mechanism. At lower ratios of Spir to actin, depolymerization was still rapid, but the higher plateau of the pyrene fluorescence curves indicated that some filaments remained in solution. At higher ratios (1:1 and higher) of WH2 domains to actin, we observed oscillations in the pyrene signal (see especially for 2.5 μM Spir-CD in supplemental Fig. S1*A*). We also see oscillations when using light scattering instead of pyrene to detect polymer (supplemental Fig. S1*B*). This behavior is reminiscent of the "ringing" described for Cobl (9) and may reflect the dual activities of Spir: nucleation and depolymerization, competing under certain conditions.

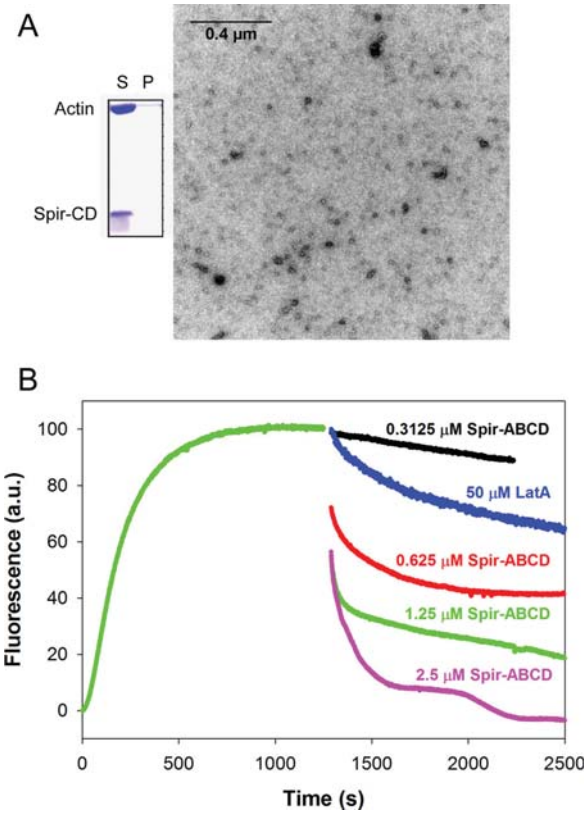

FIGURE 1. **Rapid actin filament depolymerization by Spir.** *A*, a co-sedimentation assay of 6 μM Spir-CD added to 6 μM F-actin. Spir-CD can be seen in the supernatant (*S*) (but not in the pellet (*P*)) with actin that has mostly depolymerized after a 15-min incubation. Representative EM image of actin incubated with a stoichiometric amount of Spir-CD for 15 min. Some short filaments remain, but the majority of the fields imaged have no F-actin. *B*, fluorescence curves of 5 μM F-actin (2.5% pyrene labeled actin) upon the addition of Spir-ABCD (concentrations as indicated) show rapid depolymerization. The actin polymerization was monitored for 1200 s before Spir was added. Depolymerization is dose-dependent and is complete above stoichiometric Spir concentrations. Filaments exhibit faster depolymerization in the presence of Spir than in the presence of sequestration agent, LatA.

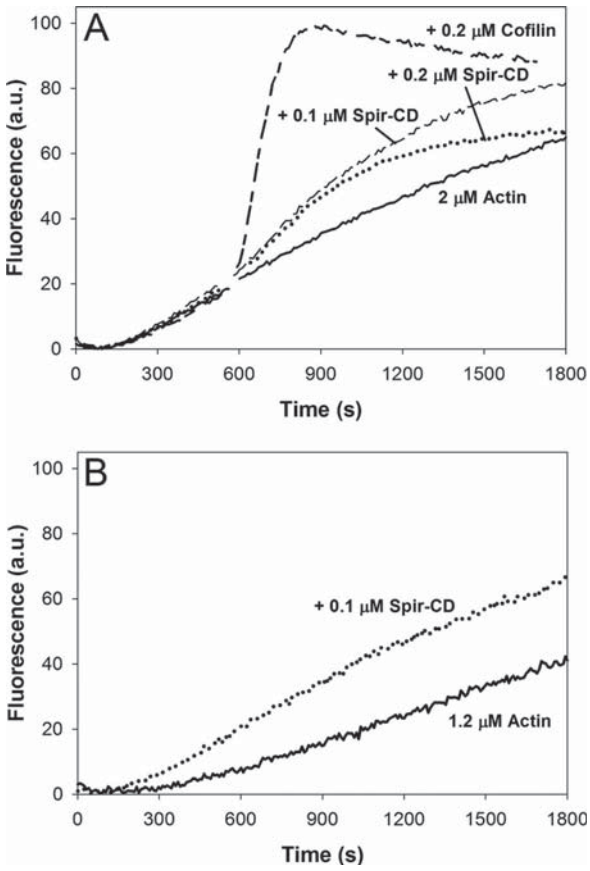

FIGURE 2. **Spir severs weakly in bulk assays.** *A*, 2.5% pyrene-labeled actin was polymerized for ~9 min before the addition of either Spir-CD or cofilin. The polymerization rate accelerates strongly after the addition of 0.2 μM cofilin, but only a small rate increase is apparent upon the addition of 0.1 or 0.2 μM Spir-CD. *B*, weak nucleation is apparent when Spir-CD is added to 1.2 μM G-actin, the amount remaining at the time of addition in *A*.

Severing by Drosophila Spir—Bosch *et al.* (8) reported that Spir severs filaments, prompting us to ask whether severing causes the rapid depolymerization observed in this study. To do so, we compared the strength of severing by Spir with that of cofilin. We first tested the effect of adding Spir-CD or cofilin to actin, midpolymerization. Under these conditions cofilin severs filaments, thereby creating new barbed ends and strongly increasing the polymerization rate of actin (21). Indeed, the addition of 0.2 μM cofilin to 2.5 μM actin ~9 min after polymerization was initiated results in a dramatic increase in the polymerization rate (Fig. 2*A*). In contrast, the addition of 0.2 μM Spir-CD causes only a modest increase in the polymerization rate (Fig. 2*A*). Because Spir also nucleates filaments (1, 8), we assessed the contribution of nucleation under these conditions. We calculated that 1.2 μM actin monomer remained at the time that Spir was added and then tested the ability of Spir to nucleate this low concentration of actin. The addition of 0.1 μM Spir causes an increase in polymerization rate and a slight decrease in the lag phase, indicating that Spir can nucleate even at a low actin concentration (Fig. 2*B*). Thus, nucleation may also contribute to the change seen in our "severing" assay. Taken together, these data suggest that the severing activity of Spir is weak under these conditions.

The original observation of severing was made with hSpir1 (8), and we were working with Dm Spir. To ascertain whether Dm Spir can in fact sever, we also used EM. Filaments were immobilized on grids and incubated with a 10-fold excess of Spir-CD. After 3 min, the grids were washed and stained with uranyl acetate. We observed fragments of filaments aligned linearly, which suggests that Dm Spir severs actin filaments (supplemental Fig. S2*A*).

Mechanism of Rapid F-actin Depolymerization—To observe the effect of Spir on actin filaments more directly, we used TIRF microscopy. In each experiment, labeled actin was polymerized and then added to a flow cell. Filaments were held on the surface through biotin-streptavidin bonds. When substoichiometric concentrations of either Spir-ABCD or Spir-CD were added, severing was observed only rarely (data not shown). At approx-

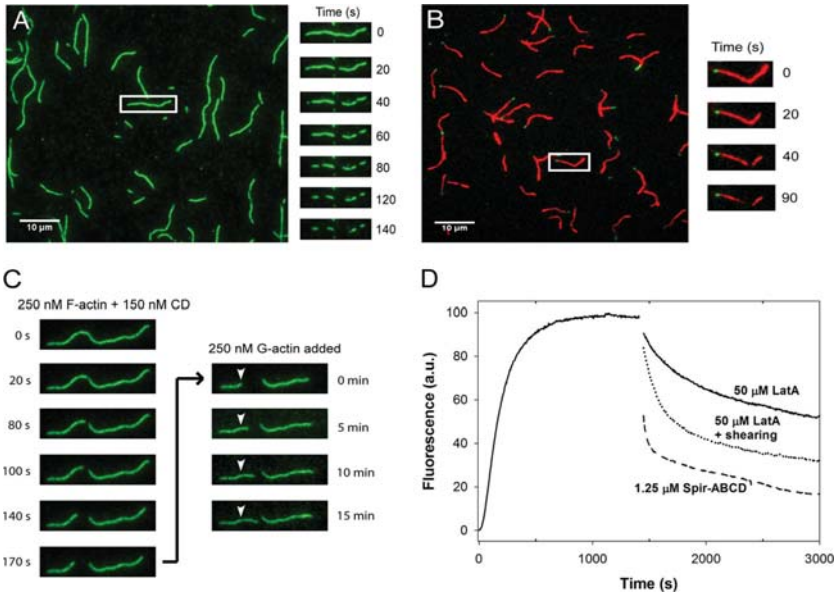

FIGURE 3. **Spir severs and depolymerizes actin filaments from the barbed end.** *A*, Cy3b-labeled actin filaments were diluted to 200 nM in TIRF buffer before immobilization in flow cells. Time lapse images were recorded for 3 min immediately after 100 nM Spir-ABCD was added. Severing events were observed, and filaments depolymerized faster at one end. Images at 20-s intervals are shown for one filament. *B*, polarity marked filaments are grown off of AlexaFluor488-phalloidin-stabilized seeds. The addition of 100 nM Spir-ABCD induced both severing and depolymerization of the barbed ends. *C*, typical Cy3b-labeled actin filament. Time course of filament changes after the addition of 150 nM Spir-CD. Phalloidin was added after 180 s to stabilize existing filaments, and then 250 nM labeled G-actin was added. Growth at one side of the cut site and one end of the filament confirms the polarity of the filament. *D*, to mimic the effect of severing combined with sequestering, we mechanically sheared 5 μM F-actin by pipetting several times and then adding LatA. The combination of these treatments led to depolymerization that was much faster than the addition of LatA alone. The addition of stoichiometric Spir-ABCD is shown for comparison.

imately stoichiometric concentrations, severing events and depolymerization of actin filaments were both evident (Fig. 3*A* and supplemental Fig. S2*B*). When we increased Spir-ABCD or Spir-CD concentrations another 2-fold, filaments disappeared too quickly to distinguish between severing and depolymerization (data not shown). Severing rates at stoichiometric concentrations of Spir-ABCD and Spir-CD were similar (Spir-ABCD: $(0.34 \pm 0.26) \times 10^{-2}$ and Spir-CD: $(0.14 \pm 0.19) \times 10^{-2}$ cuts/μm/s, $n = \sim 50$ filaments each). The addition of Spir-ABCD and Spir-CD did not affect all filaments. Spir-ABCD did not sever three of the filaments, and Spir-CD did not sever approximately half of the filaments analyzed. Filaments that were not severed were included in the calculations of average severing rates. For comparison, we measured severing rates of yeast cofilin (with yeast actin). When eight times less cofilin was added, the rates were still more than 10 times faster ($(4.0 \pm 1.4) \times 10^{-2}$ cuts/μm/s, $n = 25$), and all of the filaments observed were severed. We also asked whether Spir-ABCD could sever in the presence of actin monomers, to compare with conditions in the pyrene assay. We mixed Spir-ABCD with stoichiometric amounts of G-actin before adding them to filaments in a flow cell (supplemental Fig. S3). Under these conditions, both severing and depolymerization activity were markedly decreased ($(0.05 \pm 0.11) \times 10^{-2}$, $n = 74$; supplemental Fig. S3). Taken together, our results demonstrate that Spir is a weak severer and that this activity alone could not account for the rapid depolymerization we observe.

Filament shortening was observed when Spir (ABCD or CD) was added in TIRF experiments. Shortening was also observed when just the buffer was exchanged in the flow chamber as a control. In such control experiments, approximately one-quarter of the filaments shrank, whereas virtually every filament was affected when Spir-ABCD was added. In both cases, shortening occurred predominantly from one end of each filament. We measured depolymerization rates from each end and found that one end shortened ~15 times faster than the other, consistent with differences in the kinetics of barbed and pointed ends of actin filaments (supplemental Fig. S2*C*). To confirm that the rapidly shortening end was the barbed end of the filament, we made polarity marked filaments in the flow chamber (see the supplemental methods). Upon addition of Spir-ABCD, we observed rapid depolymerization at the barbed ends as expected (Fig. 3*B*). Eventually, only the phalloidin-stabilized actin seeds remained, indicating that Spir is not able to depolymerize or sever phalloidin-stabilized filaments (data not shown). Two lines of evidence suggest that stabilizing the pointed ends did not bias our observation. First, polarity marked filaments that were severed also depolymerized predominantly from their barbed ends at the cut point. Second, we confirmed that the shortening end was the barbed end in unmarked filaments. To do so, Spir was added to filaments in a flow chamber for 2 min. Then phalloidin was added to the chamber to halt the reaction. Next, 250 nM labeled G-actin was added, and the growth of filaments was monitored. New growth extended from the depolymerized ends, confirming that barbed end depolymerization was dominant in our assay (Fig. 3*C* and supplemental Fig. S2*D*).

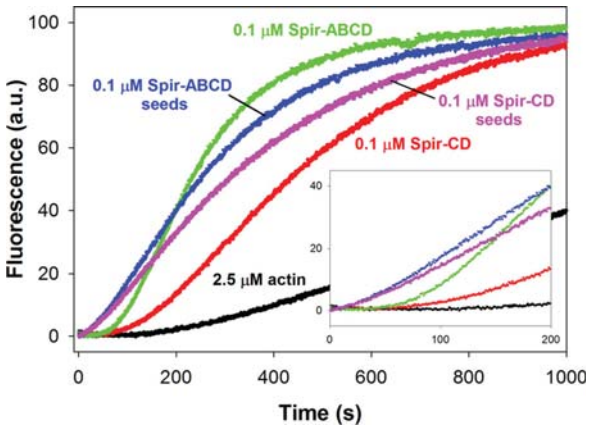

FIGURE 4. **Spir-ABCD and Spir-CD seeds enhance actin polymerization.** Spir-ABCD and Spir-CD seeds, created by incubating stoichiometric ratios of Spir and actin in 2 mM $MgCl_2$ and 50 mM KCl (*blue* and *magenta traces*), exhibit faster nucleation of filaments as indicated by the shorter lag times compared with actin alone (*black*) and actin mixed with either Spir-ABCD or Spir-CD at time 0 (*green* and *red*).

The combination of TIRF experiments and bulk assays suggests that depolymerization, whether by sequestration or active depolymerization, is the major activity causing rapid loss of filaments. This activity is enhanced by weak severing producing additional barbed ends for depolymerization under these conditions. To test this hypothesis, we returned to the pyrene assay. This time, when adding LatA, we mixed the solution by pipetting several times with the expectation that we would shear actin filaments, mimicking the effect of a severer. Indeed, the depolymerization rate was much greater with pipetting compared with adding LatA with gentle mixing (Fig. 3*D*). This observation demonstrates that synergy between sequestering and severing results in rapid filament disassembly and supports our hypothesis that Spir is acting by combining these mechanisms.

Spir-Actin Complexes Include Nuclei—To better understand how Spir can nucleate, sever, depolymerize, and/or sequester actin, we examined the arrangement of actin monomers in Spir-actin complexes. We first mixed stoichiometric concentrations of Spir (ABCD or CD) with actin under polymerizing conditions (50 mM KCl and 1 mM $MgCl_2$) and then added this solution to monomeric actin (2.5% pyrene-actin), such that the final concentrations were 0.1 μM Spir and 2.5 μM actin. We observed polymerization with virtually no lag time (Fig. 4), suggesting that small seeds or nuclei were present in this Spir-actin mixture. This observation was surprising based on findings with hSpir1 (8). That study reported cooperative binding of four actin monomers to Spir and a stable structure described as a sequestration complex, as opposed to a nucleus. For comparison, we added 0.1 μM Spir (ABCD or CD) to 2.5 μM actin and monitored these standard polymerization reactions. As expected, in these cases there was a detectable acceleration of actin nucleation, with the lag time reduced to ~50 s (*versus* ~100 s for actin alone) and polymerization rates faster than for actin alone. To further compare these five conditions, we calculated the concentration of barbed ends at half-maximal polymerization. In all cases where Spir was present, there were at least four times more barbed ends compared with spontaneous polymerization, consistent with improved nucleation of actin leading to a greater number of filaments. However, because polymerization rates are not explosive when we add either Spir-actin complexes or just Spir to monomeric actin, we assume that there is a mixture of species present in the solution. Again, based on the barbed end concentration at half-maximal polymerization, we estimate that ~1/100th of the Spir molecules form nuclei and speculate that many of the remaining molecules bind actin in sequestration structures based on our earlier EM studies (1) and findings with hSpir1 (8).

Solution Structure of Spir-Actin Complexes—To examine the Spir-actin complexes in solution, we used spectroscopy, cross-linking, and analytical ultracentrifugation. We used yeast actin mutants to examine both longitudinal and lateral contacts between actin monomers associated with Spir. To study longitudinal contacts, we labeled the yeast actin mutant Q41C with pyrene (at Cys-41 and Cys-374). Residue 41 is within the DNase I binding loop, and pyrene probes bound to Cys-41 and Cys-374 from adjacent longitudinal monomers in F-actin will stack, producing excimer emission at 470 nm (22). We monitored excimer emission in the presence of stoichiometric concentrations of Spir-ABCD or Spir-CD under nonpolymerizing (in G buffer) and polymerizing (added $MgCl_2$ and KCl) conditions. If four actin monomers bind Spir-ABCD, or two bind Spir-CD, in a filament-like configuration, we expect the amplitude of excimer fluorescence to be ~75% or ~50% that of polymerized actin, respectively. Excimer emission of stoichiometric actin and Spir-ABCD in G buffer was 44 ± 6% that of polymerized actin (Fig. 5*A*). The addition of salts increased the excimer emission (to 67 ± 2%), indicating that the orientation and/or affinity of actin and Spir are sensitive to solvent conditions. Increased excimer emission in the presence of salts was also observed for Spir-CD, but the excimer signal was much lower than could be expected for stoichiometric actin binding in a filament-like configuration (16 ± 3% *versus* 50%; Fig. 5*A*). The signal is also much lower than the expected two-thirds of that with Spir-ABCD, indicating structural differences in monomer stacking between Spir-ABCD-actin and Spir-CD-actin complexes. The addition of an excess of actin did not change the excimer emission levels, suggesting that the lower levels were not caused by insufficient actin binding and indicating that further structural changes were unlikely (data not shown).

The interpretation of the above excimer results must be qualified by the assay dependence on the stacking of pyrene probes. Thus, in our case, excimer emission does not report directly and strictly on filament-like positions of the labeled residues. Instead, it reports on their longitudinal or lateral stacking, which requires proximities, within ~3–18 Å. A useful example is that of cofilin-decorated actin filaments. Cofilin binding enhances excimer emission above that of unbound filaments. However, in contrast to excimer increase, FRET measurements show an increased distance between Cys-41 and Cys-374 probe pairs upon cofilin binding (22). In agreement with FRET results, cofilin inhibits the normal cross-linking of actin monomers via the same cysteines that are used for excimer experiments. With this in mind, we also probed the complexes of Spir with the Q41C actin mutant with cross-linking reagents. As expected,

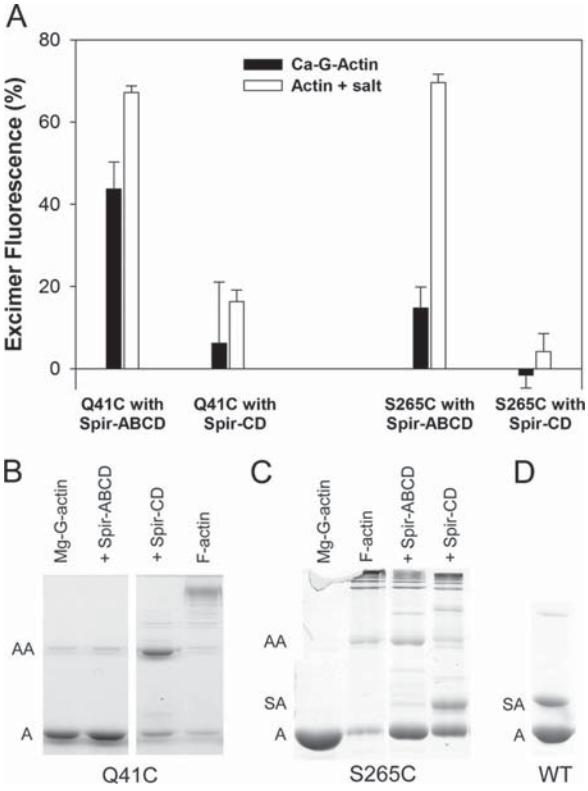

FIGURE 5. **Longitudinal and lateral actin contacts induced by Spir.** *A*, yeast actin mutants Q41C and S265C incubated with Spir-ABCD or Spir-CD were monitored for excimer formation under nonpolymerizing and polymerizing conditions. Excimer fluorescence is plotted relative to that of the corresponding F-actin controls (100%). Stoichiometric concentrations of Spir-ABCD and Q41C showed excimer fluorescence under nonpolymerizing conditions. Minimal excimer formation was visible in all other Ca-G-actin cases. Under polymerizing conditions, Spir-ABCD incubated with either Q41C or S265C produced high excimer fluorescence. *B*, cross-linking of Q41C in the presence of Spir-ABCD or Spir-CD is shown. 5 μM yeast actin mutant Q41C converted to Mg-G-actin was incubated with stoichiometric concentrations of either Spir-ABCD or Spir-CD and the cross-linker MTS1. In the presence of Spir-CD, actin dimer formation is strong compared with the Mg-G-actin (with a trace level of cross-linking) and F-actin (cross-linked into higher order oligomers) controls. In contrast, little cross-linking is evident when Q41C is incubated with Spir-ABCD. *C*, cross-linking of S265C in the presence of Spir-ABCD or Spir-CD. Conditions were the same as in *B*. Cross-linking with S265C and Spir-ABCD or Spir-CD both result in higher order oligomers. A band between actin monomer and dimer is detected only for Spir-CD and S265C. We interpret this as cross-linking between Spir and actin. *D*, cross-linking with Spir-CD and wild type yeast actin. A band above the actin monomers confirms that Spir-CD cross-links to actin Cys-374. *A* indicates molecular weight consistent with an actin monomer. *AA* indicates an actin dimer. *SA* indicates Spir-CD-actin.

Q41C F-actin alone was cross-linked by MTS-1, a homo-bifunctional cysteine cross-linker, but Mg-G-actin was not (Fig. 5*B*). When we treated Spir-CD and Q41C with MTS-1, the major species detected was ~84 kDa, consistent with an actin dimer (Fig. 5*B*). However, when we added MTS-1 to Q41C in the presence of Spir-ABCD, no cross-linking was observed. Other homo-bifunctional cross-linkers of varying lengths ($CuCl_2$, MTS-3, and MTS-6) produced similar results. These data confirm that the Spir-ABCD-actin structures are distinct from Spir-CD-actin structures and actin filaments. Actin bound to Spir-ABCD is stabilized in a structure that holds the neighboring pyrene rings close enough to produce excimer emission but not close enough to be cross-linked. Thus, the excimer emission is not reflecting precise filament-like configuration in this case. In contrast, the Spir-CD-actin complex is flexible, allowing cross-linkers to capture monomers when they are close to a filament-like configuration, although they are not close enough to each other or oriented correctly on average to give eximer emission levels proportional to Spir-ABCD-actin.

We performed analogous experiments with yeast actin mutated to Cys at Ser-265. Pyrene excimer emission from labeled Cys-265 and Cys-374 reflects lateral proximity within the actin filament (23), which is not expected if Spir-ABCD and Spir-CD bind actin in strictly longitudinal structures (1, 8). Excimer emission was negligible for Spir-CD and actin, regardless of the buffer conditions (Fig. 5*A*). Surprisingly, we detected high excimer emission when stoichiometric amounts of Spir-ABCD and actin were combined under polymerizing conditions (Fig. 5*A*). We also performed cross-linking experiments with S265C actin. Consistent with excimer emission data, we observed lateral actin cross-linking in the presence of Spir-ABCD (Fig. 5*C*). This cross-linking was weak but reproducible (with ~80% of the actin remaining in the monomer form), confirming lateral contacts between actin monomers in the presence of Spir-ABCD. This result differs from Spir-ABCD+Q41C actin, in which no cross-linking is observed. Perhaps, the lateral contacts approximate filamentous orientations more closely than the longitudinal contacts. As with Q41C actin, S265C actin was cross-linked in the presence of Spir-CD, despite low excimer emission. We also note that, despite low overall cross-linking of lateral actin contacts, higher order oligomers were generated with Spir-CD in contrast to the dimer observed when longitudinal contacts were cross-linked.

We also detected a band between actin monomers and dimers in the Spir-CD/S265 actin cross-linking experiment (Fig. 5*C*). We interpret this cross-linking as another indication of the flexibility of the Spir-CD-actin structures. To learn more about the orientation of contacts being detected, we performed cross-linking with Spir-CD and wild type actin. We observed a Spir-actin band in this case as well. Because Spir-CD has only one cysteine (Cys-459 within linker 3) we conclude that Spir Cys-459 can be cross-linked to actin through its sole reactive cysteine, Cys-374.

To further examine the solution structure of Spir-actin complexes, we measured their sedimentation velocity coefficients. As before, we combined Spir-ABCD and Spir-CD with stoichiometric concentrations of actin under polymerizing (with $MgCl_2$ and KCl) and nonpolymerizing (in G buffer) conditions. In all cases, the sedimentation coefficient(s) were larger in the presence of salts, consistent with the increase in actin contacts observed under these conditions in the excimer experiments described above (Table 1). In the presence of salts, the observed sedimentation coefficient for Spir-CD and actin (4.65 S) approached the theoretical sedimentation coefficient of an actin dimer (4.94 S). In contrast, the sedimentation coefficient for stoichiometric ratios of actin and Spir-ABCD was less than that of an actin trimer. Asymmetry in the $g(s)$ plot for Spir-ABCD indicates a mixture of species (supplemental Fig. S4). This mixture of species could represent a variable number of

TABLE 1

Comparison of observed and theoretical sedimentation coefficients (in Svedbergs) of Spir constructs incubated with actin at stoichiometric ratios under polymerizing and nonpolymerizing conditions

The theoretical *S* values for actin oligomers were calculated as described under "Experimental Procedures" (+ salt indicates 2 mM $MgCl_2$ and 50 mM KCl).

Observed sedimentation coefficients	*S*	Theoretical sedimentation coefficients	*S*
Actin	3.25	Actin	3.25
Actin + Spir-CD	3.80	2 actin prolated ellipsoid	4.94
Actin + Spir-CD (+ salt)	4.65	3 actin prolated ellipsoid	6.08
Actin + Spir-ABCD	5.80	3 actin oblate ellipsoid	6.49
Actin + Spir-ABCD (+salt)	6.25	3 actin spherical	6.76
		4 actin prolated ellipsoid	6.93
		4 actin oblate ellipsoid	7.86
		4 actin spherical	8.19

actin monomers bound to Spir-ABCD, as well as a mixture of orientations of monomers within the structure. In either case, we do not observe full occupancy of WH2 domains of Spir-ABCD in an elongated structure.

Crystal Structure of Spir-Actin Complex—We co-crystallized Spir-CD with nonpolymerizing ECP-cleaved actin (24) to obtain high resolution data about the Spir-actin complex. Crystals were acquired with a starting ratio of 1 Spir-CD:1 actin, and the complex we observed contained only one actin monomer per Spir-CD. At 2.8 Å resolution, we determined that actin was consistently bound to Spir-D (Fig. 6). As expected, the WH2 domains forms an α-helix that binds in the hydrophobic cleft between subdomains 1 and 3. The C-terminal half of WH2-D extends along subdomain 1 toward subdomain 2. The configuration of Spir-D is similar to that in other reported WH2-actin co-crystal structures (*e.g.* root mean square = 0.472 Å with respect to the WH2 domain of WASP (17)) and similar to the previously published structure of Spir-D-actin (which did not include linker 3 or Spir-C; root mean square = 0.563 Å (16)). Our structure suggests that linker 3 does not fold back to bind the same monomer as Spir-D, instead favoring a conformation in which it is reaching away, leaving Spir-C more able to bind an actin monomer. However, Spir-C and most of the linker between C and D were disordered in the structure and could not be mapped.

In fact pairs of Spir-CD-actin complexes were cross-linked to each other through a disulfide bond between Cys-374 in actin and Cys-459 in Spir (Fig. 6). The cross-linking is most likely driven by crystal packing, capturing the same transient interaction we detected in chemical cross-linking experiments. This structure could reflect a severing mechanism. If linker 3 can insert between subunits of a filament it would destabilize the structure. However, we note that we do not detect significant Spir-actin cross-linking with Spir-ABCD. Thus, we believe that the anti-parallel dimer reflects the flexibility inherent in the association of Spir-CD with actin. Potentially arguing against this is the fact that we do not observe cross-linking between Spir-CD and Q41C actin. Instead, we interpret this as evidence that the Q41C actin dimers form rapidly, preventing significant Spir-actin cross-linking.

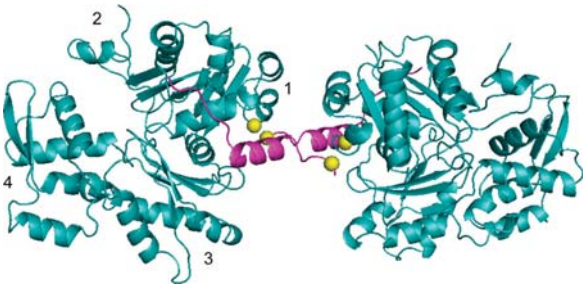

FIGURE 6. **Crystal structure of Spir-D (*magenta*) with ECP-cleaved actin (*cyan*) forming an anti-parallel dimer.** Spir-D is positioned next to the W-loop of actin between subdomains 1 and 3. Subdomains are indicated on the *left* actin monomer. Part of linker 3 between Spir-C and -D is shown. Spir-C and part of actin subdomain 2 are disordered in the crystal. Actin Cys-374 and Spir Cys-459 (shown as *yellow balls*) form a disulfide bond, creating an anti-parallel dimer.

DISCUSSION

Spir Severing—Spir can nucleate, sever, and depolymerize filaments *in vitro*. We found that a construct containing only two WH2 domains, Spir-CD, is sufficient to sever, consistent with recent findings for the WH2 nucleator Cobl (9). As is the case for nucleation, the severing activity of a construct containing four WH2 domains, Spir-ABCD, is more potent than one with two WH2 domains. Some of the difference may be due to the obvious fact that Spir-ABCD has twice as many WH2 domains, but our data show that the constructs actually behave differently when bound to actin. By combining the spectroscopic and cross-linking data with the solution and crystal structure data, we infer that Spir-CD-actin structures are more flexible than Spir-ABCD-actin. The relative stiffness of Spir-ABCD-actin compared with Spir-CD-actin may explain its stronger severing activity.

Both bulk assays and single filament assays show that the severing activity of Spir is quite weak. Under the conditions used here, it is approximately 2 orders of magnitude weaker than the classical severing protein, cofilin. We only observed significant amounts of severing at concentrations of Spir close to stoichiometric with actin, conditions that are unlikely to exist in the cell. Furthermore, severing is even weaker when actin monomers are present. This result explains our earlier observation that Spir does not sever at measurable levels in seeded polymerization assays (1). We therefore conclude that Spir is not a significant *in vivo* severing factor.

Spir Depolymerization—The severing activity of Spir alone is insufficient to explain the rapid depolymerization observed in bulk assays. TIRF experiments show that filaments also shrink in the presence of Spir (Fig. 3). Depolymerization occurred predominantly at one end of the filament, which we determined is the barbed end. Spir has been shown to sequester actin monomers (1, 8). Because bulk depolymerization rates were significantly higher for Spir than the sequestering agent, LatA, we are

intrigued by the possibility that there is a difference in depolymerization mechanisms. However, data from TIRF experiments and pyrene bulk assays do not support this idea. Filaments shorten in control TIRF experiments as fast as they do when Spir is added. The major difference was in the number of filaments shortening, which may be a function of surface interactions and severing. Filaments depolymerize faster in pyrene bulk assays when sheared prior to the addition of LatA. Thus, the enhanced depolymerization rates observed in bulk experiments may reflect how even weak severing activity can markedly accelerate overall depolymerization rates.

Spir-Actin Complexes—Although Spir-CD binds two actin monomers (in the presence of $MgCl_2$ and KCl) as expected, it is noteworthy that Spir-ABCD did not bind four actin monomers (on average) in sedimentation velocity experiments. Tight cooperative binding of four actin monomers was reported for the N-terminal construct of hSpir-1 (8). Perhaps the difference is due to the constructs used. However, Dm Spir-NT and Dm Spir-ABCD have equivalent nucleation activity and the only domain in the N terminus of Spir outside of the WH2 cluster, the KIND domain, does not bind actin (25, 26). Furthermore, earlier EM studies showed little difference between Spir-NT and Spir-ABCD in complex with actin (lengths of 22 ± 4 *versus* 26 ± 5 nm, respectively; (1)). Likewise, rigid body modeling of small angle x-ray scattering data by Sitar *et al.* (27) produced little difference between the WH2 domains and actin of Spir-NT and Spir-ABCD.

Although cross-linking of actin in the presence of Spir-CD captures a filament-like orientation, Spir-ABCD brings more actins into close proximity, including some lateral interactions, both of which may make it the stronger nucleator. The absence of strong longitudinal actin cross-linking in the presence of Spir-ABCD suggests that the contacts are not precisely filament-like. Sitar *et al.* (27) consistently predict elongated structures for Dm Spir bound to actin from small angle x-ray scattering data. They also conclude that these complexes are not strictly filament-like. They do not observe lateral interactions, but our data suggest that they are a small fraction of all interactions. Deviations between their models and measured values are well explained if there is a mixture of species in these experiments.

It is interesting to speculate whether Spir can form distinct complexes with actin: a nucleus and a sequestration complex. Perhaps fully occupied Spir is stable and effectively sequesters actin, as described for the SA_4 complex (8). Here we present evidence of alternate, perhaps less stable, Spir-actin complexes with actin making lateral contacts in addition to longitudinal contacts. Such structures are good candidates for filament nucleation. Indeed, we observed accelerated actin polymerization under these same conditions, consistent with nuclei being present. However, the number of filament seeds formed by Spir-actin must be relatively small, judging by the level of actin polymerization acceleration. Together these data suggest that the dominant species observed is not the nucleus, adding to the challenge of understanding how Spir nucleates.

Ducka *et al.* (16) observed enhanced pyrene fluorescence when at least 4 mol of actin were added per mole of Spir-BCD (3 WH2 domains). They interpreted this as evidence that lateral monomer interactions are necessary to stabilize longitudinal contacts between monomers bound to Spir in a filament-like structure. However, we observed lateral interactions between actin monomers when stoichiometric concentrations were added to Spir-ABCD in multiple experiments, and our sedimentation velocity data suggest a distribution of the number of monomers binding to Spir-ABCD. The pyrene-actin experiments of Ducka *et al.* (16) must be reconsidered in light of these results. Given the mixture of species that we detect, it is unlikely that the enhancement of pyrene fluorescence that Ducka *et al.* (16) observe is solely the product of adding a monomer in a lateral position to fully occupied WH2 domains. Instead, increasing concentrations of actin probably lead to greater occupation of WH2 domains and a concomitant change in the pyrene environment.

Concluding Remarks—The importance of the ability of Spir to nucleate and sever needs to be examined further *in vivo*. Identifying residues that are essential to severing *versus* nucleation, if possible, would be the ideal way to test which of these activities is essential. Short of this, we argue that nucleation by Spir is likely to be a critical function because it has been shown to play a positive role in the establishment of an actin-based mesh that is essential for *Drosophila* and mammalian oogenesis (13, 14). Genetic and biochemical evidence indicates that Spir coordinates with the formin Capu (Fmn2 in mammals) (11, 14, 25, 28). Capu binds two molecules of Spir and enhances its nucleation activity. Our preliminary results indicate that Capu does not influence depolymerization or lateral cross-linking by Spir. This suggests that if Spir, in fact, has multiple activities *in vivo*, regulation by factors other than Capu may play a role.

Finally, it will be important to study other WH2 nucleators with the approaches taken here to learn more about how this disparate class of nucleators works and what specific factors create the differences in their activities. To date, one common theme among this class of nucleators is that WH2 domains alone are not sufficient to create a nucleator. Instead an extra domain, such as the MBL domain of Spir, the K domain, and linker 2 of Cobl and the C-terminal dimerization domain of VopL, works with the WH2 domains (1, 2, 6, 9, 29, 30).

Acknowledgments—We thank Corie Ralston for data collection at the Advanced Light Source, Alex Shvetsov for helping with crystal conditions, Dima Kudryashov for initial work on this project, Ron Lin for help with TIRF and slide preparation, and Christina Vizcarra for sharing reagents.

REFERENCES

1. Quinlan, M. E., Heuser, J. E., Kerkhoff, E., and Mullins, R. D. (2005) *Drosophila* Spire is an actin nucleation factor. *Nature* **433,** 382–388
2. Ahuja, R., Pinyol, R., Reichenbach, N., Custer, L., Klingensmith, J., Kessels, M. M., and Qualmann, B. (2007) Cordon-Bleu is an actin nucleation factor and controls neuronal morphology. *Cell* **131,** 337–350
3. Liverman, A. D., Cheng, H. C., Trosky, J. E., Leung, D. W., Yarbrough, M. L., Burdette, D. L., Rosen, M. K., and Orth, K. (2007) Arp2/3-independent assembly of actin by *Vibrio* type III effector VopL. *Proc. Natl. Acad. Sci. U.S.A.* **104,** 17117–17122
4. Tam, V. C., Serruto, D., Dziejman, M., Brieher, W., and Mekalanos, J. J. (2007) A type III secretion system in *Vibrio cholerae* translocates a formin/spire hybrid-like actin nucleator to promote intestinal colonization. *Cell*

Host Microbe **1,** 95–107
5. Chereau, D., Boczkowska, M., Skwarek-Maruszewska, A., Fujiwara, I., Hayes, D. B., Rebowski, G., Lappalainen, P., Pollard, T. D., and Dominguez, R. (2008) Leiomodin is an actin filament nucleator in muscle cells. *Science* **320,** 239–243
6. Zuchero, J. B., Coutts, A. S., Quinlan, M. E., Thangue, N. B., and Mullins, R. D. (2009) p53-cofactor JMY is a multifunctional actin nucleation factor. *Nat. Cell Biol.* **11,** 451–459
7. Tam, V. C., Suzuki, M., Coughlin, M., Saslowsky, D., Biswas, K., Lencer, W. I., Faruque, S. M., and Mekalanos, J. J. (2010) Functional analysis of VopF activity required for colonization in *Vibrio cholerae*. *mBio* **1,** e00289–10. doi:10.1128/mBio.00289–10
8. Bosch, M., Le, K. H., Bugyi, B., Correia, J. J., Renault, L., and Carlier, M. F. (2007) Analysis of the function of Spire in actin assembly and its synergy with formin and profilin. *Mol. Cell* **28,** 555–568
9. Husson, C., Renault, L., Didry, D., Pantaloni, D., and Carlier, M. F. (2011) Cordon-Bleu uses WH2 domains as multifunctional dynamizers of actin filament assembly. *Mol. Cell* **43,** 464–477
10. Bamburg, J. R. (1999) Proteins of the ADF/cofilin family. Essential regulators of actin dynamics. *Annu. Rev. Cell Dev. Biol.* **15,** 185–230
11. Manseau, L. J., and Schüpbach, T. (1989) Cappuccino and Spire. Two unique maternal-effect loci required for both the anteroposterior and dorsoventral patterns of the *Drosophila* embryo. *Genes Dev.* **3,** 1437–1452
12. Le Goff, C., Laurent, V., Le Bon, K., Tanguy, G., Couturier, A., Le Goff, X., and Le Guellec, R. (2006) pEg6, a spire family member, is a maternal gene encoding a vegetally localized mRNA in *Xenopus* embryos. *Biol. Cell* **98,** 697–708
13. Pfender, S., Kuznetsov, V., Pleiser, S., Kerkhoff, E., and Schuh, M. (2011) Spire-type actin nucleators cooperate with Formin-2 to drive asymmetric oocyte division. *Curr. Biol.* **21,** 955–960
14. Dahlgaard, K., Raposo, A. A., Niccoli, T., and St Johnston, D. (2007) Capu and Spire assemble a cytoplasmic actin mesh that maintains microtubule organization in the *Drosophila* oocyte. *Dev. Cell* **13,** 539–553
15. Schuh, M. (2011) An actin-dependent mechanism for long-range vesicle transport. *Nat. Cell Biol.* **13,** 1431–1436
16. Ducka, A. M., Joel, P., Popowicz, G. M., Trybus, K. M., Schleicher, M., Noegel, A. A., Huber, R., Holak, T. A., and Sitar, T. (2010) Structures of actin-bound Wiskott-Aldrich syndrome protein homology 2 (WH2) domains of Spire and the implication for filament nucleation. *Proc. Natl. Acad. Sci. U.S.A.* **107,** 11757–11762
17. Chereau, D., Kerff, F., Graceffa, P., Grabarek, Z., Langsetmo, K., and Dominguez, R. (2005) Actin-bound structures of Wiskott-Aldrich syndrome protein (WASP)-homology domain 2 and the implications for filament assembly. *Proc. Natl. Acad. Sci. U.S.A.* **102,** 16644–16649
18. Rebowski, G., Namgoong, S., Boczkowska, M., Leavis, P. C., Navaza, J., and Dominguez, R. (2010) Structure of a longitudinal actin dimer assembled by tandem W domains. Implications for actin filament nucleation. *J. Mol. Biol.* **403,** 11–23
19. Ha, T., Rasnik, I., Cheng, W., Babcock, H. P., Gauss, G. H., Lohman, T. M., and Chu, S. (2002) Initiation and re-initiation of DNA unwinding by the *Escherichia coli* Rep helicase. *Nature* **419,** 638–641
20. Pavlov, D., Muhlrad, A., Cooper, J., Wear, M., and Reisler, E. (2007) Actin filament severing by cofilin. *J. Mol. Biol.* **365,** 1350–1358
21. Chan, A. Y., Bailly, M., Zebda, N., Segall, J. E., and Condeelis, J. S. (2000) Role of cofilin in epidermal growth factor-stimulated actin polymerization and lamellipod protrusion. *J. Cell Biol.* **148,** 531–542
22. Bobkov, A. A., Muhlrad, A., Kokabi, K., Vorobiev, S., Almo, S. C., and Reisler, E. (2002) Structural effects of cofilin on longitudinal contacts in F-actin. *J. Mol. Biol.* **323,** 739–750
23. Bobkov, A. A., Muhlrad, A., Shvetsov, A., Benchaar, S., Scoville, D., Almo, S. C., and Reisler, E. (2004) Cofilin (ADF) affects lateral contacts in F-actin. *J. Mol. Biol.* **337,** 93–104
24. Khaitlina, S. Y., Moraczewska, J., and Strzelecka-Gołaszewska, H. (1993) The actin/actin interactions involving the N-terminus of the DNase-I-binding loop are crucial for stabilization of the actin filament. *Eur. J. Biochem.* **218,** 911–920
25. Quinlan, M. E., Hilgert, S., Bedrossian, A., Mullins, R. D., and Kerkhoff, E. (2007) Regulatory interactions between two actin nucleators, Spire and Cappuccino. *J. Cell Biol.* **179,** 117–128
26. Ito, T., Narita, A., Hirayama, T., Taki, M., Iyoshi, S., Yamamoto, Y., Maéda, Y., and Oda, T. (2011) Human spire interacts with the barbed end of the actin filament. *J. Mol. Biol.* **408,** 18–25
27. Sitar, T., Gallinger, J., Ducka, A. M., Ikonen, T. P., Wohlhoefler, M., Schmoller, K. M., Bausch, A. R., Joel, P., Trybus, K. M., Noegel, A. A., Schleicher, M., Huber, R., and Holak, T. A. (2011) Molecular architecture of the Spire-actin nucleus and its implication for actin filament assembly. *Proc. Natl. Acad. Sci. U.S.A.* **108,** 19575–19580
28. Vizcarra, C. L., Kreutz, B., Rodal, A. A., Toms, A. V., Lu, J., Zheng, W., Quinlan, M. E., and Eck, M. J. (2011) Structure and function of the interacting domains of Spire and Fmn-family formins. *Proc. Natl. Acad. Sci. U.S.A.* **108,** 11884–11889
29. Namgoong, S., Boczkowska, M., Glista, M. J., Winkelman, J. D., Rebowski, G., Kovar, D. R., and Dominguez, R. (2011) Mechanism of actin filament nucleation by *Vibrio* VopL and implications for tandem W domain nucleation. *Nat. Struct. Mol. Biol.* **18,** 1060–1067
30. Yu, B., Cheng, H. C., Brautigam, C. A., Tomchick, D. R., and Rosen, M. K. (2011) Mechanism of actin filament nucleation by the bacterial effector VopL. *Nat. Struct. Mol. Biol.* **18,** 1068–1074

SUPPLEMENTARY INFORMATION TO:

Multiple forms of Spire-actin complexes and their functional consequences

Christine K. Chen[1], Michael R. Sawaya[1], Martin L. Phillips[1], Emil Reisler[1,2], Margot E. Quinlan[1,2,*]

[1]Department of Chemistry and Biochemistry, University of California Los Angeles, CA 90095
[2]Molecular Biology Institute, UCLA, CA 90095

SUPPLEMENTARY METHODS

Reagents - Pyrene-maleimide and Cy3b-maleimide were obtained from Molecular Probes (Eugene, OR). PEG-biotin and mPEG were purchased from Laysan Bio (Arab, AL). Neutravidin was obtained from Pierce (Rockford, IL). Biotin-maleimide and Latrunculin A (LatA) were purchased from Sigma (St. Louis, MO). Methanesulfonate (MTS) reagents were obtained from Toronto Research. Millipore-filtered water and analytical-grade reagents were used in all experiments.

Protein purification - α-actin was purified from acetone powder of rabbit skeletal muscle as described previously (1). Yeast (*S. cerevisiae*) cofilin, wild type yeast actin and actin mutants Q41C and S265C were purified as described (2).

Recombinant Dm Spir constructs (Spir-ABCD and Spir-CD) in pGEX-6P-2 were expressed and purified as described (3). Protein concentrations were determined by quantitative gels with SYPRO Red (Molecular Probes) as the stain and rabbit skeletal actin as the standard.

Protein Labeling - Both skeletal and yeast actin were labeled with pyrene-maleimide as described (4). Skeletal muscle actin was labeled with Cy3b-maleimide and biotin-maleimide using a similar approach. DTT was first removed from actin using PD-10 columns (GE Healthcare) pre-equilibrated with G-buffer (5 mM Tris, pH 8.0, 0.2 mM $CaCl_2$, and 0.2 mM ATP). Actin was polymerized with 2 mM $MgCl_2$ and 50 mM KCl for 30 minutes at room temperature, before adding 1.5-fold molar excess of Cy3b dye or 10-fold molar excess of biotin-maleimide. Reactions were incubated on ice for at least one hour. Actin was pelleted in an OPTIMA-TLX120 ultracentrifuge at 300,000 × g for 30 minutes, at 4°C. The actin pellet was resuspended in G-buffer with 1 mM DTT, and depolymerized for 2 days before spinning and characterizing actin. Percentage labeling of actin was calculated from the extinction coefficient for Cy3b ε_{561} = 130,000 $M^{-1}cm^{-1}$.

Crosslinking reactions were conducted as previously described, with some modifications (2). DTT was removed from yeast actin mutants with PD-10 columns equilibrated with 10 mM Tris pH 8.0, 0.2 mM ATP, and 0.2 mM $CaCl_2$. DTT was removed from Spir-ABCD and Spir-CD by dialysis into the same buffer. Actin was either converted to Mg-actin with ME buffer (50 μM $MgCl_2$ and 0.2 mM EGTA) or polymerized with 50 mM KCl and 2 mM $MgCl_2$ prior to incubation with Spir. Actin and Spir were combined at stoichiometric ratios. Reactions with MTS reagents were carried out for 1 minute before stopping them with 10 mM NEM.

Fluorescence Measurements - All pyrene-actin depolymerization assays were performed at 20°C, using 5 μM actin (2.5% labeled) in KMEH (50 mM KCl, 1 mM $MgCl_2$, 1 mM EGTA, 10 mM Hepes, pH 7.0) + 0.2 mM ATP unless otherwise noted. Ca-actin was converted to Mg-actin with ME buffer prior to polymerization. Fluorescence was excited at 365 nm and detected at 405 nm using an Alphascan fluorimeter (Photon Technology International).

Barbed-end concentrations were calculated as previously described (5) using the following equation: [barbed-end] = elongation rate / (k_+[G-actin]-k_-) where k_+ = 11.6 $\mu M^{-1}s^{-1}$ and k_- = 1.4 s^{-1}.

Pyrene excimer fluorescence was monitored at 20°C in G-buffer containing 100% labeled pyrene-yeast actin mutants. Fluorescence was excited at 344 nm and emission detected from 400 nm to 600 nm with a maximum emission at 475 nm. Four emission scans were averaged for each run. Excimer emission was measured with 5 μM G-actin in the presence of stoichiometric concentrations of Spir. 2 mM $MgCl_2$ and 50

mM KCl were added to the same cuvette and incubated for 15 minutes before measuring maximum emission under F-actin conditions.

Electron Microscopy - For actin filament visualization, all samples were diluted to 2 μM in F buffer and deposited on 400-mesh carbon-coated copper grids coated with formvar film (Ted Pella Inc., CA). Samples were allowed to adsorb for 60 seconds and then negatively stained with 1% uranyl acetate (w/v) for 45 seconds. Grids were observed with a JEM-1200EX (JEOL) electron microscope operated at 80 kV and magnification in the 80,000-100,000× range. The images were analyzed using IMAGE J software.

Total Internal Reflection Fluorescence Microscopy - Direct visualization of filaments was performed as previously described, with some modifications (6,7). Clean coverslips were functionalized with mPEG-biotin after silanization. Experiments were performed in flow cells with double-sided tape as spacers between functionalized coverslips and clean slides. All proteins were diluted in TIRF buffer: 50 mM KCl, 1 mM $MgCl_2$, 1 mM EGTA, 10 mM Hepes (pH 7.0), 0.2 mM ATP, 100 mM DTT, 15 mM glucose, 20 μg/mL catalase, and 100 μg/mL glucose oxidase. For immobilization of filaments, neutravidin was incubated in flow cells for one minute at a final concentration of 0.25 mg/mL prior to the addition of labeled actin. Either a G-actin mixture or F-actin was labeled with 20% Cy3b-maleimide and 1% biotin-maleimide unless otherwise noted. Concentrations are reported as the concentration of Spir or actin protein in the sample tube before adding it to the flow chamber. Samples were excited by total internal reflection illumination at 565 nm and images were captured with an Andor CCD camera controlled by Leica software on a Leica DMI6000 TIRF microscope (Buffalo Grove, IL). Images were analyzed and enhanced using Fiji software.

Polarity marked filaments were made by first creating AlexaFluor488-phalloidin stabilized actin seeds. Seeds were generated by polymerizing 5 μM actin labeled with 1% biotin in F buffer and adding AlexaFluor488-phalloidin at a 1:1 ratio. Phalloidin-stabilized filaments were sheared with a fine gel tip and then diluted to 5 nM before addition to the flow cell. After washing with TIRF buffer, a 250 nM G-actin mixture was added and allowed to incubate for 15 minutes until filaments grew to approximately 5 μm.

Analytical Ultracentrifugation - For sedimentation velocity, 400 μl samples were loaded into 12 mm double sector cells at 20 °C. Absorbance scans were obtained at 290 nm. Scans were initially collected at an intermediate speed of 22,000 rpm, for 40 to 50 minutes at 5 minute time intervals, to detect larger polymers. The speed was then increased to 55,000 rpm and scans were collected at 4 minute intervals to determine the sedimentation coefficients of smaller species. Sedimentation coefficients were obtained from the peaks of g(s) plots of sedimentation coefficient distribution, determined using the Beckman Origin-based software (Version 3.01). Partial specific volumes for the complexes were calculated as the weight average partial specific volumes, using partial specific volumes of the individual proteins and their assumed stoichiometries. Partial specific volumes of the individual proteins were calculated from their amino acid compositions and corrected to 20°C (8,9). Theoretical sedimentation coefficients were calculated using 3.25 for the sedimentation coefficient of G-actin and the following equation:

$$s_1 = s_2\left(\frac{\eta_1}{\eta_2}\right)\left(\frac{M_1}{M_2}\right)^{\frac{2}{3}}\left(\frac{1-\nu_1\rho_1}{1-\nu_2\rho_2}\right)\left(\frac{\nu_2}{\nu_1}\right)^{\frac{1}{3}}\left(\frac{1+\left(\frac{\delta_2}{\nu_2\rho_2}\right)}{1+\left(\frac{\delta_1}{\nu_1\rho_1}\right)}\right)^{\frac{1}{3}}\left(\frac{f_2}{f_1}\right)$$

where s_1 is the sedimentation coefficient of the complex, s_2 is the sedimentation coefficient of G-actin and M, ν, η , ρ, δ and *f* are the respective molecular weights, partial specific volumes, solution viscosities, solution densities, hydrations and Perrin factors. G-actin was assumed to be globular with a Perrin factor of 1, while the Perrin factors of the complexes were calculated for prolate ellipsoids with axial ratios of 2:1 for a dimer, 4:1 for a tetramer, and so forth (10).

Crystallization and Structure Determination - ECP-cleaved skeletal actin was prepared by incubating ECP32/grimelysin with actin at a 6:1 molar ratio. Cleaved actin was mixed with Spir-CD at a 1:1 molar

ratio. The protein mixture was crystallized using the hanging drop method with the drop consisting of 1 μL of protein (3 mg/mL) and 1 μL of reservoir solution (Tris pH 8.5, $MgCl_2$, PEG-8000). The crystals belonged to space group C2 with one actin monomer and one Spir CD molecule in the asymmetric unit. An x-ray diffraction data set was collected on a native crystal at the Advanced Light Source (Lawrence Berkeley National Laboratory), beamline 8.2.1, using an ADSC Quantum 315 CCD detector. Crystals were cryo-protected by a quick dip in a mixture containing 65% reservoir and 35% 2-methyl-2,4-pentanediol. Crystals were cryo-cooled to 100 K during the data collection. One hundred-forty-nine 1.0° oscillation frames were collected at a wavelength of 1.000 Å. Data reduction and scaling were performed using DENZO/SCALEPACK (11). Diffraction to 2.8 Å resolution was observed.

The crystal structure was determined by molecular replacement using the program PHASER (12), with rabbit actin (Protein Data Bank ID code 2A5X; (13)) serving as the search model, and subsequently refined using REFMAC5 (14) and Buster/TNT (15) with TLS parameterization of domain disorder (16). After each refinement step, the model was visually inspected in COOT (17), using both 2Fo-Fc and Fo-Fc difference maps. The model was validated with the following structure validation tools: PROCHECK (18), ERRAT (19), and VERIFY3D (20). All of the residues are within the most favoured and additional allowed regions of the Ramachandran plot. The Errat score, 98.1%, indicates that this percentage of residues fall below the 95% confidence limit of being erroneously modeled.

Data collection and refinement statistics are reported in Table S1. The coordinates of the final model and the merged structure factors have been deposited in the Protein Data Bank with PDB code 3UE5. The structure was illustrated using Pymol (The PyMOL Molecular Graphics System, Version 1.4, Schrödinger, LLC (http://www.pymol.org)).

SUPPLEMENTARY REFERENCES

1. Spudich, J. A., and Watt, S. (1971) *J Biol Chem* **246**, 4866-4871
2. Grintsevich, E. E., Benchaar, S. A., Warshaviak, D., Boontheung, P., Halgand, F., Whitelegge, J. P., Faull, K. F., Loo, R. R., Sept, D., Loo, J. A., and Reisler, E. (2008) *J Mol Biol* **377**, 395-409
3. Quinlan, M. E., Heuser, J. E., Kerkhoff, E., and Mullins, R. D. (2005) *Nature* **433**, 382-388
4. Kim, E., Wriggers, W., Phillips, M., Kokabi, K., Rubenstein, P. A., and Reisler, E. (2000) *J Mol Biol* **299**, 421-429
5. Pollard, T. D. (1986) *J Cell Biol* **103**, 2747-2754
6. Ha, T., Rasnik, I., Cheng, W., Babcock, H. P., Gauss, G. H., Lohman, T. M., and Chu, S. (2002) *Nature* **419**, 638-641
7. Pavlov, D., Muhlrad, A., Cooper, J., Wear, M., and Reisler, E. (2007) *J Mol Biol* **365**, 1350-1358
8. Cohn, E. J. a. E., J.T. (1943) Density and apparent specific volume of proteins. in *Proteins, Amino Acids and Peptides as Ions and Dipolar Ions* (Cohn, E. J. a. E., J.T. ed.), Reinhold Publishing Corporation, New York. pp 370-381
9. Laue, T. M., Shah, B.D., Ridgeway, T.M., and Pelletier, S.L. (1992) Computer-Aided Interpretation of Analytical Sedimentation Data for Proteins. in *Analytical Ultracentrifugation in Biochemistry and Polymer Science* (S.E. Harding, A. J. R. a. J. C. H. ed.), The Royal Society of Chemistry, Cambridge, Great Britain. pp 90-125
10. Perrin, F. (1934) *J. Phys. Rad. Ser. VII* **5**, 497-511
11. Otwinowski, Z. a. M., W. (1997) *Methods in Enzymology: Mcromolecular Crystallography, part A* **276**, 307-326
12. McCoy, A. J., Grosse-Kunstleve, R. W., Adams, P. D., Winn, M. D., Storoni, L. C., and Read, R. J. (2007) *J Appl Crystallogr* **40**, 658-674
13. Kudryashov, D. S., Sawaya, M. R., Adisetiyo, H., Norcross, T., Hegyi, G., Reisler, E., and Yeates, T. O. (2005) *Proc Natl Acad Sci U S A* **102**, 13105-13110
14. Murshudov, G. N., Vagin, A. A., and Dodson, E. J. (1997) *Acta Crystallogr D Biol Crystallogr* **53**, 240-255

15. Blanc, E., Roversi, P., Vonrhein, C., Flensburg, C., Lea, S. M., and Bricogne, G. (2004) *Acta Crystallogr D Biol Crystallogr* **60**, 2210-2221
16. Winn, M. D., Murshudov, G. N., and Papiz, M. Z. (2003) *Methods Enzymol* **374**, 300-321
17. Emsley, P., Lohkamp, B., Scott, W. G., and Cowtan, K. (2010) *Acta Crystallogr D Biol Crystallogr* **66**, 486-501
18. Laskowski, R. A., MacArthur, M.W., Moss, D.S., and Thornton, J.M. (1993) *Journal of Applied Crystallography* **26**, 283-291
19. Colovos, C., and Yeates, T. O. (1993) *Protein Sci* **2**, 1511-1519
20. Luthy, R., Bowie, J. U., and Eisenberg, D. (1992) *Nature* **356**, 83-85

SUPPLEMENTARY FIGURE LEGENDS

Figure S1. Actin filament depolymerization by Spir-CD is dose-dependent. A) Experimental conditions are the same as in Figure 1b except for using Spir-CD instead of Spir-ABCD. LatA was used for comparison of depolymerization rates to that by a known sequestering agent. Note the oscillation upon addition of 2.5 μM Spir-CD to F-actin. B) Light scattering of 10 μM F-actin in the presence of Spir-CD reveals traces similar to the pyrene assays at the same stoichiometric concentrations.

Figure S2. Spir severs and depolymerizes from the barbed end of F-actin. A) A representative EM image showing severed actin filaments (indicated by arrows). After adsorption to EM grids, filaments were exposed to Spir-CD for 3 minutes. B) Experiment identical to that shown in Figure 3a except for the presence of Spir-CD in lieu of Spir-ABCD. Concentrations used were 250 nM F-actin and 150 nM Spir-CD. C) Depolymerization rates were measured for filaments in the presence of Spir-ABCD (n=20). Five typical traces for barbed (lower traces) and pointed end (upper traces) shortening as well as average rates (thick lines with standard deviations for each time point) are shown. Linear fits to the average shortening traces were used to estimate depolymerization rates. D) Experiment like that in Figure 3c except in the presence of 150 nM Spir-ABCD. Growth of filaments can be seen off the barbed end, which is the end that depolymerizes rapidly.

Figure S3. Actin monomer inhibits Spir severing activity. Spir-ABCD was added to F-actin and filaments were observed for three minutes. +monomers indicates that Spir was pre-incubated with a stoichiometric concentration of G-actin prior to addition to F-actin. Typical fields before and after Spir addition are shown. Only four filaments were severed in the +monomers field. The rate of filament severing is $0.05 \pm 0.11 \times 10^{-2}$ cuts/μm/sec, n = 74. Conditions: 100 nM Spir-ABCD +/- 400 nM G-actin added to 250 nM F-actin in TIRF buffer.

Figure S4. Results from sedimentation velocity experiments with actin and Spir-ABCD. The peak s values are smaller than expected for an SA_4 complex. The asymmetry in the peaks is evidence of multiple species. A) G-actin and Spir-ABCD were mixed at stoichiometric ratios before centrifugation. B) G-actin and Spir-ABCD were mixed with 2 mM $MgCl_2$ and 50 mM KCl and incubated for one hour at RT prior to centrifugation.

Table S1 Data collection and refinement statistics

	ECP Actin-Spir
Data collection	
Space group	C2
Cell dimensions	
a, *b*, *c* (Å)	84.8, 53.6, 100.6
a, *b*, *g* (°)	90.0, 92.7, 90.0
Resolution (Å)	2.8 (2.9-2.8)
R_{sym}	0.105 (0.237)
I/sI	9.2 (2.4)
Completeness (%)	89.6 (55.4)
Redundancy	2.7 (2.0)
Refinement	
Resolution (Å)	2.8
No. reflections	10358
$R_{work/}$ R_{free}	0.197/0.240
No. atoms	
Protein	3040
Ligand/ion	74
Water	40
B-factors (Å^2)	
Protein	48.6
Ligand/ion	35.7
R.m.s deviations	
Bond lengths (Å)	0.009
Bond angles (º)	1.1

*Highest resolution shell is shown in parenthesis.

Figure S1 Chen et al.

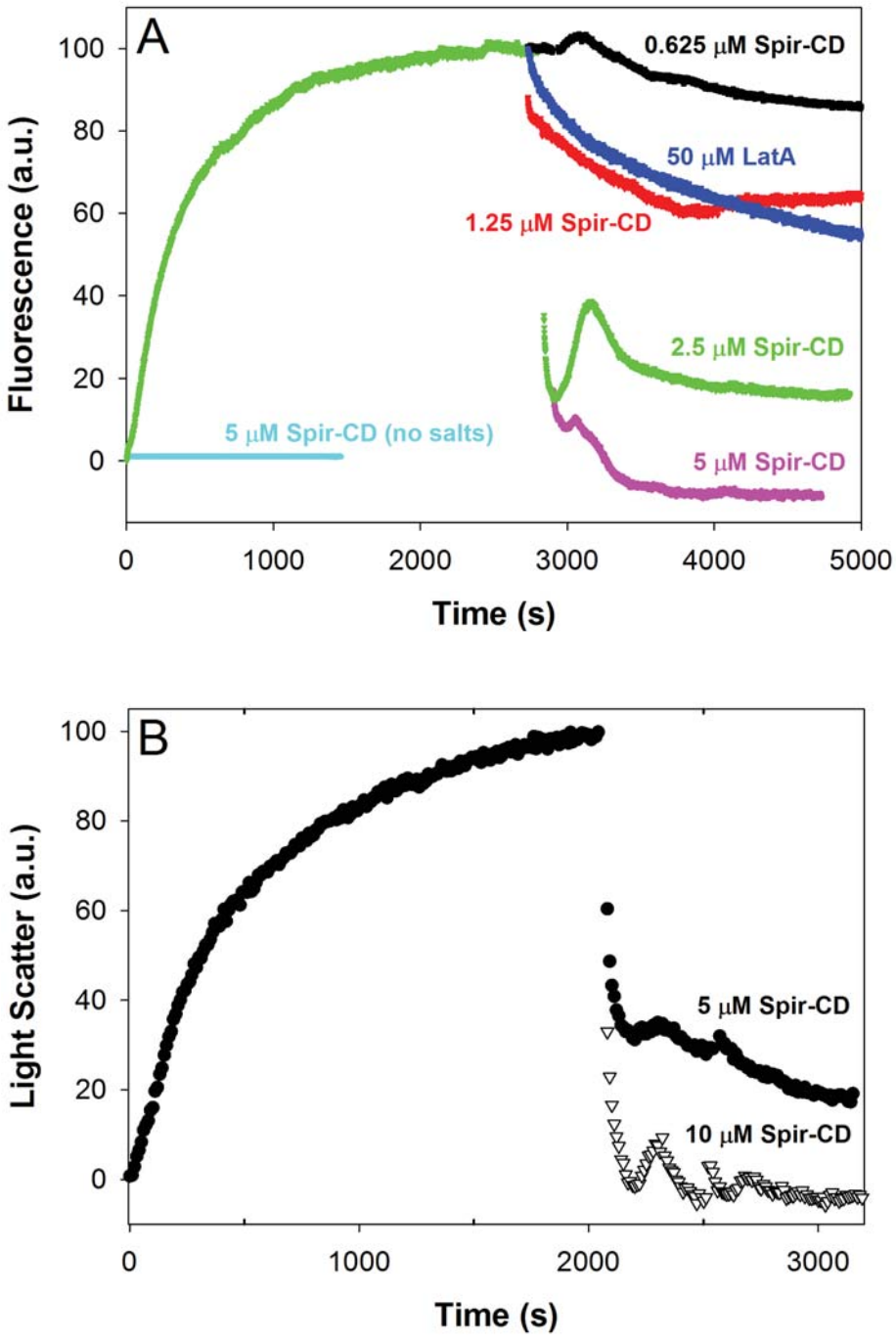

Figure S2 Chen et al.

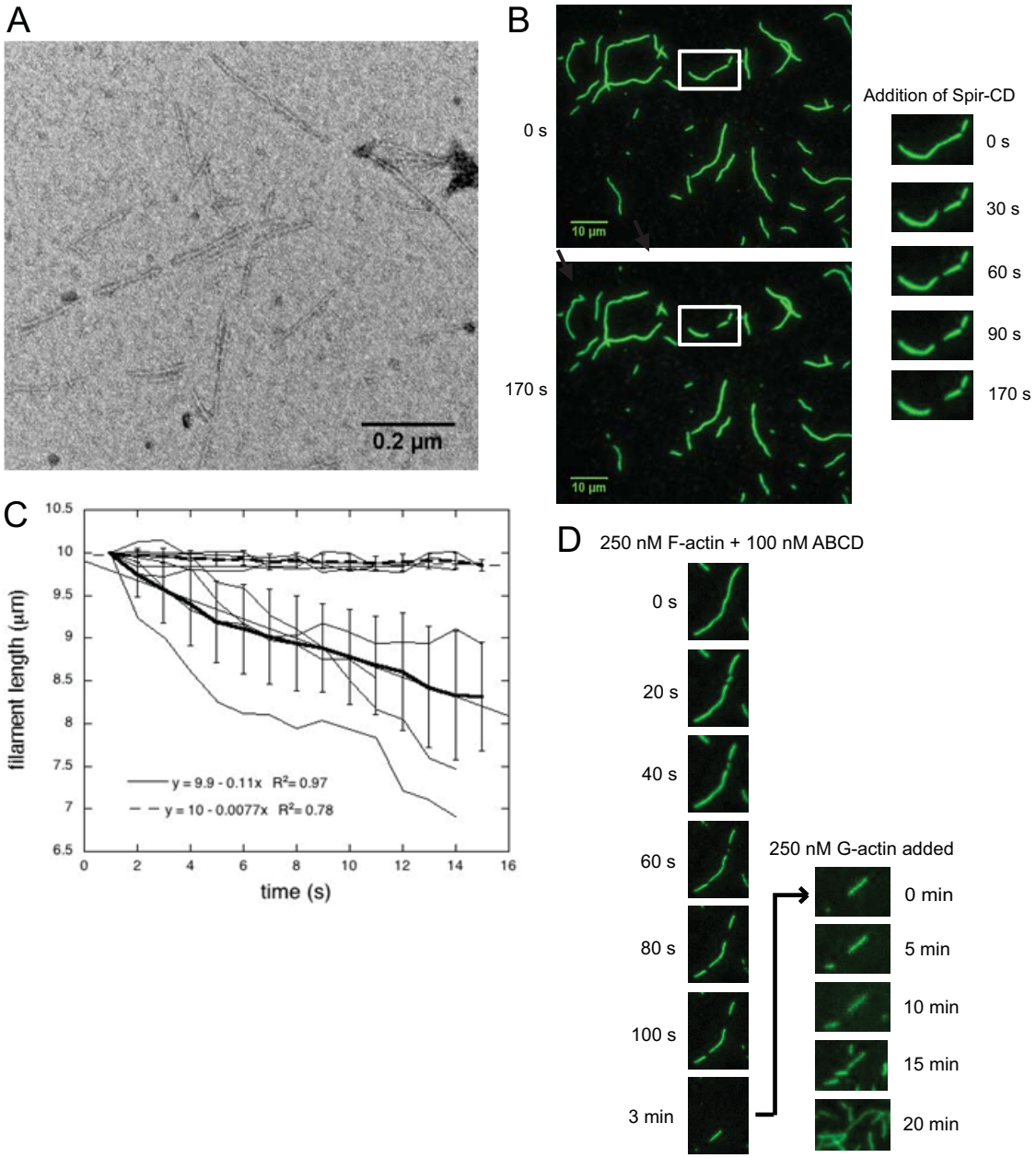

Figure S3 Chen et al.

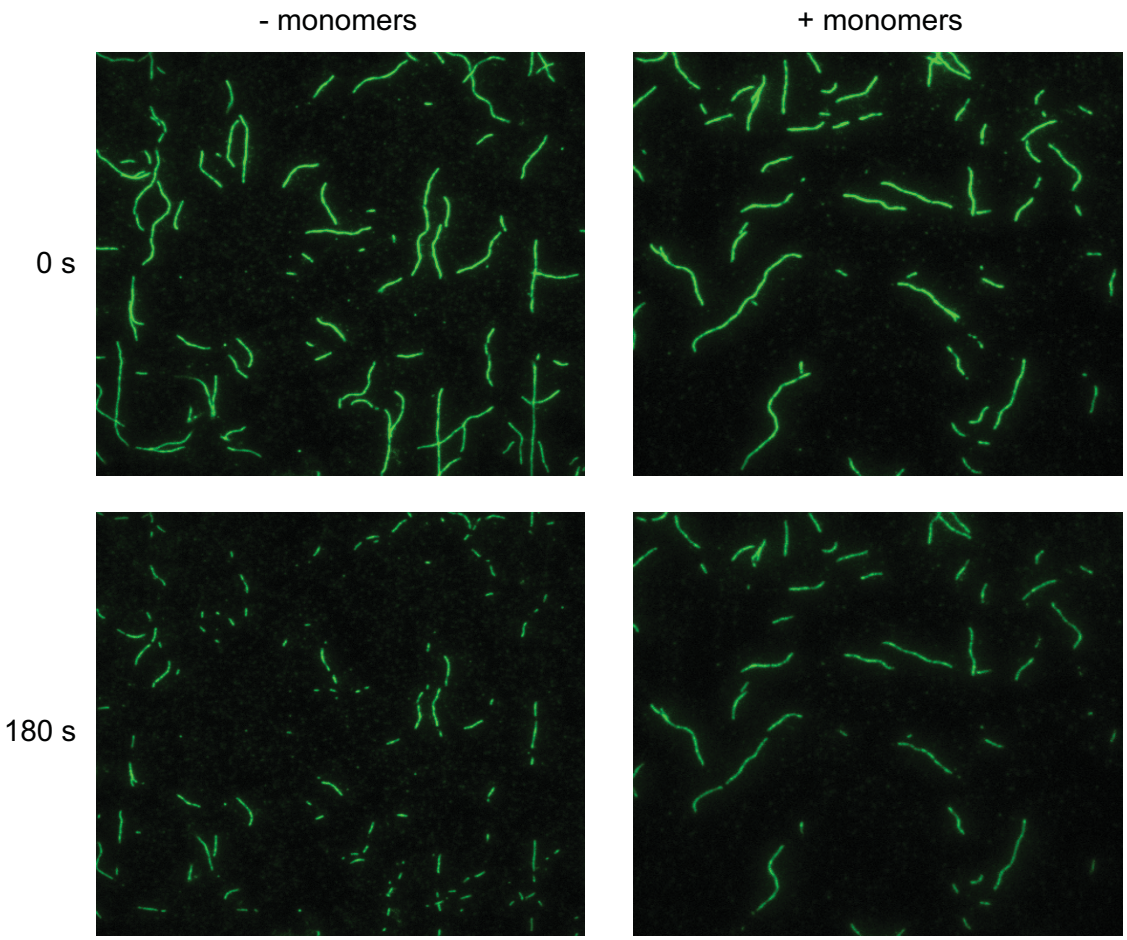

Figure S4 Chen et al.

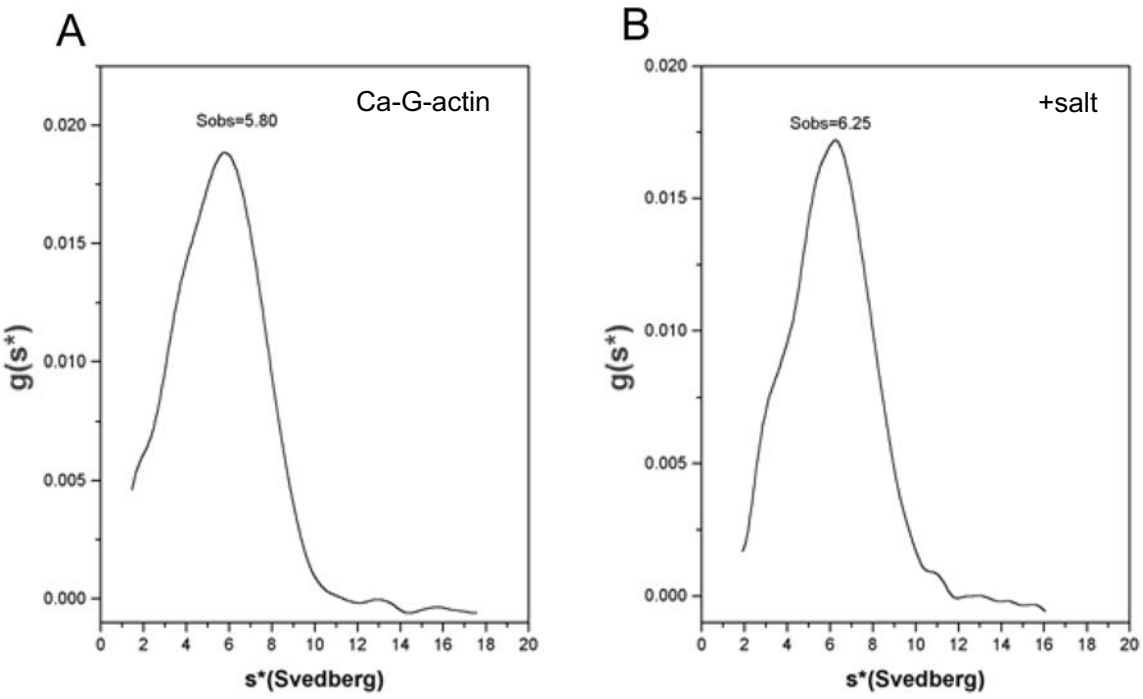

Chapter 3

Additional aspects of the multiple forms of Spir-actin complexes

ABSTRACT

Chapter 2 focuses on understanding how Spire can sever and nucleate actin filaments and sequester actin monomers *in vitro*. Our goal was to determine which functions are physiologically relevant. Chapter 3 is a continuation of this exploration, further characterizing Spire and its many functions. To study the effects of Spire on actin filaments depolymerization, we examined their complexes by analytical ultracentrifugation. We observed multiple species, with two of these corresponding to an actin monomer and tetramer bound to Spire. We also studied actin depolymerization and cross-linking in the presence of Cappuccino, a formin that binds to the KIND domain of Spire. We did not detect additional effects by Cappuccino. We examined the binding of Spire to actin using fluorescently-labeled yeast actin mutants. We propose that the binding occurs in two non-equivalent steps. We solved another crystal structure of the Spire-actin complex which is similar to the structure shown in Chapter 2, but deviates with the placement of another actin in the asymmetric unit. In conclusion, we propose that Spire-actin complexes contain both polymerization nuclei and sequestration structures as previously proposed.

INTRODUCTION

Spire (Spir) belongs to a class of Wasp homology 2 (WH2)-nucleators that nucleates actin filaments through the use of its four actin-monomer-binding WH2 domains (1). Spir was found to sever filaments and sequester monomers in addition to nucleating new filaments (2). It still remains to be determined which of these activities are dominant *in vivo* and/or when the different activities are physiologically relevant. Here, we focus on further characterizing Spir and its many activities *in vitro*.

The four tandem WH2 domains of Spir (Spir-ABCD) show maximal nucleation of actin, equivalent to that by the N-terminal half of Spir (Spir-NT), which contains the cluster of these WH2 domains. The two C-terminal WH2 domains (Spir-CD) are sufficient to nucleate, albeit at a slower rate. Models of the nucleation mechanism vary in details. A common idea is that the closely spaced WH2 domains bind actin monomers in an elongated longitudinal structure, as observed by electron microscopy and detected by analytical ultracentrifugation (1, 2). The alignment of four actin monomers would act as a template for additional monomers. However, the orientation and mobility of adjacent monomers with respect to each other before elongation begins remains unclear. Bosch et al. (2) report that the N-terminal half of human Spir1 (hSpir1) binds four actin monomers into a stable sequestration complex (SA_4). Rebowski et al. (3) crystallized a structure of longitudinal actin dimers bound to artificially tethered N-Wasp WH2 domains. They observed that the actin monomers are rotated ~60° more than adjacent monomers in control F-actin. They interpret this structure as a weak nucleation complex and question the function of Spir as a nucleator. However, the nucleation activity of Spir is sequence specific. The sequence between WH2 domains, especially linker 3 between Spir-C and Spir-D, as well as the specific order of WH2 domains in Spir contribute significantly to the observed nucleation

activity (1,4), making it unclear how relevant this crystal structure is to understanding Spir. Ducka et al. (5) co-crystalized Spir with actin, and resolved only the last WH2 domain (Spir-D) bound to actin, which overlays with our crystal structure in the previous chapter. Important information regarding the other WH2 domains and the linkers (disordered) was missing in their structure. Their model proposes an elongated longitudinal configuration of actin monomers, but the lack of atomic information for the linkers and corresponding WH2 domains leaves to speculation the orientation of actins bound to adjacent WH2 domains. Thus, more work is required to understand how Spir associates with actin monomers and nucleates filaments.

The N-terminus of Spir contains a kinase non-catalytic C-lobe domain (KIND), which binds tightly to the formin homology 2 (FH2) domain of Cappuccino (Capu). In genetic studies of *Drosophila* oogenesis, loss of the actin network by *cappuccino* mutants cannot be rescued by overexpression of Spir, but loss of the network due to *spire* mutants can be partially rescued by expression of Capu (6). Because both proteins exhibit nucleation activity, a question was raised about the function of these proteins with dual roles in the cell. Quinlan et al. (7) showed that the KIND domain competes with microtubules and F-actin for Capu's binding and inhibits its ability to nucleate actin. In contrast, nucleation by Spir is enhanced by binding to the C-terminal half of Capu. Thus, the interaction of the two proteins results in the exclusive use of Capu to boost Spir's nucleation ability.

In order to study nucleation and severing by Spir, we analyzed the effects of *Drosophila melanogaster* (Dm) Spir on actin monomers and filaments. We found by velocity sedimentation that incubation of Dm Spir with actin filaments results in two types of species, corresponding to Spir-bound actin monomers and tetramers. We also tested the effects of Capu and Spir on F-actin and found that Capu has no additional effects on F-actin depolymerization or cross-linking. We

further confirm Spir's sequestration activity in a polymerization assay. Notably, titration of fluorescent actin with Spir shows its bi-modal phase binding to actin. Finally, our crystal structure confirms the positioning of Spir domain D on actin and the disorder of domain C. Together, our data suggest that Spir-actin interactions are more complex than originally believed.

METHODS

Protein purification and labeling

Skeletal actin, yeast actin mutants, Spir constructs, and Capu were purified as previously described (1, 8-10). Acanthamoeba actin was a generous gift from the Quinlan lab. Skeletal actin and yeast actin mutant F169C were labeled with pyrene (Molecular Probes) as previously described (11). Yeast actin mutant A167C was labeled with acrylodan by a similar method. DTT was removed with G-50 beads (Sigma Aldrich) and labeled in G-buffer (5 mM Hepes, pH 7.5, 0.2 mM $CaCl_2$, and 0.2 mM ATP). Excess label was removed with G-50 beads. Extent of labeling was determined with pyrene extinction coefficient ε_{344} = 22,000 $M^{-1}cm^{-1}$ and acrylodan extinction coefficient ε_{391} = 20,000 $M^{-1}cm^{-1}$, respectively.

Analytical Ultracentrifugation

For sedimentation velocity, 400 μl samples were loaded into 12 mm double sector cells at 20 °C. Absorbance scans were obtained at λ = 290 nm. Scans were initially collected at an intermediate speed of 22,000 rpm, for 40 to 50 minutes at 5 minute time intervals, to detect larger polymers. The speed was then increased to 55,000 rpm and scans were collected at 4 minute intervals to determine the sedimentation coefficients of smaller species. Sedimentation coefficients were obtained from the peaks of g(s) plots of sedimentation coefficients distribution, determined using the Beckman Origin-based software (Version 3.01). Partial specific volumes for the complexes were calculated as the weight average partial specific volumes, using partial specific volumes of the individual proteins and their assumed stoichiometries. Partial specific

volumes of the individual proteins were calculated from their amino acid compositions and corrected to 20°C (12, 13).

Fluorescence experiments

All pyrene-actin polymerization and depolymerization assays were performed at 20°C, using 5 µM actin (2.5% labeled) in KMEH (50 mM KCl, 1 mM $MgCl_2$, 1 mM EGTA, 10 mM Hepes, pH 7.0) + 0.2 mM ATP, unless otherwise noted. Ca-actin was converted to Mg-actin with ME buffer (50 µM $MgCl_2$, 0.2 mM EGTA) prior to its polymerization. Pyrene-actin was excited at λ = 365 nm and detected at λ = 405 nm using an Alphascan fluorimeter (Photon Technology International).

To test binding of Spir to acrylodan and pyrene-labeled actins, both labeled actins were first converted to Mg-actin by adding 0.1 mM $MgCl_2$ and 0.2 mM EGTA. ATP-actin was converted to ADP-actin by adding 0.5 mM ATP, 1 mM glucose, and 3 units/mL of hexokinase. Excitation was set to λ = 344 nm and detected at λ = 377 nm for acrylodan-actin. Pyrene-actin fluorescence was measured as above.

Cross-linking experiment

Cross-linking reactions with yeast actin mutant S265C were carried out with N,N'-p-phenylenedimaleimide (PPDM). 6 uM actin was incubated in G-buffer with either 3 uM CD, 1.5 uM ABCD, 1.5 uM NT-Spir, or 1.5 uM NT-Spir and 0.75 uM Capu for 15 minutes. Actin was then polymerized in the presence of 2 mM $MgCl_2$ and 50 mM KCl. pPDM was added in 1.5X molar excess to actin. Reaction time-points were taken at 30 seconds and 30 minutes. Reactions were stopped with 10 mM DTT and the products were visualized by SDS-PAGE.

Crystal Structure Determination

Acanthamoeba actin was mixed with Spir-CD at a 2:1 molar ratio. The protein mixture was crystallized using the hanging drop method with a drop consisting of equal parts of protein (~3 mg/mL) and reservoir solution (0.2 M NaSCN, 20% PEG3350, 0.1 M $MgCl_2$, 5 mM DTT). The crystals belonged to space group $P2_12_12_1$ with one actin monomer and one Spir-CD molecule in the asymmetric unit. An x-ray diffraction data set was collected at the Advanced Photon Source (Argonne National Laboratory), beamline 24-ID-C, using an ADSC Quantum 315 CCD detector. Crystals were cryo-protected by a quick dip in a mixture containing 65% reservoir solution and 35% 2-methyl-2,4-pentanediol. Crystals were cryo-cooled to 100 K during the data collection. One hundred-fifteen 1.0° oscillation frames were collected at a wavelength of 0.9793 Å. Data reduction and scaling were performed using DENZO/SCALEPACK (14). Diffraction to 2.8 Å resolution was observed.

The crystal structure was determined by molecular replacement using the program PHASER (15), with rabbit actin (Protein Data Bank ID code 2A5X; 16) serving as the search model, and subsequently refined using REFMAC5 (17) and Buster/TNT (18) with TLS parameterization of domain disorder (19). After each refinement step, the model was visually inspected in COOT (20), using both 2Fo-Fc and Fo-Fc difference maps. The model was validated with the following structure validation tools: PROCHECK (21), ERRAT (22), and VERIFY3D (23). All of the residues are within the most favoured or additional allowed regions of the Ramachandran plot. The Errat score, 97.3%, indicates that this percentage of residues fall below than 95% confidence limit of being erroneously modeled. Data collection and refinement statistics are reported in Table 1. The coordinates of the final model and the merged structure

factors have been deposited in the Protein Data Bank with PDB code 4EFH. The structure was illustrated using Pymol (24).

RESULTS

We showed in the previous chapter that Spir forms a heterogeneous mixture of actin complexes when incubated at stoichiometric concentrations (which refers to the full occupancy of each WH2 domain by actin). For example, 1 mol of Spir-CD would be incubated with 2 mol of actin and 1 mol of Spir-ABCD would be incubated with 4 mol of actin. In addition to analyzing the different species formed upon incubation of Spir with G-actin at stoichiometric concentrations, we examined by analytical ultracentrifugation the species present after Spir was added to F-actin. Previous results in pyrene fluorescence assays showed that Spir was able to depolymerize F-actin (Chapter 2, Figure 1). When added at stoichiometric ratios, Spir appears to cause ~80% depolymerization of actin. When we analyzed such solutions by EM, we saw very few filaments and mostly depolymerized actin, matching the fluorescence data. With sedimentation velocity, we observed coefficients of 3.4 S and 7.4 S (Figure 1a). According to Table 1 in Chapter 2, these numbers correspond to the hypothetical values for one actin bound to Spir-CD and 4 actins bound to Spir-CD. Spir-CD was not shown to dimerize on its own, but these results suggest the presence of dimeric species in solutions of depolymerized F-actin. Asymmetry of both peaks in the g(s) plots indicates a heterogeneous mixture of species, either varying in shape (or orientation), or in the number of actin monomers bound. The lower molecular weight species comprise ~60% of the total (Figure 1b). The amount of higher oligomeric species in the low speed analytical ultracentrifugation run was negligible (not shown), but these could be detectable in the pyrene fluorescence assay and by EM.

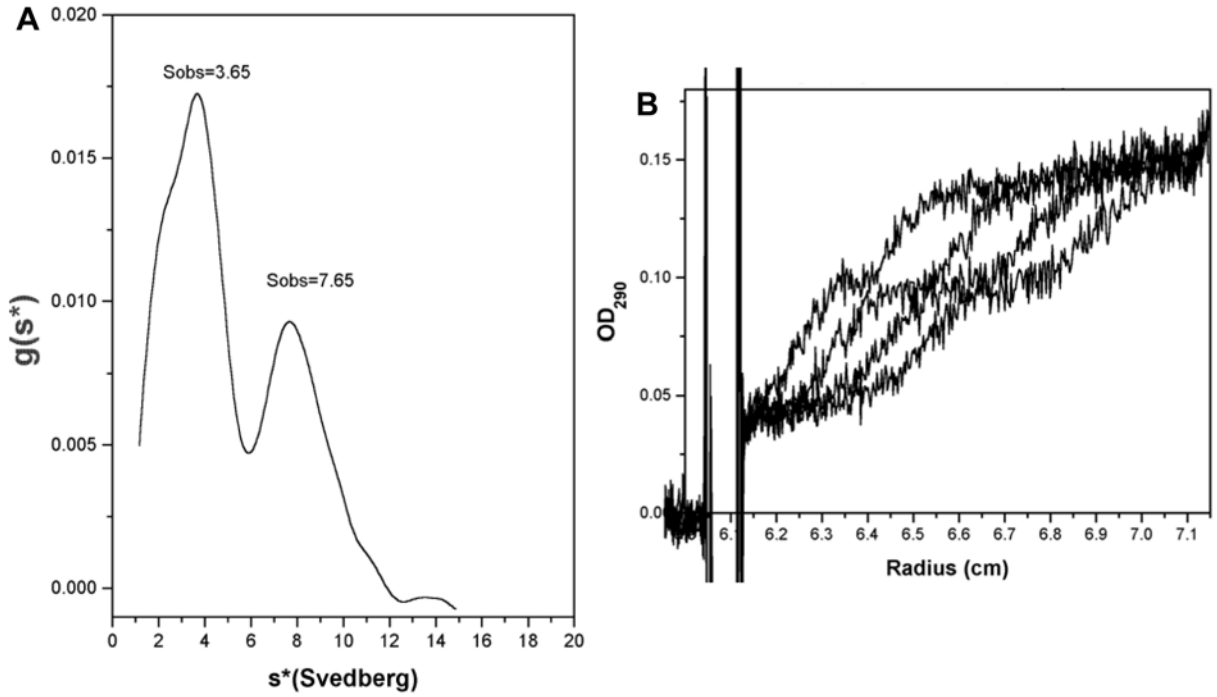

Figure 1. Spir-actin complexes detected after Spir induced depolymerization of F-actin. A. Spir-CD was added to F-actin at stoichiometric ratios before ultracentrifugation. Two sedimentation coefficient (s) peaks were observed, corresponding to Spir-bound actin and Spir-bound actin tetramer. Asymmetry of these peaks is indicative of the heterogeneity of Spir-actin complexes. B. 20-minute scans taken before derivatization at 55,000 rpm. The amount of lower molecular weight species (~60% of the total) is greater than the amount of higher molecular weight species.

Capu does not enhance Spir-induced depolymerization or cross-linking

Although Spir can act independently on F-actin, the question remains whether it can be shown to function synergistically with Capu *in vitro*. We combined Capu with NT-Spir at a 1:2 ratio and added the complex at the same Spir:actin ratio in a pyrene depolymerization assay (Figure 2a). The two pyrene fluorescence traces overlap, suggesting that Capu - when combined with Spir - has no effect on depolymerization. Because Capu was shown to aid in actin dimerization upon binding to the KIND domain of NT-Spir, we also tested Capu's effect on lateral dimer cross-linking in yeast actin mutant S265C (Figure 2b). Time points taken at 30 sec and 30 minutes show no difference in the band density at ~84 kDa, suggesting that Capu does not enhance the effect of Spir on lateral dimer cross-linking. Other bands present on the gel suggest Capu's cross-linking to NT-Spir.

Spir-actin complexes exhibit multifunctionality upon polymerization

We previously showed that Spir-actin seeds are able to nucleate actin filaments at low stoichiometric ratios decreasing the lag phase in nucleation assays better than Spir alone (Chapter 2, Figure 4). We then tested if Spir-actin seeds can polyemerize on their own and if they nucleate filaments, as more G-actin is added (Figure 3). The Spir-actin seeds started to form filaments, as indicated by pyrene fluorescence increase (to ~30% fluorescence of fully polymerized filaments). After a short delay the fluorescence decreased, plateauing at ~15% fluorescence of polymerized actin. This oscillation is similar to the oscillation seen with Cordon-Bleu (25). Husson et al. proposed that the oscillation was due to a combination of effects: nucleation, severing, and depolymerization occurring in sequential order. At each actin

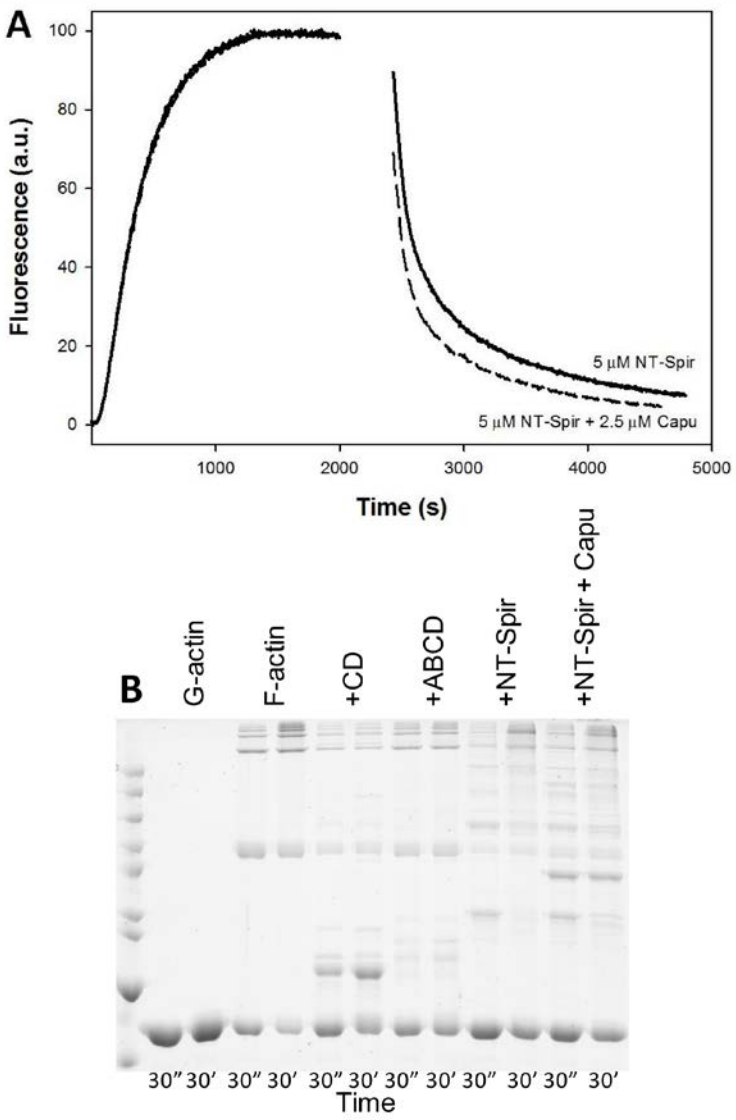

Figure 2. Capu has no effect on Spir induced depolymerization and cross-linking of actin. A. NT-Spir added at a 1:1 mole ratio to actin depolymerizes completely F-actin. The Spir-Capu complex did not show significantly different effect on depolymeriztion of F-actin when added at the same mole ratio as Spir alone. B. Cross-linking of yeast actin mutant S265C by PPDM is not enhanced by the addition of Capu. Time-points were taken at 30 seconds and 30 minutes. Spir was added to actin at stoichiometric ratios.

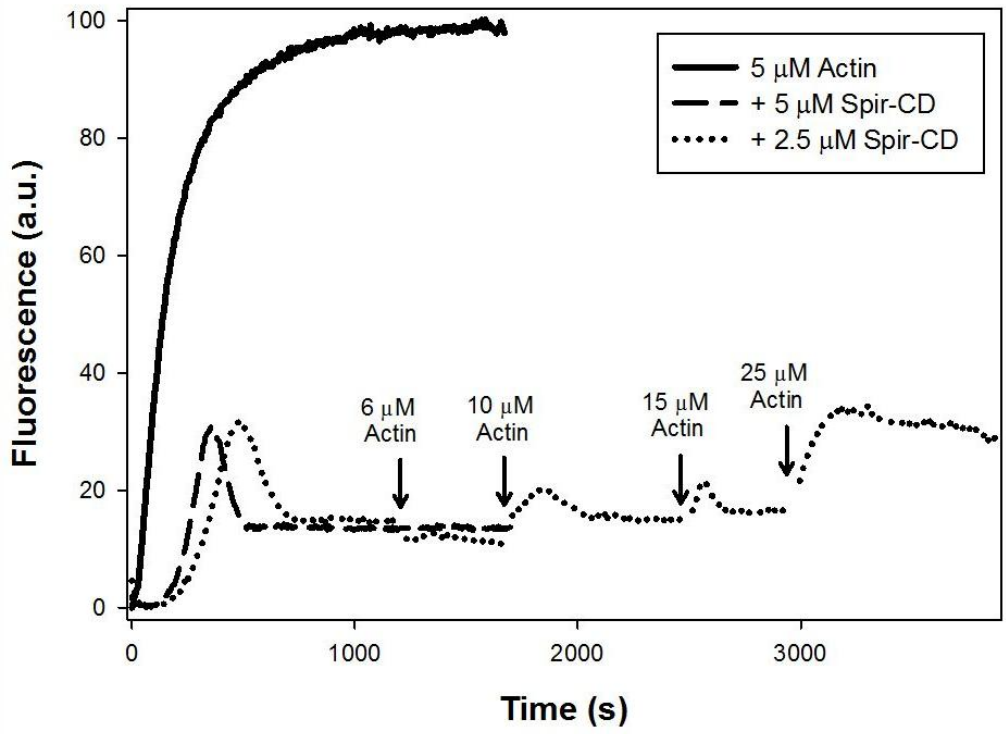

Figure 3. Spir-actin seeds do not polymerize. Spir-CD was added to G-actin (5 μM) at 1:1 and 1:2 mole ratios and then polymerized with 1X KMEH. Aliquots of actin were then added to the complex to final actin concentrations of 6, 10, 15, and 25 μM, respectively. The additional amount of actin was not able to rescue its polymerization as shown by the lower levels of fluorescence compared to actin polymerized alone.

addition, the oscillation occurs again, but pyrene fluorescence never reaches the same maximum as in fully polymerized actin. The final actin concentration was 25 uM actin, which is 10 times more than the amount of Spir in the reaction. Thus, the Spir-actin complex was not able to fully polymerize filaments even though previous nucleation assays showed that a 10-fold actin excess nucleated to form filaments when added to Spir at the beginning of the polymerization (Chapter 2, Figure 2). These results suggest a strong sequestration complex that renders the Spir-actin seeds non-polymerizable at high concentrations.

Spir binding to actin

Sitar et al. (26) proposed that each WH2 domain in Spir binds to actin with similar affinity. Our crystal structure suggests the possibility of different affinities since only the D domain could be resolved in the crystals. Different affinities are suggested also by incomplete occupation of all WH2 domains in the analysis of sedimentation velocity experiments. The affinity of actin for each WH2 domain in Spire was further tested in a binding assay. Spir was titrated with yeast actin mutants labeled at A167C or F169C with either acrylodan or pyrene, respectively (Figure 4). These mutants were chosen because WH2 domains bind near the W-loop of actin (residues 165-172). Spir was added in aliquots of 0.25 μM to an initial actin concentration of 5 μM. The fluorescence increased with each Spir addition up to ~1.25 μM and then started to decrease. This bimodal fluorescence change suggests that there are two binding modes of Spir, to a strong binding site and then to a weaker binding site.

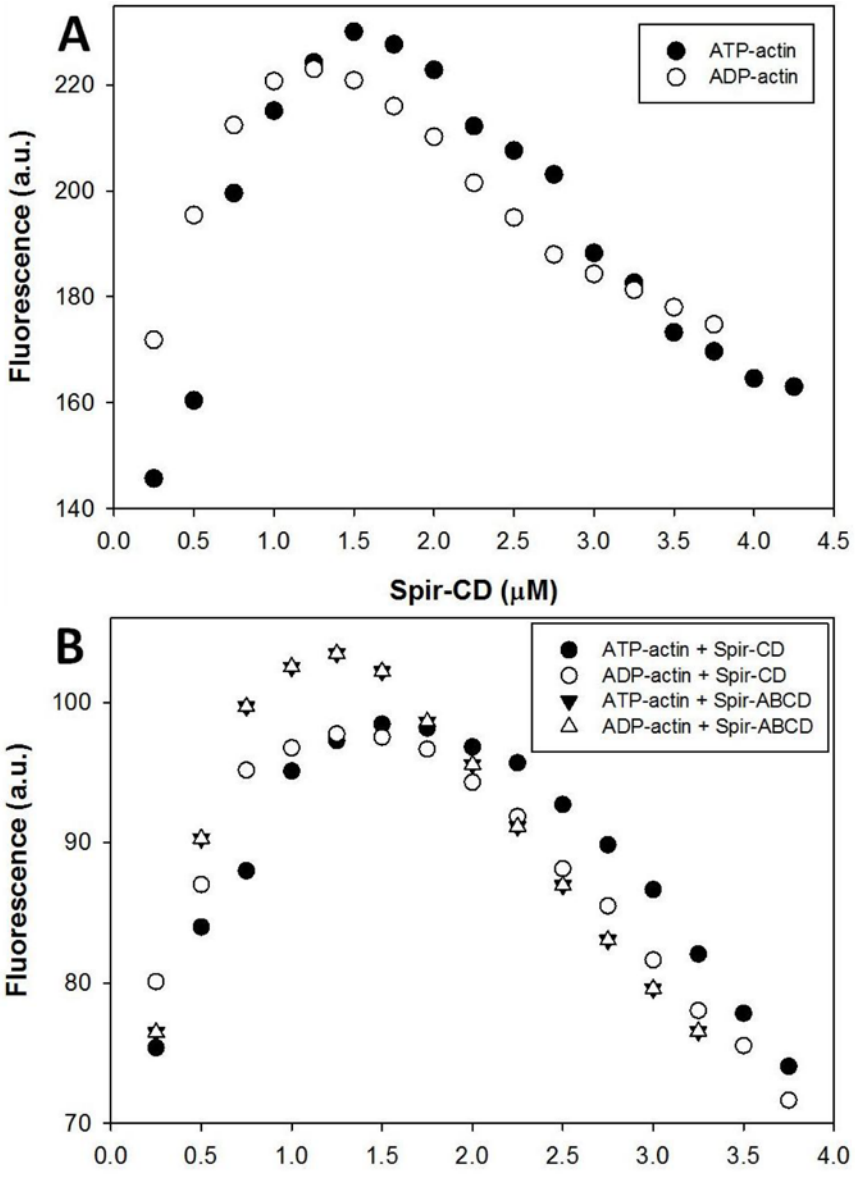

Figure 4. Binding of Spir to labeled actin causes a bimodal change in fluorescence. A. Aliquots of Spir-CD were added to 5 μM pyrene-labeled yeast actin mutant F169C. The fluorescence reaches a maximum at ~1.25-1.50 μM Spir-CD added and then declines with every addition. B. Spir was added to 5 μM acrylodan-labeled yeast actin mutant A167C for each titration point. The fluorescence reaches a maximum for both Spir-ABCD and Spir-CD at ~1.25-1.50 μM. The fluorescence then declines with every additional aliquot of Spir (as in A).

Crystal structure of Spir in complex with actin

The previous crystal structure of the complex provided insight into the flexibility of Spir-CD (Chapter 2, Figure 6) but did not allow us to map the vital linkers on actin, and to deduce how the actin molecules are arranged in a nucleating complex. Although models for that exist or can be generated, a high resolution structure would provide valuable insight into the ability of Spir to form either a nucleation or sequestration complex. Thus, we further pursued solving a crystal structure by modifying several factors. First, acanthamoeba actin was used in place of skeletal actin. Second, high amounts of DTT were used to ensure that Cys374 on actin would remain reduced. Third, the ratio for complex formation was altered to 1:2 Spir to actin. These changes resulted in a crystal structure that showed a different positioning of actin in the asymmetric unit. However, once again, only the D domain of Spir was resolved, with the entire C domain remaining disordered. The structure shown here (Figure 5) is not physiologically relevant, but is instead an example of the inherent flexibility of Spir-CD.

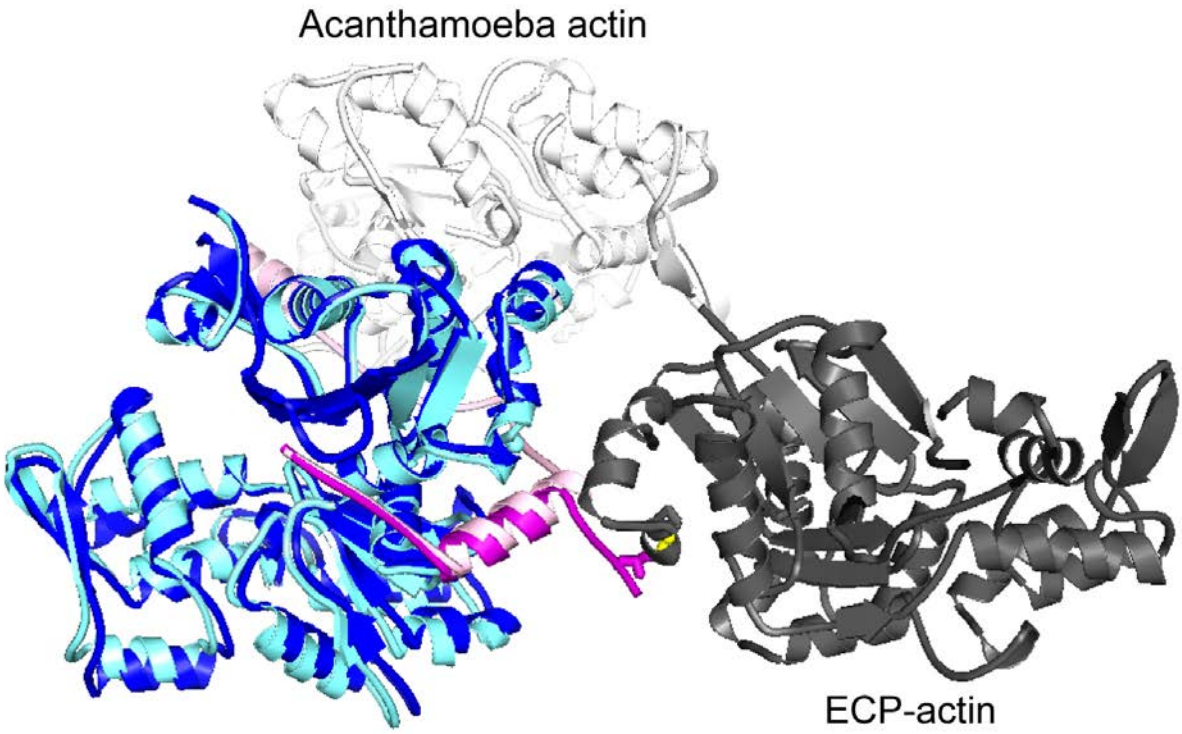

Figure 5. Overlay of crystal structures for Spir-CD with Acanthamoeba actin and ECP-cleaved actin. Spir-D (shown in magenta for the ECP-cleaved actin structure and in light pink for the Acanthamoeba actin structure) align next to the W-loop of the actin structure. Spir-C is disordered in both crystal structures. Actin subunits were modeled into the asymmetric unit of the crystal structure using Pymol. Actin Cys-374 (shown as yellow balls) and Spir Cys-459 form a disulfide bond, creating an anti-parallel dimer from the ECP-cleaved actin protomers. The actin protomer in the crystal structure of unmodified Acanthamoeba actin (PDB code 4EFH) is positioned longitudinally ~60° from the asymmetric unit of the ECP-cleaved actin structure.

Table 1 Data collection and refinement statistics

	Acanthamoeba Actin-Spir
Data collection	
Space group	$P2_12_12_1$
Cell dimensions	
a, *b*, *c* (Å)	53.0, 71.8, 126.1
α, β, γ (°)	90.0, 90.0, 90.0
Resolution (Å)	2.5 (2.59-2.50)
R_{sym}	0.141 (0.491)
$I/\sigma I$	11.2 (3.3)
Completeness (%)	99.5 (100)
Redundancy	4.4 (4.5)
Refinement	
Resolution (Å)	2.5
No. reflections	17414
$R_{work/}$ R_{free}	0.165/0.207
No. atoms	
Protein	2999
Ligand/ion	29
Water	130
B-factors (Å^2)	
Protein	35.6
Ligand/ion	28.2
Water	34.5
R.m.s deviations	
Bond lengths (Å)	0.010
Bond angles (º)	1.1

*Statistics for the highest resolution shell are shown in parentheses.

DISCUSSION

Here, we show evidence of the complex nature of Spir-actin interactions and their implications in the nucleation and sequestration activity of Spir *in vitro*. We also show its potential binding modes for G-actin. Although conflicting results suggest that Spir is either a nucleator or a sequestering agent, we observe both activities with Spir. Husson et al. (25) described recently the multifunctional features of Cobl, another tandem WH2-containing protein belonging to the same group of actin nucleators as Spir. They conclude that Cobl is able to nucleate, sever, and depolymerize F-actin. Their first line of evidence stems from a polymerization assay, in which they added equimolar concentrations of Cobl to actin. Under polymerizing conditions, the pyrene fluorescence initially increases to ~50% of the fluorescence for fully polymerized F-actin. The fluorescence then decreases to ~20%, and remains unchanged for the duration of the assay. Using theoretical algorithms, the authors predicted that the oscillation seen in the assay corresponds to the following events: nucleation of the filaments, severing of filaments, and their depolymerization. The oscillating curve is reminiscent of the oscillations seen in our seed experiments involving stoichiometric ratios of Spir and actin (Figure 3). Thus, we conclude that Spir exhibits multifunctional properties similar to Cobl.

Sitar et al. (26) recently published results suggesting that all WH2 domains of Spir bind to actin with equal binding affinities. Our data suggests otherwise. In Chapter 2, we observed by analytical ultracentrifugation that Spir and actin form complexes of different stoichiometries. If each WH2 domain has the same affinity, we should observe a discrete peak corresponding to a Spir:actin complex of 1:4. Our next line of evidence supporting different binding affinities comes from the fluorescence assay in which the titration of Spir causes a bimodal change in fluorescence. This suggests that the occupancy of the WH2 domains by actin changes, with Spir

exhibiting a weak binding site and a strong binding site for actin. We can also infer from the crystal structures that the Spir domains have different affinities for actin since in both cases, we were able to crystallize actin only with Spir-D. Ducka et al. (5) also encountered this constraint, suggesting that either the intrinsic disorder of Spir-C and/or linker 3 or a different affinity of actin for Spir-C preclude its crystallization with actin. However, their method for measuring binding affinity would also need to be supported by an alternative approach, as calorimetry measurements have significant standard errors.

Since existing evidence suggests that Spir and Capu work synergistically both *in vivo* and *in vitro* (7, 10, 27), it would be valuable to examine Spir's multifunctionality in conjunction with Capu, to provide further insight into their roles in *Drosophila* oogenesis. We were not able to observe any enhancement of actin depolymerization by Spir due to Capu, suggesting that Capu has no added value as either a severer of actin or its sequestering agent. Capu was originally shown to enhance the nucleation by Spir so this conclusion is not surprising. Spir's mechanism of severing and sequestration may be specific to Spir alone, and the *in vivo* relevance of these functions has not been confirmed. Capu's inability to enhance cross-linking of Spir-actin dimers in the S265C yeast actin mutant is more puzzling. Because the cross-linking assay is a useful tool for accessing the lateral configuration of actin oligomers, it can also detect the presence of possible nuclei. Spir alone enhances the cross-linking of S265C. Since Capu is believed to dimerize Spir and thus enhance actin nucleation (7), we expected to observe increased cross-linking, but the addition of Capu had no effect on this reaction. We note additional bands, corresponding to Capu alone and possibly Capu cross-linked to actin. Perhaps Capu's cross-linking to actin inhibits its ability to dimerize Spir and enhance actin cross-linking. If Spir does

have multiple functions *in vivo*, then factors other than Capu may be involved in regulating its function.

In conclusion, the techniques used here were useful in providing evidence for Spir's diverse activities, but distinguishing between the structures that produce a nucleating complex versus a sequestration complex is difficult. Most importantly, we still need to resolve Spir's *in vivo* role as either a nucleator or severer. Evidence for Spir's nucleator activity *in vivo* is more established in light of evidence supporting its role in establishing an actin mesh during *Drosophila* oogenesis. It would be also interesting to identify the specific residues necessary for either nucleation or severing activity. Previous data suggests that the nucleation activity of Spir is sequence specific (1). For example, linker 3 between Spir-C and Spir-D is critical for Spir's depolymerization activity (not shown). In a more recent study, the acidic residues directly preceding the WH2 domains of Cobl were proposed to contribute to its various activities (25). Most likely, specific residues in the linker regions, and/or WH2 domains other than the D domain, impact Spir's binding affinity to actin, thus affecting its specific activities.

REFERENCES

1. Quinlan, M. E.; Heuser, J. E.; Kerkhoff, E.; Dyche Mullins, R., *Nature* **2005,** 433, (7024), 382-388.

2. Bosch, M.; Le, K. H. D.; Bugyi, B.; Correia, J. J.; Renault, L.; Carlier, M.-F., *Molecular Cell* **2007,** 28, (4), 555-568.

3. Rebowski, G.; Boczkowska, M.; Hayes, D. B.; Guo, L.; Irving, T. C.; Dominguez, R., *Proceedings of the National Academy of Sciences* **2008,** 105, (31), 10785-10790.

4. Zuchero, J. B.; Coutts, A. S.; Quinlan, M. E.; Thangue, N. B.; and Mullins, R. D., *Nature Cell Biology* **2009**, 11, 451–459.

5. Ducka, A. M.; Joel, P.; Popowicz, G. M.; Trybus, K. M.; Schleicher, M.; Noegel, A. A.; Huber, R.; Holak, T. A.; Sitar, T., *Proceedings of the National Academy of Sciences* **2010,** 107, (26), 11757-11762.

6. Rosales-Nieves, A. E.; Johndrow, J. E.; Keller, L. C.; Magie, C. R.; Pinto-Santini, D. M.; Parkhurst, S. M., *Nat Cell Biol* **2006,** 8, (4), 367-376.

7. Quinlan, M. E.; Hilgert, S.; Bedrossian, A.; Mullins, R. D.; Kerkhoff, E., *The Journal of Cell Biology* **2007,** 179, (1), 117-128.

8. Spudich, J. A.; Watt, S., *Journal of Biological Chemistry* **1971,** 246, (15), 4866-4871.

9. Grintsevich, E. E.; Benchaar, S. A.; Warshaviak, D.; Boontheung, P.; Halgand, F. d. r.; Whitelegge, J. P.; Faull, K. F.; Ogorzalek Loo, R. R.; Sept, D.; Loo, J. A.; Reisler, E., *Journal of Molecular Biology* **2008,** 377, (2), 395-409.

10. Vizcarra, C. L.; Kreutz, B.; Rodal, A. A.; Toms, A. V.; Lu, J.; Zheng, W.; Quinlan, M. E.; Eck, M. J., *Proceedings of the National Academy of Sciences* **2011,** 108, (29), 11884-11889.

11. Kudryashov, D. S.; Grintsevich, E. E.; Rubenstein, P. A.; Reisler, E., *Journal of Biological Chemistry* **2010,** 285, (33), 25591-25601.

12. Cohn, E. J. a. E., J.T. (1943) Density and apparent specific volume of proteins. in *Proteins, Amino Acids and Peptides as Ions and Dipolar Ions* (Cohn, E. J. a. E., J.T. ed.), Reinhold Publishing Corporation, New York. pp 370-381

13. Laue, T. M., Shah, B.D., Ridgeway, T.M., and Pelletier, S.L. (1992) Computer-Aided Interpretation of Analytical Sedimentation Data for Proteins. in *Analytical Ultracentrifugation in Biochemistry and Polymer Science* (S.E. Harding, A. J. R. a. J. C. H. ed.), The Royal Society of Chemistry, Cambridge, Great Britain. pp 90-125

14. Otwinowski Z. and Minor W., *Methods in Enzymology*: *Macromolecular Crystallography, part A*, **1997**, 276, 307-326.

15. McCoy, A.J.; G. K. R.; Adams, P.D.; Winn, M.D.; Storoni, L.C.; Read R.J., *J Appl Crystallogr* **2007,** 40, (4), 658-674.

16. Kudryashov, D. S.; Sawaya, M. R.; Adisetiyo, H.; Norcross, T.; Hegyi, G. r.; Reisler, E.; Yeates, T. O., *Proceedings of the National Academy of Sciences of the United States of America* **2005,** 102, (37), 13105-13110.

17. Murshudov, G.N.; V. A.; Dodson, E.J., *Acta Crystallogr D Biol Crystallogr* **1997,** 53, (3), 240-255.

18. Blanc, E.; R. P.; Vonrhein, C.; Flensburg, C.; Lea, S.M.; Bricogne, G., *Acta Crystallogr D Biol Crystallogr* **2004,** 60, (12), 2210-21.

19. Winn, M.D.; Murshudov, G.N.; Papiz, M.Z., *Methods Enzymol* **2003**,374, 300-21.

20. Emsley, P.; Lohkamp, B.; Scott, W. G.; Cowtan, K., *Acta Crystallographica Section D* **2010,** 66, (4), 486-501.

21. Laskowski, R. A.; MacArthur, M. W.; Moss, D. S.; Thornton, J. M., *Journal of Applied Crystallography* **1993,** 26, 283-291.

22. Colovos, C.; Yeates, T. O., *Protein Science* **1993,** 2, (9), 1511-1519.

23. Luthy, R.; Bowie, J. U.; Eisenberg, D., *Nature* **1992,** 356, (6364), 83-85.

24. The PyMOL Molecular Graphics System, Version 1.4, Schrödinger, LLC (http://www.pymol.org).

25. Husson, C.; Renault, L.; Didry, D.; Pantaloni, D.; Carlier, M.-F., *Molecular Cell* **2011,** 43, (3), 464-477.

26. Sitar, T.; Gallinger, J.; Ducka, A. M.; Ikonen, T. P.; Wohlhoefler, M.; Schmoller, K. M.; Bausch, A. R.; Joel, P.; Trybus, K. M.; Noegel, A. A.; Schleicher, M.; Huber, R.; Holak, T. A., *Proceedings of the National Academy of Sciences* **2011,** 108, (49), 19575-19580.

27. Dahlgaard, K.; Raposo, A. A. S. F.; Niccoli, T.; St Johnston, D., *Developmental Cell* **2007,** 13, (4), 539-553.

Chapter 4

Cofilin-linked changes in actin filament flexibility promote severing

Biophysical Journal Volume 101 July 2011 151–159

Cofilin-Linked Changes in Actin Filament Flexibility Promote Severing

Brannon R. McCullough,[†] Elena E. Grintsevich,[‡] Christine K. Chen,[‡] Hyeran Kang,[†] Alan L. Hutchison,[†] Arnon Henn,[†] Wenxiang Cao,[†] Cristian Suarez,[§] Jean-Louis Martiel,[§] Laurent Blanchoin,[§] Emil Reisler,[‡] and Enrique M. De La Cruz[†]*

[†]Department of Molecular Biophysics and Biochemistry, Yale University, New Haven, Connecticut; [‡]Department of Chemistry and Biochemistry, University of California, Los Angeles, California; and [§]Institut de Recherches en Sciences et Technologies pour le Vivant, Laboratoire de Physiologie Cellulaire & Végétale, Centre d'Etudes Atomiques-Centre National de la Recherche Scientifique, Institut National de la Recherche Agronomique, Université Joseph Fourier, Grenoble, France

ABSTRACT The actin regulatory protein, cofilin, increases the bending and twisting elasticity of actin filaments and severs them. It has been proposed that filaments partially decorated with cofilin accumulate stress from thermally driven shape fluctuations at bare (stiff) and decorated (compliant) boundaries, thereby promoting severing. This mechanics-based severing model predicts that changes in actin filament compliance due to cofilin binding affect severing activity. Here, we test this prediction by evaluating how the severing activities of vertebrate and yeast cofilactin scale with the flexural rigidities determined from analysis of shape fluctuations. Yeast actin filaments are more compliant in bending than vertebrate actin filaments. Severing activities of cofilactin isoforms correlate with changes in filament flexibility. Vertebrate cofilin binds but does not increase the yeast actin filament flexibility, and does not sever them. Imaging of filament thermal fluctuations reveals that severing events are associated with local bending and fragmentation when deformations attain a critical angle. The critical severing angle at boundaries between bare and cofilin-decorated segments is smaller than in bare or fully decorated filaments. These measurements support a cofilin-severing mechanism in which mechanical asymmetry promotes local stress accumulation and fragmentation at boundaries of bare and cofilin-decorated segments, analogous to failure of some nonprotein materials.

INTRODUCTION

Cofilin is an actin filament severing protein that contributes to overall assembly dynamics and motility by increasing the number of free filament ends from which free subunits associate and dissociate (1–4). Severing occurs without coupling to energy sources such as ATP hydrolysis. Severing is instead driven by cofilin binding and linked reactions (5).

Cofilin alters the helical structure of filaments (6,7) and increases the conformational dynamics of subunits such that they are more compliant in bending (8–10) and twisting (11). These changes in filament mechanical properties suggest that alterations of filament mechanics and dynamics could promote their fragmentation. The observed surface tethering-dependence of cofilin severing activity (12) is consistent with filament mechanics playing a critical role in severing.

We proposed that a local asymmetry in actin filament (bending-and-twisting) mechanics and discontinuity in topology localizes stress at boundaries and promotes severing, analogous to fatigue fractures of nonprotein materials (8,13,14). Consistent with this model, cofilin severing is maximal at substoichiometric binding densities (12,15) and scales with the density of boundaries between bare and cofilin-decorated segments (14), for some (16,17) but not all (12,15,18) cofilactin isoforms. In cases where severing activity peaks at cofilin binding densities smaller than those yielding the maximum number of boundaries (12,15,18), surface tethering sites could potentially act as mechanical barriers to filament fluctuations, similar to boundaries, thereby promoting severing (12).

This mechanical asymmetry model also predicts that cofilin-linked changes in filament elasticity influence severing. To evaluate whether alteration of filament elasticity by cofilin scales with filament severing, we measured the severing activities and bending mechanics from thermal fluctuations in shape of various cofilactin isoforms. Cofilin isoforms that alter weakly the actin filament bending stiffness display weak severing activity. In addition, imaging thermally driven fragmentation of fluctuating filaments indicates that severing at boundaries of bare and cofilin-decorated segments occurs at smaller filament deformations than fragmentation of homogenous (bare or cofilin-saturated) filaments. These results support a model in which cofilin-linked stress accumulation and severing occur at bare and cofilin-decorated boundaries possessing a local mechanical asymmetry.

MATERIALS AND METHODS

Protein purification

All reagents were the highest purity commercially available and came from Sigma-Aldrich (St. Louis, MO), unless otherwise noted. Rabbit skeletal muscle actin was purified and labeled with pyrenyl iodoacetamide (Molecular Probes, Eugene, OR (13)), Alexa 488 succinimidyl ester (Molecular Probes (8)) for flexibility and steady-state length assays, or biotin-maleimide

Submitted April 26, 2011, and accepted for publication May 24, 2011.

*Correspondence: enrique.delacruz@yale.edu

Arnon Henn's present address is Faculty of Biology, Technion - Israel Institute of Technology, Haifa, Israel.

Editor: Roberto Dominguez.

0006-3495/11/07/0151/9 $2.00

doi: 10.1016/j.bpj.2011.05.049

(Sigma-Aldrich) and Cy3b-maleimide (GE Healthcare, Waukesha, WI) for real-time severing assays by using a method similar to that used for pyrene labeling yeast actin (19). The material was then gel-filtered over Sephacryl S300 (Sigma-Aldrich) at 4°C in G-buffer (5 mM Tris (pH 7.5), 0.2 mM ATP, 0.2 mM $CaCl_2$, 0.5 mM DTT, 1 mM NaN_3). *Saccharomyces cerevisiae* actin was purified and labeled with pyrene maleimide or similarly labeled with biotin-maleimide (Sigma-Aldrich) and Cy3b-maleimide (GE Healthcare) for real-time severing assays as described in Northrop et al. (19) or Alexa 488 succinimidyl ester (Molecular Probes (8)) for flexibility and steady-state length assays.

The labeling efficiency was ~0.8–1.0 pyrene and ~0.8 Alexa 488 fluorophores per actin monomer. Ca^{2+}-actin monomers were converted to Mg^{2+}-actin monomers with 0.2 mM EGTA and 50 μM $MgCl_2$ then polymerized with 0.1 vol 10× polymerization buffer yielding $KMI_{6.8}$ buffer (50 mM KCl, 2 mM $MgCl_2$, 2 mM DTT, 0.2 mM ATP, 20 mM imidazole, pH 6.8). Recombinant human nonmuscle cofilin-1, *Schizosaccharomyces pombe* ADF/cofilin, and actophorin were purified as described in De La Cruz (13). *S. cerevisiae* cofilin was purified as described in Grintsevich et al. (20). *S. cerevisiae* cofilin (D34C, C62A mutant) was labeled with Alexa-488 as described in Suarez et al. (21).

Equilibrium binding to actin filaments

Equilibrium binding of cofilin and pyrene actin filaments was monitored by fluorescence with a Quantamaster fluorimeter (Photon Technologies International, South Brunswick, NJ) thermostatically controlled at 25(±0.1)° C. Samples were excited at 366 nm and the observed fluorescence intensities at 407 nm were converted to filament binding densities (ν) as described (5,13,22). Equilibrium binding isotherms were fitted to the numerical solutions of an implicit bimolecular binding equation (23) with the stoichiometry and binding affinity as unconstrained fitting parameters. Fit parameters are subject to large experimental error due to stoichiometric binding limitations. Measurements were made in $KMI_{6.8}$ buffer at total concentrations of 2 μM for vertebrate and 1.6 μM for yeast actin.

Determination of filament flexural rigidity

Images of individual labeled bare and fully cofilin-decorated fluorescently-labeled actin filaments in supplemented $KMI_{6.8}$ buffer ($KMI_{6.8}$ buffer supplemented with 15 mM dextrose, 100 mM DTT, 0.1 mg mL^{-1} glucose oxidase, and 20 μg mL^{-1} catalase) were acquired using an Eclipse TE300 microscope (Nikon, Melville, NY) equipped with a Coolsnap HQ-cooled charge-coupled device camera (Roper Scientific, Tucson, AZ) and MetaMorph image acquisition software (Molecular Devices, Downingtown, PA) as described in McCullough et al. (8). The bending persistence length (L_p) was determined by fitting the average angular (θ) cosine correlation of a segment of length s to the following two-dimensional correlation function:

$$\langle C(s)\rangle \;=\; \langle \cos[\theta(s)-\theta(0)]\rangle \;=\; e^{\frac{-s}{2L_p}}. \qquad (1)$$

Analysis of filaments undergoing thermal fluctuations and those adsorbed to poly-L-lysine-treated slides using Eq. 1 yielded comparable results.

Real-time severing assay

Direct visualization of filament severing by total internal reflectance fluorescence microscopy was performed essentially as described in Pavlov et al. (12) except filaments (comprised of 1% biotinylated and 15% Cy3b-labeled subunits) were tethered to the coverslip surface with neutravidin (24) and cofilin was added to the flow cell with a chamber volume of 18 μL. Final conditions were $KMEI_{6.8}$ buffer supplemented with 15 mM dextrose, 100 mM DTT, 0.1 mg mL^{-1} glucose oxidase, and 20 μg mL^{-1} catalase and the indicated cofilin concentration. We assessed severing from the average filament length after a minute upon the addition of cofilin to the flow cell.

Equilibrium length severing assay

Samples of 6 μM Alexa-488 labeled actin and cofilin concentrations yielding a range of binding densities were equilibrated for 60 min, serial-diluted to 100–200 nM total actin in buffer containing cofilin concentrations to not alter the binding density, adsorbed to poly-L-lysine treated slides, and imaged as done for the determination of filament flexural rigidity. The average filament length, L_{avg}, at different cofilin binding densities was measured to estimate the apparent boundary-severing rate, using equations describing the relationship between L_{avg} and severing (25,26) that were modified as follows.

The total filament number (N) depends on severing and annealing events according to the reaction scheme

$$N \underset{k_{anneal}}{\overset{k_{sever}}{\rightleftharpoons}} N + dN, \qquad (2)$$

where $dN > 0$. The rate of change in filament number (dN/dt; normalized by the total number of filament subunits, n) is given by the apparent normalized second-order annealing rate constant (k_{anneal}, in units of subunits s^{-1} $filament^{-1}$) and the apparent normalized filament severing rate (k_{sever}, in units of filaments s^{-1} $subunit^{-1}$) according to

$$\frac{d(N/n)}{dt} \;=\; k_{sever} - (N/n)^2 k_{anneal}. \qquad (3)$$

The average filament length (L_{avg}) is equivalent to the total population of filament subunits divided by the total number of filaments ($L_{avg} = n/N$). The values of n, N, and L_{avg} do not change ($dn/dt = 0$, $dN/dt = 0$, and $dL_{avg}/dt = 0$) under steady-state conditions, such that

$$k_{sever} \;=\; (N/n)^2 k_{anneal} \;=\; L_{avg}^{-2} k_{anneal}, \qquad (4)$$

and L_{avg} simplifies to the following function of k_{anneal} and k_{sever}:

$$L_{avg} \;=\; \sqrt{\frac{k_{anneal}}{k_{sever}}}. \qquad (5)$$

Therefore, an increase in k_{sever} yields shorter average filament lengths (when changes in k_{anneal} are small).

To distinguish between severing at boundaries and symmetric sites, we express k_{sever} in terms of the normalized fraction of subunits at boundaries of bare and cofilin-decorated segments (b) as

$$L_{avg} \;=\; \sqrt{\frac{k_{anneal}}{(1-b)k_{sever,sym} + bk_{sever,boundary}}}, \qquad (6)$$

where $k_{sever,sym}$ (filaments s^{-1} symmetric $subunit^{-1}$) is the boundary-independent apparent rate for actin filament severing at symmetric sites; $k_{sever,boundary}$ is the apparent severing rate for cofilin-induced actin filament severing at boundaries (filaments s^{-1} boundary $subunit^{-1}$). The fraction of occupied sites at boundaries (b) is a function of the cofilin binding density (ν) according to

$$b \;=\; \nu(1-\nu) \qquad (7)$$

for noncooperative binding or

$$b \;=\; \frac{1-\sqrt{(1-2\nu)^2 + 4\omega\nu(1-2\nu)}}{2(1-\omega)} \qquad (8)$$

for cooperative binding, where ω is the thermodynamic cooperativity parameter (13,22). Note that all sites are symmetric when no boundaries are present ($b = 0$ when $k_{sever,sym} = k_{sever}$).

This model assumes that the severing probability, and therefore k_{sever}, is equivalent at identical filament sites (e.g., unoccupied, isolated, singly-contiguous, doubly-contiguous, as defined by a one-dimensional lattice of binding sites (13,22)). Long filaments sever more readily than shorter filaments because they have more potential sites at which to sever. This length-dependence of the severing process is explicitly accounted for in Eq. 3.

To estimate the apparent severing rate at boundaries, we fit L_{avg} as a function of binding density (Eqs. 6–8) with the cooperativity parameter (ω) for cooperative human cofilin binding constrained to experimentally determined values obtained under comparable conditions (13). The rate of spontaneous (i.e., cofilin-independent) actin filament severing ($k_{sev} = 1 \times 10^{-6}$ filaments s^{-1} subunit^{-1}; see Fig. 2 (25,27)) was constrained during the fitting procedure. The fits yielded an apparent annealing rate of 4.6 ± 0.2 and 5.7 ± 0.2 subunits s^{-1} filament^{-1} for vertebrate and yeast actin filaments, respectively.

Determination of the critical severing angle

Individual, thermally fluctuating Alexa-488-labeled actin (100–200 nM total actin) and cofilactin (addition of 1.4 μM total cofilin) filaments in supplemented $KMI_{6.6}$ buffer were imaged as done for determination of filament flexural rigidity. Irreversible filament severing events were identified, cropped, and digitally processed to enhance resolution (8). Severing at boundaries of bare and cofilin-decorated segments was observed by imaging Alexa-488 labeled *S. cerevisiae* yeast cofilin (D34C, C62A mutant) binding to Alexa568-labeled actin filaments using total internal reflectance fluorescence (21). The angle between filament segments before severing was determined from two consecutive, post- and pre-severing, frames ($n = 10$ for bare actin and saturated cofilactin filaments; $n = 20$ for fragmentation at boundaries of partially decorated filaments). The acquisition rate was 10 frames per second in experiments using fluorescently-labeled cofilin, which is well below the observed (see Fig. 4) or predicted (8) bending relaxation time, indicating adequate temporal sampling of the bending angle before severing. Individual measurement errors were within 95% confidence for all events.

Energy, forces, and internal work in elastic filaments

The equilibrium equations for an inextensible actin filament segment subject to a bending deformation (28) were used to estimate the net shear force associated with filament conformations. We used the classical Euler bending (θ, ϕ) and twisting (ψ) angles to parameterize the orientation of the filament with arc-length (s) to derive the total elastic free energy function (H, normalized by k_BT) with inextensibility constraints,

$$\left(\frac{H}{k_BT}\right) = \frac{L_B}{2}\left(\left(\frac{d\theta}{ds}\right)^2 + \sin^2\theta\left(\frac{d\phi}{ds}\right)^2\right) + \frac{L_T}{2}\left(\frac{d\psi}{ds} + \cos\theta\frac{d\phi}{ds}\right)^2 + F_x\sin\theta\cos\phi + F_y\sin\theta\sin\phi + F_z\cos\theta, \tag{9}$$

where F_x, F_y, and F_z are the three components of the internal force associated with the inextensibility condition; L_B and L_T are the bending and twisting persistence lengths, respectively. We introduce the three moments (A_1, A_2, and A_3) associated with the three Euler angles θ, ϕ, ψ,

$$A_1 = \frac{\partial H}{\partial(d\theta/ds)}, A_2 = \frac{\partial H}{\partial(d\phi/ds)}, A_3 = \frac{\partial H}{\partial(d\psi/ds)} \tag{10}$$

to simplify the energy function

$$\left(\frac{H}{k_BT}\right) = \frac{(A_1)^2}{2L_B} + \frac{(A_3)^2}{2L_T} + \frac{(A_2 - A_3\cos\theta)^2}{2L_B\sin^2\theta} + F_x\sin\theta\cos\phi + F_y\sin\theta\sin\phi + F_z\cos\theta \tag{11}$$

and obtain the equilibrium equations for the filament (28)

$$\begin{aligned}
\frac{d\theta}{ds} &= \frac{A_1}{L_B}\\
\frac{d\phi}{ds} &= \frac{(A_2 - A_3\cos\theta)}{L_B\sin^2\theta}\\
\frac{d\psi}{ds} &= \frac{A_3}{L_T} + \frac{\cos\theta(A_2 - A_3\cos\theta)}{L_B\sin^2\theta}\\
\frac{dA_1}{ds} &= \left(-F_x\cos\phi\cos\theta - F_y\sin\phi\cos\theta + F_z\sin\theta\right) + \frac{(A_2 - A_3\cos\theta)(A_2\cos\theta - A_3)}{L_B\sin^3\theta}\\
\frac{dA_2}{ds} &= \sin\theta\left(F_x\sin\phi - F_y\cos\phi\right)\\
\frac{dA_3}{ds} &= 0,
\end{aligned} \tag{12}$$

supplemented with the inextensibility conditions

$$\begin{aligned}
\frac{dX}{ds} &= \sin\theta\cos\phi\\
\frac{dY}{ds} &= \sin\theta\sin\phi\\
\frac{dZ}{ds} &= \cos\theta,
\end{aligned} \tag{13}$$

where $X(s)$, $Y(s)$, and Z(s) are the spatial coordinates of s. In absence of an externally applied force, the internal force components (F_x, F_y, F_z) are constants determined from the solution to Eq. 10.

We solve Eq. 11 with boundary conditions at the ends ($s = 0$, $s = L$) of a filament segment of length, L. Both filament ends are constrained to bend with zero elevation ($Z(0) = Z(L) = 0$; $\theta(0) = \theta(L) = \pi/2$) and to not twist ($\psi(0) = \psi(L) = 0$). The azimuthal angle, ϕ, is set to 0 and varied at $s = L$ so that the angle between the two unit tangent vectors is ϕ (L). These conditions deal with position (X, Y, and Z) or orientation (θ, ϕ, ψ) variables only. Therefore, the internal force (F_x, F_y, F_z) and moments (A_1, A_2, A_3) are determined by solving Eq. 12 with the above boundary conditions. The shear force, $\mathbf{F}_{shear}$, is calculated from the projection of the internal force on a plane orthogonal to the tangent vector at one-half of the segment length,

$$\mathbf{F}_{shear} = (\mathbf{I} - \mathbf{t}\otimes\mathbf{t})\mathbf{F}, \tag{14}$$

where $\mathbf{F}$ is the vector of components (F_x, F_y, F_z), $\mathbf{t}$ is the unit tangent vector expressed at $s = L/2$, and $\mathbf{I}$ the identity matrix. The shear work done by the shear force over a distance of one actin filament diameter was calculated by multiplying the shear force by the filament diameter of 6 nm and converting to thermal energy (k_BT).

RESULTS

Yeast actin filaments are more compliant in bending than vertebrate actin filaments

The bending persistence length (L_p) of a semiflexible polymer such as an actin filament is determined by the bending stiffness, or (apparent) flexural rigidity (κ), according to

$$L_p = \frac{\kappa}{k_B T}. \quad (15)$$

L_p is the characteristic length over which angular correlations of filaments undergoing thermally (k_BT)-driven shape fluctuations diminish (stiff filaments have longer L_p lengths than flexible ones). Thus, the filament L_p is determined from the average angular correlation along the contour length of individual filaments undergoing thermally driven fluctuations in shape (Fig. 1).

Vertebrate muscle actin filaments have an L_p of 9.4 μm (Fig. 1 *A*; Table 1), in agreement with previous determinations made under slightly different buffer conditions (8,29,30), and as predicted from normal mode analysis (31) and all-atom molecular dynamics simulations (32,33). *S. cerevisiae* (herein referred to as "yeast") actin filaments are more flexible in bending than vertebrate filaments, displaying an L_p of 5.5 μm (Fig. 1 *B*; Table 1), in accord with greater conformational dynamics (34–36) and instability (37,38).

Vertebrate cofilin does not increase the flexibility of yeast actin filaments

Vertebrate cofilactin filaments bend more readily than bare filaments (Fig. 1 *A* (8,10)), as indicated by the reduction in their persistence length from 9.4 to 3.0 μm (Table 1). Similarly, yeast cofilactin filaments are approximately threefold more compliant in bending than their bare filament counterparts, displaying a persistence length of 2.0 μm compared to 5.5 μm (Fig. 1 *B*; Table 1). Yeast cofilin increases the flexibility of vertebrate actin filaments approximately fivefold (Table 1); the persistence length of saturated filaments is 1.9 μm (Fig. 1 *A*; Table 1).

In contrast, vertebrate cofilin does not significantly affect the bending flexibility of yeast actin filaments. Yeast filaments saturated with human cofilin have a persistence length of 5.9 μm, comparable to that of bare filaments (5.5 μm; Fig. 1 *B*; Table 1). Fluorescence quenching of pyrene-labeled yeast actin (Fig. 1 *C*) and cosedimentation of Alexa-488-labeled yeast actin (data not shown) confirm strong binding under our experimental conditions ($K_d = 16 \pm 4$ nM), revealing that vertebrate (human cofilin-1) cofilin binds yeast actin filaments but does not significantly alter their overall filament flexural rigidity.

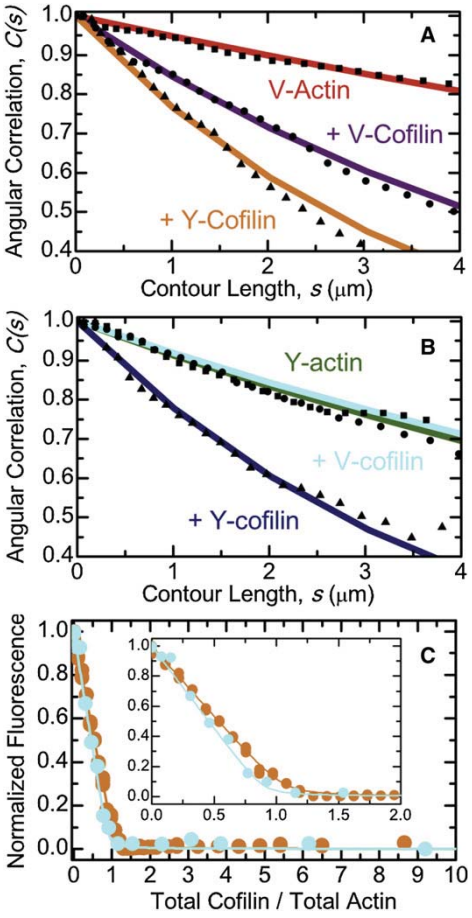

FIGURE 1 Bending flexibility of yeast and vertebrate cofilactin filaments. (*A*) The best fits of the average angular correlation of vertebrate muscle actin filaments to the two-dimensional persistence length function (Eq. 1): bare (*red*), fully decorated human cofilin-1 (*violet*), or yeast cofilin (*orange*). (*B*) The best fits of the average angular correlation of yeast actin filaments to the two-dimensional persistence length function (Eq. 1): bare (*green*), fully decorated human cofilin-1 (*blue*), or yeast cofilin (*cyan*). (*C*) Equilibrium binding of cofilin and actin filaments: yeast cofilin and vertebrate muscle actin filaments (*orange*), vertebrate cofilin and yeast actin filaments (*blue*). (*Solid line* through the data) Best fit to the numerical solutions of an implicit bimolecular binding isotherm (23), yielding binding affinities <50 nM (52).

Cofilin severing efficiency correlates with linked changes in filament elasticity

It was previously demonstrated that (vertebrate) cofilin increases the bending flexibility of (vertebrate) actin filaments (8), and suggested that local asymmetry in filament mechanics at boundaries of bare and cofilin-decorated segments promotes stress accumulation and severing (8,14). This model leads to two notable predictions that can be experimentally tested: 1), human cofilin severs weakly yeast actin filaments, because its binding does not alter appreciably their elasticity; and 2), combinations of

TABLE 1 Summary of actin and cofilactin filament bending parameters

Actin	Cofilin	L_p (μm)
Vertebrate	—	9.4 (± 0.7)
Vertebrate	Human-1	3.0 (± 0.2)
Vertebrate	Yeast	1.9 (± 0.3)
Vertebrate	Yeast (*S. pombe*)	2.2 (± 0.1)
Vertebrate	Actophorin	2.8 (± 0.3)
Yeast	—	5.5 (± 0.5)
Yeast	Human-1	5.9 (± 0.4)
Yeast	Yeast	2.0 (± 0.2)

Conditions are $KMI_{6.8}$ buffer, 25°C. Yeast is *S. cerevisiae* unless noted.

cofilactin displaying enhanced filament flexibility promote severing.

We evaluated these predictions through direct imaging of severing events (Fig. 2) and the [cofilin]-dependence of the average filament length distribution at steady state (Fig. 3). Vertebrate actin filaments are severed readily by vertebrate and yeast cofilin in real-time severing assays (Fig. 2), as previously reported (12,15). Similarly, yeast actin filaments are severed efficiently by yeast cofilin (Fig. 2 (39)). In contrast, no detectable severing of yeast actin filaments is observed upon addition of vertebrate cofilin (Figs. 2 and 3).

Filament severing by cofilin scales nonmonotonically with the binding density and is maximal when filaments

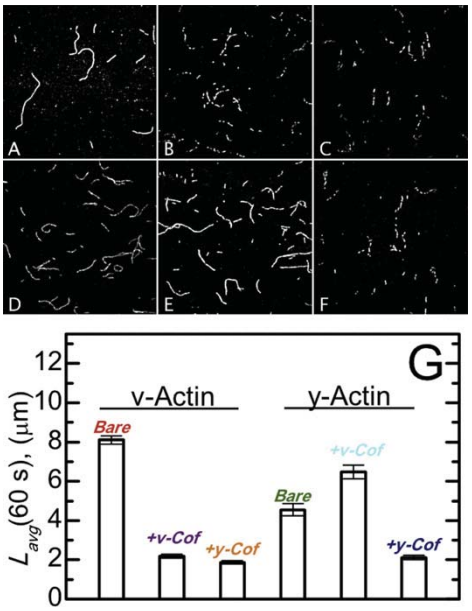

FIGURE 2 Real-time actin filament severing by cofilin. Fluorescent images of vertebrate muscle (*A–C*) or yeast (*D–F*) actin filaments 1 min after the addition of buffer (*A* and *D*), 250 nM vertebrate cofilin (*B* and *E*), or 250 nM yeast cofilin (*C* and *F*). (*G*) The average filament length of samples shown in panels *A–F* for sample sizes (number of filaments) of 393 (bare v-actin), 443 (v-actin + v-cofilin), 402 (v-actin + y-cofilin), 1647 (bare y-actin), 1466 (y-actin + v-cofilin), and 417 (y-actin + y-cofilin).

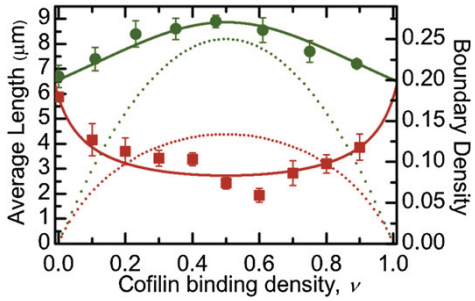

FIGURE 3 Dependence of average actin filament length on cofilin binding density. The vertebrate cofilin binding density-dependence of the average vertebrate (*red*) and yeast (*green*) actin filament steady-state length. (*Dotted lines*) Density of boundaries between bare and cofilin-decorated filament segments along vertebrate (*red*) and yeast (*green*) actin filaments calculated from the binding density and equilibrium binding constants (13,14). The sample size ranged from 100 to 200 filaments at each binding density. Uncertainty bars represent standard errors of the mean.

are partially saturated (12,14,15). These real-time severing measurements were made at identical conditions [cofilin] for all cofilactin isoforms, raising the possibility that the observed severing efficiencies reflect differences in cofilin binding and boundary density on the approach to equilibrium (22) during an experiment, because the affinities and cooperativities differ among the isoforms. We therefore evaluated the yeast and vertebrate filament steady-state length distribution over a range of vertebrate [cofilin] and binding densities (Fig. 3). We did not evaluate severing by yeast cofilin in a similar way because thorough characterization of that process, including the [cofilin]-dependence, has been previously reported (12).

Vertebrate actin filaments have a mean length, L_{avg}, of ~7 μm at steady-state (Fig. 3), as previously reported (25,40). Severing decreases the steady-state L_{avg} (26). Vertebrate cofilin shortens the L_{avg} for vertebrate actin filaments in a manner that scales with the density of bare and cofilin-decorated boundaries (peak at a binding density of ~0.5; Fig. 3 (14)), indicative of an increased actin filament severing rate. To assess the severing rate at boundaries of bare and cofilin-decorated segments, we modified equations for L_{avg} from severing-dependent actin polymerization models (25,26) to yield expressions relating L_{avg} to the dependence of severing activity on the cofilin-binding density (Eqs. 6–8; see Materials and Methods). The best fit of the binding density-dependence of L_{avg} to Eqs. 6 and 8 indicates that the severing rate at vertebrate cofilin boundaries along vertebrate filaments is 10-fold greater than within bare or cofilin-decorated clusters ($k_{sever,sym} = 1 \times 10^{-6}$ filaments s^{-1} symmetric subunit^{-1}; $k_{sever,boundary} = 2.7\ (\pm\ 0.5) \times 10^{-5}$ filaments s^{-1} boundary subunit^{-1}). Analysis of severing rates in real-time assays (Fig. 2) yields a comparable severing rate ($k_{sever} = 2.6\ (\pm\ 0.1) \times 10^{-5}$ filaments s^{-1} subunit^{-1}).

In contrast to its effect on vertebrate actin, vertebrate cofilin does not shorten the average length of yeast actin filaments (Fig. 3) over a broad range of binding densities, indicating attenuated severing activity as observed in real-time severing assays (Fig. 2). The apparent severing rate at bare and cofilin-decorated boundaries estimated from the binding density-dependence of L_{avg} (Eqs. 6 and 7) yields comparable severing rates at boundaries and within clusters ($k_{sever,sym} = 1 \times 10^{-6}$ filaments s^{-1} symmetric subunit^{-1}; $k_{sever,boundary} = -8\ (\pm 1) \times 10^{-7}$ filaments s^{-1} boundary subunit^{-1}; the negative value of $k_{sever,boundary}$ obtained from the best fit of the data results from a reduced severing activity). The overall apparent severing rate, accounting for contributions from both symmetric and boundary subunits, is 5.5 $(\pm 1) \times 10^{-7}$ filaments s^{-1} subunit^{-1} at the peak boundary density, comparable to the severing rate determined in real-time assays (Fig. 2; $k_{sever} = 6.1\ (\pm\ 4.1) \times 10^{-7}$ filaments s^{-1} subunit^{-1}) and suggest that vertebrate cofilin partially protects yeast actin from fragmentation at intermediate binding densities (Figs. 2 and 3), the molecular basis of which requires further investigation. More importantly, these data reveal that there is a correlation between changes in filament elasticity and cofilin severing activity, consistent with the hypothesis that stress accumulation at boundaries of mechanical asymmetry promotes filament fragmentation (8,12).

Cofilin alters the reversibility of filament bending deformations

We measured the bending deformation at breakage sites of freely-fluctuating filaments (Fig. 4). Observed severing events are associated with a localized bending at the site of fragmentation (Fig. 4). The angle at which local deformation becomes irreversible and filaments sever (i.e., critical bending angle), depends on bound cofilin, such that cofilactin filaments sever at higher critical angles than bare actin filaments ($\theta_{crit} = 73\ \pm\ 7^\circ$ versus $57\ \pm\ 9^\circ$; Fig. 4, *D* and *E*). The critical severing angle is lowest for severing events at boundaries between bare and cofilin-decorated segments ($\theta_{crit} = 31\ \pm\ 6^\circ$; Fig. 4 *F*) and hingelike motions are observed before severing ((21); Fig. 4 *C*).

The internal shear force and work resulting from a given filament bending deformation were estimated through simulation of the elastic free energy function of a filament segment constrained by a bending angle (see Materials

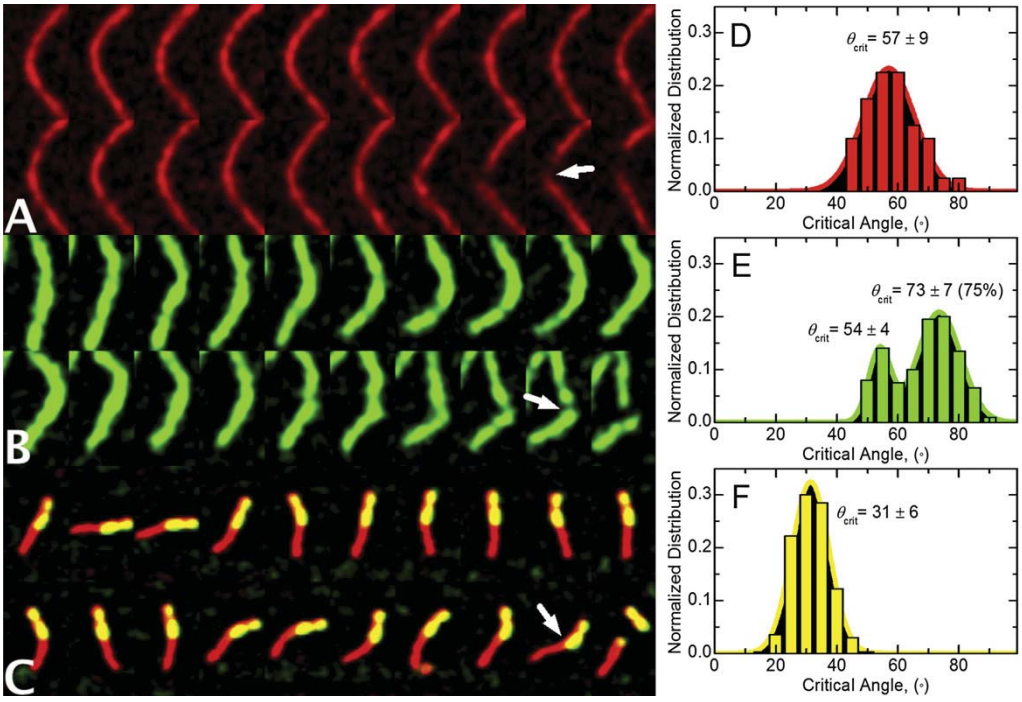

FIGURE 4 Modulation of the critical actin filament severing angle by cofilin. Subsequent fluorescent images acquired at 100-ms intervals of a thermally fluctuating vertebrate muscle (*A*) actin or (*B*) cofilactin filament conformations before fragmentation. (*C*) Subsequent fluorescent images acquired at 5 s intervals of a thermally fluctuating vertebrate muscle actin filament partially decorated with yeast cofilin (21) before fragmentation. (*Arrows*) Bending vertex from hingelike motion. The average critical angle for severing of (*D*) bare vertebrate actin ($n = 10$), (*E*) vertebrate cofilactin ($n = 10$), or (*F*) at boundaries of bare and cofilin-decorated segments ($n = 20$). (*Solid lines*) Best fits of the data to normal distributions. Unimodal and bimodal random fitting distributions of the cofilactin severing angles evaluated using the ANOVA F-test indicate that a bimodal distribution is statistically warranted with >99.9% confidence. Using Satterthwaites's approximation, the statistical probability that we observed a difference between populations by chance is <0.1%.

and Methods, and Eqs. 9–14). We assume that the internal force orthogonal to the tangent vector reflects the shear force. Compliant cofilactin filament bending introduces less shear force than equivalent bending of stiffer bare actin filaments. As a result, they sever at larger bending angles than bare filaments; cofilactin filaments must bend more to introduce comparable shear forces (Fig. 5).

To estimate the shear energy required to sever a filament, the shear work across the filament diameter ($d = 6$ nm) was calculated from the shear force at the critical severing angle. We estimate the shear energy associated with severing of an actin filament to be ~20 k_BT (Fig. 5), comparable to the standard free energy change associated with phalloidin-stabilized filament fragmentation ($\Delta G^\circ = 28.5\ k_BT$ (27)). The shear energy for cofilactin filament severing is estimated to be ~10 k_BT (Fig. 5), assuming a comparable shear displacement. In this study, filaments are constrained to fluctuate in two dimensions, so filament elastic free energy contributions (Eq. 9) originating from twist-bend coupling (41) are minimized and therefore not considered in the calculations. The mechanical properties of filaments partially decorated with cofilin are uncertain, so we did not attempt to calculate the shear force and work associated with bending at boundaries.

DISCUSSION

Isoform-dependent actin filament flexibility

Biochemical studies indicate that despite being 86% identical (94% homologous), yeast and vertebrate muscle actin filaments display distinct functional properties that have physiological significance, as substitution of yeast actin with vertebrate muscle actin is lethal (42). Yeast actin polymerizes (36,38), exchanges nucleotide (43), and releases P_i more rapidly (44) than vertebrate muscle actin. Yeast actin filaments "breathe" and bind phalloidin between adjacent subunits more rapidly (35), twist more readily (34), and fragment more easily (38) than vertebrate muscle actin filaments. Analysis of the bending fluctuations in this study (Fig. 1) indicates that yeast actin filaments are also more compliant in bending than vertebrate actin filaments, consistent with previous reports that they appear qualitatively less rigid (37). The enhanced yeast actin filament bending and twisting flexibility, structural dynamics, and susceptibility to fragmentation result from weaker inter- and intrasubunit filament contacts than in vertebrate actin filaments (41,45,46).

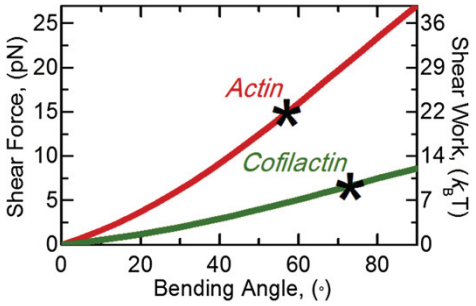

FIGURE 5 Calculated applied shear force from bending of actin and cofilactin filaments. Simulations of the equilibrium equations for an inextensible elastic filament with ends constrained by an applied bending angle are used to determine internal forces and moments. The projection of the internal force expressed at one-half the arc-length is the applied shear force (*left axis*) for a bare (*red*) or fully cofilin-decorated (*green*) actin filament from a bending angle. The applied shear force over the diameter of a filament (6 nm) is the applied shear work (*right axis*) from a bending angle and is an estimate of the energy required to sever a filament. (*Asterisks*) Estimated shear force and work associated with the critical severing angles (Fig. 4) for bare and fully cofilin-decorated actin filaments.

Enhanced filament compliance promotes severing by cofilin

Cofilin severing activity correlates with its effect on actin filament flexibility. Vertebrate cofilin binds but has minimal effects on yeast actin filament bending stiffness (Table 1) and does not sever them to an appreciable extent (Figs. 2 and 3). Yeast (*S. cerevisiae* and *S. pombe*) cofilin severs vertebrate actin filaments more efficiently than vertebrate cofilin—as determined by a decrease in the average filament length (Fig. 2 *G*; see (15,18) for *S. pombe cofilin* severing analysis)—and also increases the filament bending flexibility to a greater extent (Table 1). Yeast cofilin severs yeast actin filaments similarly to vertebrate actin filaments (Fig. 2 *G*) and yields comparable filament elasticities (Table 1).

Cofilin binding increases the radial mass of filaments. One would expect decorated filaments to be more stiff than bare ones because they have a larger geometric moment (47). However, cofilin lowers the filament stiffness, indicating that the apparent elastic modulus is lower and that the strength of filament inter- and intrasubunit contacts are compromised (8). The observation that vertebrate cofilin binds yeast actin filaments without altering their overall stiffness suggest that the mass contributions to the geometric moment are balanced by changes in the apparent elastic modulus.

Stress accumulation promotes severing at boundaries of bare and cofilin-decorated segments

We hypothesized that a local asymmetry in filament mechanics localizes stress from thermally driven shape fluctuations and promotes preferential severing at the boundaries of bare and cofilin-decorated segments along filaments (8,14). Bending vertex and hingelike motions are observed at breakage sites (Fig. 4), particularly at boundaries between bare and cofilin-decorated segments (Fig. 4 *C*). Consistent with stress accumulation promoting filament severing,

severing at boundaries coincides with a smaller critical angle for breakage (Fig. 4). That is, bending deformations at boundaries are irreversible at smaller angles than within homogenous (bare or fully decorated) filament segments.

The critical severing angle distribution of cofilactin filaments is bimodal (Fig. 4 *E*). A small fraction (~25%) of cofilactin severing events occurs with a critical angle comparable to bare actin (54 ± 4°); the majority of cofilactin severing events are at a larger critical angle (73 ± 7°). This bimodal distribution suggests that a fraction of cofilactin adopts a conformation with mechanical properties like that of native actin (7,48,49), and is consistent with multiple, isoenergetic cofilactin equilibrium conformations identified from spectroscopic (11) and kinetic (22,50) studies. A larger severing angle for cofilactin filaments is expected because enhanced elasticity will allow them to bend more under an equivalent load.

The shear force and work introduced by bending a bare actin filament is greater than on a cofilactin filament because the former is stiffer (Fig. 5). Consequently, cofilactin filaments bend more than bare filaments before severing (Fig. 4). We note that the shear work (~10 k_BT) at the cofilactin filament critical angle (73°) is approximately equal to that of a bare filament bent to the critical severing angle at boundaries of partially decorated filaments (31°). This observation suggests that boundaries have bare and cofilactin-like properties, namely the energetic stability (i.e., shear work needed to sever) of cofilactin and the stiffness (deformation needed to introduce a given shear force) of bare actin filaments.

Collectively, these measurements favor a mechanism in which enhanced filament elasticity with cofilin binding introduces a local asymmetry in filament topology and mechanics at boundaries of bare and cofilin-decorated segments that generates the accumulation of stress, thereby promoting filament severing (8,14,21). According to this mechanism, any mechanical barrier such as that introduced by myosin motors and cross-linking proteins (provided the filament binding densities do not completely inhibit cofilin binding (51)) would promote stress accumulation and severing by cofilin. In this manner, mechanical discontinuities along filaments act as stress accumulators, analogous to mechanical defects in nonprotein materials (Fig. 6 (14)).

We thank John A. Cooper (Washington University in St. Louis) for providing yeast cofilin and yeast actin used in the early stages of this work.

This work is supported by the American Heart Association (grant No. 0940075N awarded to E.M.D.L.C.), the National Institutes of Health (grant No. GM071688 and No. GM071688-03S1 awarded to E.M.D.L.C.), the Agence Nationale de la Recherche (grant No. ANR-08-Blanc-0012 awarded to L.B.), and the United States Public Health Service (grant No. USPHS GM077190 awarded to E.R.). B.R.M. was supported by American Heart Association predoctoral award No. 09PRE2230014. E.M.D.L.C. is an American Heart Association Established Investigator, and is a recipient of the National Science Foundation CAREER Award No. MCB-0546353 as well as being a Hellman Family Fellow.

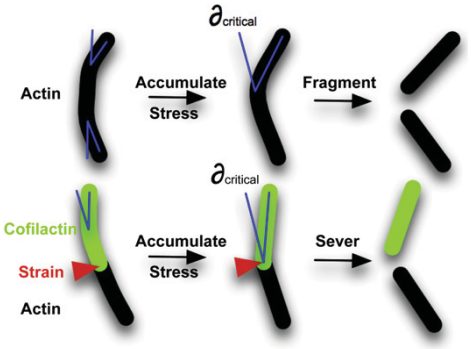

FIGURE 6 Model for cofilin-dependent actin filament severing. The strain required to fragment a filament is reached at a critical bending angle. A local gradient in filament bending mechanics localizes mechanical stress from thermal fluctuations at boundaries between bare and cofilin-bound segments which accumulates, thereby promoting the severing of filaments.

REFERENCES

1. Condeelis, J. 2001. How is actin polymerization nucleated in vivo? *Trends Cell Biol.* 11:288–293.
2. Michelot, A., J. Berro, …, L. Blanchoin. 2007. Actin-filament stochastic dynamics mediated by ADF/cofilin. *Curr. Biol.* 17:825–833.
3. Roland, J., J. Berro, …, J. L. Martiel. 2008. Stochastic severing of actin filaments by actin depolymerizing factor/cofilin controls the emergence of a steady dynamical regime. *Biophys. J.* 94:2082–2094.
4. Oser, M., and J. Condeelis. 2009. The cofilin activity cycle in lamellipodia and invadopodia. *J. Cell. Biochem.* 108:1252–1262.
5. Cao, W., J. P. Goodarzi, and E. M. De La Cruz. 2006. Energetics and kinetics of cooperative cofilin-actin filament interactions. *J. Mol. Biol.* 361:257–267.
6. McGough, A., B. Pope, …, A. Weeds. 1997. Cofilin changes the twist of F-actin: implications for actin filament dynamics and cellular function. *J. Cell Biol.* 138:771–781.
7. Galkin, V. E., A. Orlova, …, E. H. Egelman. 2001. Actin depolymerizing factor stabilizes an existing state of F-actin and can change the tilt of F-actin subunits. *J. Cell Biol.* 153:75–86.
8. McCullough, B. R., L. Blanchoin, …, E. M. De la Cruz. 2008. Cofilin increases the bending flexibility of actin filaments: implications for severing and cell mechanics. *J. Mol. Biol.* 381:550–558.
9. Pfaendtner, J., E. M. De La Cruz, and G. A. Voth. 2010. Actin filament remodeling by actin depolymerization factor/cofilin. *Proc. Natl. Acad. Sci. USA.* 107:7299–7304.
10. Sharma, S., E. E. Grintsevich, …, J. K. Gimzewski. 2011. Atomic force microscopy reveals drebrin induced remodeling of F-actin with subnanometer resolution. *Nano Lett.* 11:825–827.
11. Prochniewicz, E., N. Janson, …, E. M. De la Cruz. 2005. Cofilin increases the torsional flexibility and dynamics of actin filaments. *J. Mol. Biol.* 353:990–1000.
12. Pavlov, D., A. Muhlrad, …, E. Reisler. 2007. Actin filament severing by cofilin. *J. Mol. Biol.* 365:1350–1358.
13. De La Cruz, E. M. 2005. Cofilin binding to muscle and non-muscle actin filaments: isoform-dependent cooperative interactions. *J. Mol. Biol.* 346:557–564.
14. De La Cruz, E. M. 2009. How cofilin severs an actin filament. *Biophys. Rev.* 1:51–59.
15. Andrianantoandro, E., and T. D. Pollard. 2006. Mechanism of actin filament turnover by severing and nucleation at different concentrations of ADF/cofilin. *Mol. Cell.* 24:13–23.

16. Yeoh, S., B. Pope, …, A. Weeds. 2002. Determining the differences in actin binding by human ADF and cofilin. *J. Mol. Biol.* 315:911–925.

17. Bobkov, A. A., A. Muhlrad, …, E. Reisler. 2006. Cooperative effects of cofilin (ADF) on actin structure suggest allosteric mechanism of cofilin function. *J. Mol. Biol.* 356:325–334.

18. Chan, C., C. C. Beltzner, and T. D. Pollard. 2009. Cofilin dissociates Arp2/3 complex and branches from actin filaments. *Curr. Biol.* 19:537–545.

19. Northrop, J., A. Weber, …, T. P. Walsh. 1986. Different calcium dependence of the capping and cutting activities of villin. *J. Biol. Chem.* 261:9274–9281.

20. Grintsevich, E. E., S. A. Benchaar, …, E. Reisler. 2008. Mapping the cofilin binding site on yeast G-actin by chemical cross-linking. *J. Mol. Biol.* 378:540–550.

21. Suarez, C., J. Roland, …, L. Blanchoin. 2011. Cofilin tunes the nucleotide state of actin filaments and severs at bare and decorated segment boundaries. *Curr. Biol.* 21:862–868.

22. De La Cruz, E. M., and D. Sept. 2010. The kinetics of cooperative cofilin binding reveals two states of the cofilin-actin filament. *Biophys. J.* 98:1893–1901.

23. Cao, W., M. M. Coman, …, E. M. De La Cruz. 2011. Mechanism of MSS116 ATPase reveals functional diversity of dead-box proteins. *J. Mol. Biol.* 409:399–414.

24. Ha, T., I. Rasnik, …, S. Chu. 2002. Initiation and re-initiation of DNA unwinding by the *Escherichia coli* Rep helicase. *Nature.* 419:638–641.

25. Sept, D., J. Xu, …, J. A. McCammon. 1999. Annealing accounts for the length of actin filaments formed by spontaneous polymerization. *Biophys. J.* 77:2911–2919.

26. Carlsson, A. E. 2006. Stimulation of actin polymerization by filament severing. *Biophys. J.* 90:413–422.

27. Kinosian, H. J., L. A. Selden, …, L. C. Gershman. 1993. Actin filament annealing in the presence of ATP and phalloidin. *Biochemistry.* 32:12353–12357.

28. Berro, J., A. Michelot, …, J. L. Martiel. 2007. Attachment conditions control actin filament buckling and the production of forces. *Biophys. J.* 92:2546–2558.

29. Isambert, H., P. Venier, …, M. F. Carlier. 1995. Flexibility of actin filaments derived from thermal fluctuations. Effect of bound nucleotide, phalloidin, and muscle regulatory proteins. *J. Biol. Chem.* 270: 11437–11444.

30. Greenberg, M. J., C.-L. A. Wang, …, J. R. Moore. 2008. Modulation of actin mechanics by caldesmon and tropomyosin. *Cell Motil. Cytoskel.* 65:156–164.

31. ben-Avraham, D., and M. M. Tirion. 1995. Dynamic and elastic properties of F-actin: a normal-modes analysis. *Biophys. J.* 68:1231–1245.

32. Chu, J. W., and G. A. Voth. 2005. Allostery of actin filaments: molecular dynamics simulations and coarse-grained analysis. *Proc. Natl. Acad. Sci. USA.* 102:13111–13116.

33. Pfaendtner, J., D. Branduardi, …, G. A. Voth. 2009. Nucleotide-dependent conformational states of actin. *Proc. Natl. Acad. Sci. USA.* 106:12723–12728.

34. Prochniewicz, E., and D. D. Thomas. 1999. Differences in structural dynamics of muscle and yeast actin accompany differences in functional interactions with myosin. *Biochemistry.* 38:14860–14867.

35. De La Cruz, E. M., and T. D. Pollard. 1996. Kinetics and thermodynamics of phalloidin binding to actin filaments from three divergent species. *Biochemistry.* 35:14054–14061.

36. Kim, E., C. J. Miller, and E. Reisler. 1996. Polymerization and in vitro motility properties of yeast actin: a comparison with rabbit skeletal α-actin. *Biochemistry.* 35:16566–16572.

37. Kron, S. J., D. G. Drubin, …, J. A. Spudich. 1992. Yeast actin filaments display ATP-dependent sliding movement over surfaces coated with rabbit muscle myosin. *Proc. Natl. Acad. Sci. USA.* 89:4466–4470.

38. Buzan, J. M., and C. Frieden. 1996. Yeast actin: polymerization kinetic studies of wild type and a poorly polymerizing mutant. *Proc. Natl. Acad. Sci. USA.* 93:91–95.

39. Bergeron, E. W., R. Wedemeyer, …, H. L. Bartlett. 2011. Allele-specific effects of thoracic aortic aneurysm and dissection (TAAD) $\{\alpha\}$-smooth muscle actin mutations on actin function. *J. Biol. Chem.* 286:11356–11369.

40. Xu, J., J. F. Casella, and T. D. Pollard. 1999. Effect of capping protein, CapZ, on the length of actin filaments and mechanical properties of actin filament networks. *Cell Motil. Cytoskeleton.* 42:73–81.

41. De La Cruz, E. M., J. Roland, …, J. L. Martiel. 2010. Origin of twist-bend coupling in actin filaments. *Biophys. J.* 99:1852–1860.

42. McKane, M., K.-K. Wen, …, P. A. Rubenstein. 2006. Effect of the substitution of muscle actin-specific subdomain 1 and 2 residues in yeast actin on actin function. *J. Biol. Chem.* 281:29916–29928.

43. Chen, X., R. K. Cook, and P. A. Rubenstein. 1993. Yeast actin with a mutation in the "hydrophobic plug" between subdomains 3 and 4 (L266D) displays a cold-sensitive polymerization defect. *J. Cell Biol.* 123:1185–1195.

44. Yao, X., and P. A. Rubenstein. 2001. F-actin-like ATPase activity in a polymerization-defective mutant yeast actin (V266G/L267G). *J. Biol. Chem.* 276:25598–25604.

45. Orlova, A., X. Chen, …, E. H. Egelman. 1997. Modulation of yeast F-actin structure by a mutation in the nucleotide-binding cleft. *J. Mol. Biol.* 271:235–243.

46. Stokasimov, E., and P. A. Rubenstein. 2009. Actin isoform-specific conformational differences observed with hydrogen/deuterium exchange and mass spectrometry. *J. Biol. Chem.* 284:25421–25430.

47. Gittes, F., B. Mickey, …, J. Howard. 1993. Flexural rigidity of microtubules and actin filaments measured from thermal fluctuations in shape. *J. Cell Biol.* 120:923–934.

48. Orlova, A., A. Shvetsov, …, E. Reisler. 2004. Actin-destabilizing factors disrupt filaments by means of a time reversal of polymerization. *Proc. Natl. Acad. Sci. USA.* 101:17664–17668.

49. Kozuka, J., H. Yokota, …, T. Yanagida. 2006. Dynamic polymorphism of single actin molecules in the actin filament. *Nat. Chem. Biol.* 2: 83–86.

50. Kueh, H. Y., W. M. Brieher, and T. J. Mitchison. 2008. Dynamic stabilization of actin filaments. *Proc. Natl. Acad. Sci. USA.* 105:16531–16536.

51. Schmoller, K. M., C. Semmrich, and A. R. Bausch. 2011. Slow down of actin depolymerization by cross-linking molecules. *J. Struct. Biol.* 173:350–357.

52. Bobkov, A. A., A. Muhlrad, …, E. Reisler. 2002. Structural effects of cofilin on longitudinal contacts in F-actin. *J. Mol. Biol.* 323:739–750.

Chapter 4

Supplemental Information

INTRODUCTION

In this chapter, we examined the change in persistence length of both vertebrate and yeast F-actin upon binding of vertebrate and yeast cofilin. Although yeast actin filaments are more compliant in bending than vertebrate actin filaments, we observed that human cofilin 1 (hCof1) binds to yeast actin filaments but neither increases filament flexibility nor severs them. In contrast, yeast cofilin is able to increase filament flexibility of both skeletal and yeast actin while efficiently severing them, thereby allowing us to correlate severing activity with changes in filament flexibility. Consistent with previous models, cofilin severing is maximal under subsaturating conditions (1, 2) and scales with the density of boundaries between bare and cofilin-decorated segments (3, 4). Imaging of filament thermal fluctuations reveals that severing events are associated with local bending and fragmentation when deformations attain a critical angle. These measurements support a cofilin-severing mechanism in which mechanical asymmetry promotes local stress accumulation and fragmentation at boundaries of bare and cofilin-decorated segments.

Previous results have also shown a dependence of severing on different cofilin isoforms. For example, *S. pombe* cofilin severs skeletal actin filaments more rapidly than human cofilin at optimal concentrations (2). Other proteins in the ADF family also possess different severing activities under different conditions. For example, budding yeast twinfilin, which has two ADF homology domains, severs *in vitro* only at low pH (5), unlike yeast cofilin, which exhibits pH-independent severing (6).

Using TIRF microscopy, we examined further severing of different actin isoforms by different cofilin isoforms in an effort to understand the differences in severing activities. Yeast

cofilin is an effective severer of yeast actin at low ratios of cofilin to actin and continues to sever even at high ratios. In contrast, hCof1 is not an effective severer of yeast actin at low ratios but is able to sever filaments when added in large excess, contradicting previous observations that severing occurs only, or mainly, at subsaturating conditions. EM image analysis of yeast F-actin decorated with hCof1 shows filament twist of ~162° i.e., the same as the twist induced by yeast cofilin. Because the same hcof1 severs skeletal actin filaments (albeit at slower rate than yeast cofilin), our results raise questions about actin filament properties that contribute to their severing by cofilins.

METHODS

All proteins and reagents were obtained as described previously in the manuscript.

Total Internal Reflective Fluorescence (TIRF) Microscopy

Experiments were executed as described in the manuscript, with a few exceptions. To measure length distributions in a bulk assay, actin was first polymerized in F-buffer (10 mM imidazole, 2 mM $MgCl_2$, 50 mM KCl, 1 mM EGTA, 0.2 mM ATP, 1 mM DTT, pH 6.8). F-actin was then diluted to 1 μM with the addition of cofilin, and allowed to react for 1 minute before dilution into F-buffer containing 100-fold molar excess of phalloidin. Filaments were immobilized on poly-Lysine coated coverslips. Fiji software was used to analyze the filaments.

Electron Microscopy (EM) Reconstructions

Actin filament twist in the presence and absence of yeast cofilin and human cofilin-1 was obtained from the analysis of electron microscopy images of these filaments. F-actin was incubated with either yeast cofilin or human cofilin-1 at a 1:1 ratio and applied to carbon-coated grids. Grids were stained with 1% uranyl acetate and analyzed as previously described (7).

SUPPLEMENTAL DATA

We examined previously the change in persistence length of both vertebrate and yeast F-actin upon binding of vertebrate and yeast cofilin. Although yeast actin filaments are more compliant in bending than vertebrate actin filaments, we observed that human cofilin-1 (hCof1) binds to yeast actin filaments but neither increases filament flexibility nor severs them. In contrast, yeast cofilin increases the flexibility of both skeletal and yeast actin filaments, while efficiently severing them, thereby allowing us to correlate severing activity with changes in filament flexibility. Consistent with previous models, cofilin severing is maximal under subsaturating conditions (1) and scales with the density of boundaries between bare and cofilin-decorated segments (3).

Using TIRF microscopy, we examined more extensively the severing of filaments of different actin isoforms by different cofilin isoforms. We measured the severing rates (cuts/μm·sec) for yeast actin with increasing concentrations of either yeast cofilin or hCof1 and also compared these rates to the rates of hCof1 severing of skeletal actin (Figure 1). We found that yeast cofilin is an effective severer of yeast F-actin at low ratios of cofilin to actin and continues to sever even at high ratios. In contrast, hCof1 is not an effective severer of yeast F-actin at low ratios but is able to sever filaments when added in excess, contradicting previous observations that severing occurs only, or mainly, under subsaturating conditions. Severing is also enhanced, although to a lesser extent than with yeast cofilin, when hCof1 is incubated with skeletal actin. This raises questions to what extent severing is cofilin-isoform dependent or actin-isoform dependent.

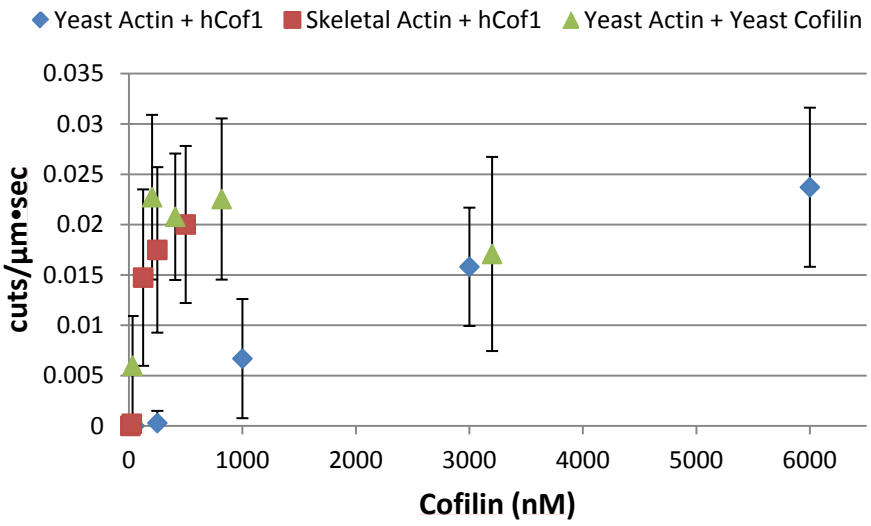

Figure S1. Severing rates of skeletal and yeast actin by yeast cofilin and human cofilin1 (hCof1). Filament severing was monitored via TIRF microscopy. A final concentration of 250 nM actin was flowed into chambers; cofilins were introduced at the indicated concentrations. Consecutive images were processed using Fiji software and severing rates were measured as the number of cuts made per µm of filament length per second. Yeast cofilin at low concentrations (50 nM) severs yeast actin filaments effectively. At low concentrations, human cofilin severs skeletal actin at slower rates than yeast cofilin; at higher concentrations, the two cofilins sever skeletal F-actin at similar rates. The severing of yeast actin filaments by human cofilin proceeds efficiently only at much higher concentrations than with yeast cofilin.

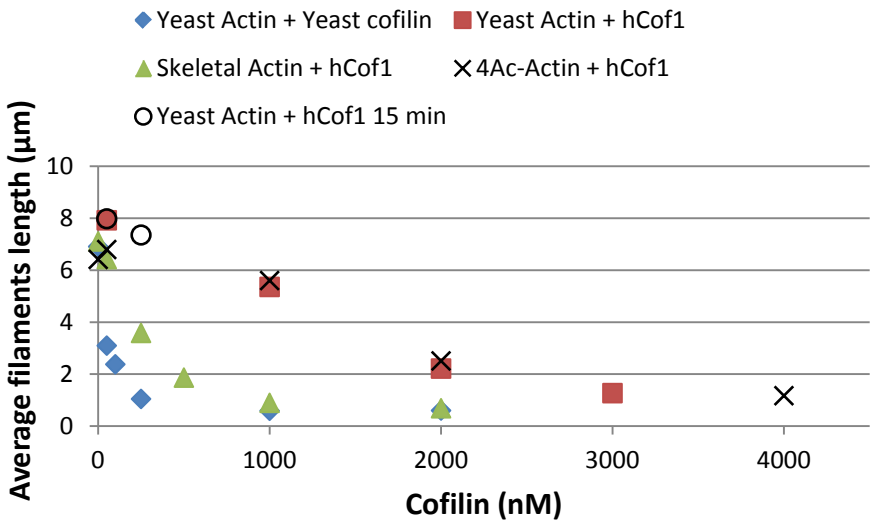

Figure S2. The average length of yeast actin filaments shortens at high concentrations of hCof1. 1 µM actin was incubated for one minute with cofilin (at the indicated concentrations) before immobilization on poly-Lys coverslips. Filament images were obtained with TIRF microscopy and analyzed using Fiji software. On average, filament shortening occurred at low concentrations of yeast cofilin added to yeast actin and hCof1 added to skeletal actin. Filament shortening was more evident at equimolar concentrations for hCof1 for both WT yeast actin and its 4 acidic N-teminal mutant.

We were able to correlate the real-time severing data with measurements of filament length in bulk assays. The average filament length decreases with increasing amounts of either cofilin (Figure 2). Incubation of hCof1with yeast F-actin resulted in an average filament length similar to the control at low concentrations of hCof1, but the average filament length decreased significantly at higher concentrations of hCof1, correlating with the real-time severing data. Yeast cofilin on yeast F-actin and hCof1 on skeletal F-actin exhibited the same effect but at lower concentrations. The distributions of filament lengths supports the severing data, showing the existence of filaments <1μm at high concentrations of cofilin (Figure 3 and 4). Although previous data showed similar binding affinities for both hCof1 and yeast cofilin to yeast F-actin, we incubated hCof1 with yeast F-actin for 15 minutes instead of 1 minute to ensure equilibration. At low concentrations, the average filament length remained similar to the control indicating little severing even with a longer incubation time. Therefore, we conclude that the differences in severing are dependent on concentrations rather than binding affinities. Because hCof1 severs skeletal F-actin better than yeast F-actin, we used a yeast actin mutant with four acidic residues at the N-terminus (Met-Asp-Glu-Asp-Glu-Val; obtained as previously described (8) to mimic the sequence of skeletal actin. The motivation for that test was the previous observation on cofilin cross-linking (by EDC) to the N-terminal acidic residues on skeletal actins (9). Using this yeast actin mutant (4Ac-actin), we observed similar length distributions as with wild-type yeast actin indicating that the N-terminus of actin is not relevant to the severing of actin by cofilin.

Because we are able to observe severing by both yeast cofilin and hCof1, we used EM reconstructions to measure the twist of F-actin decorated with saturating concentrations of cofilin. Yeast F-actin decorated with either hCof1 or yeast cofilin resulted in a twist of ~162° relative to adjacent subunits (Figure 5) suggesting that hCof1 and yeast cofilin induce similar

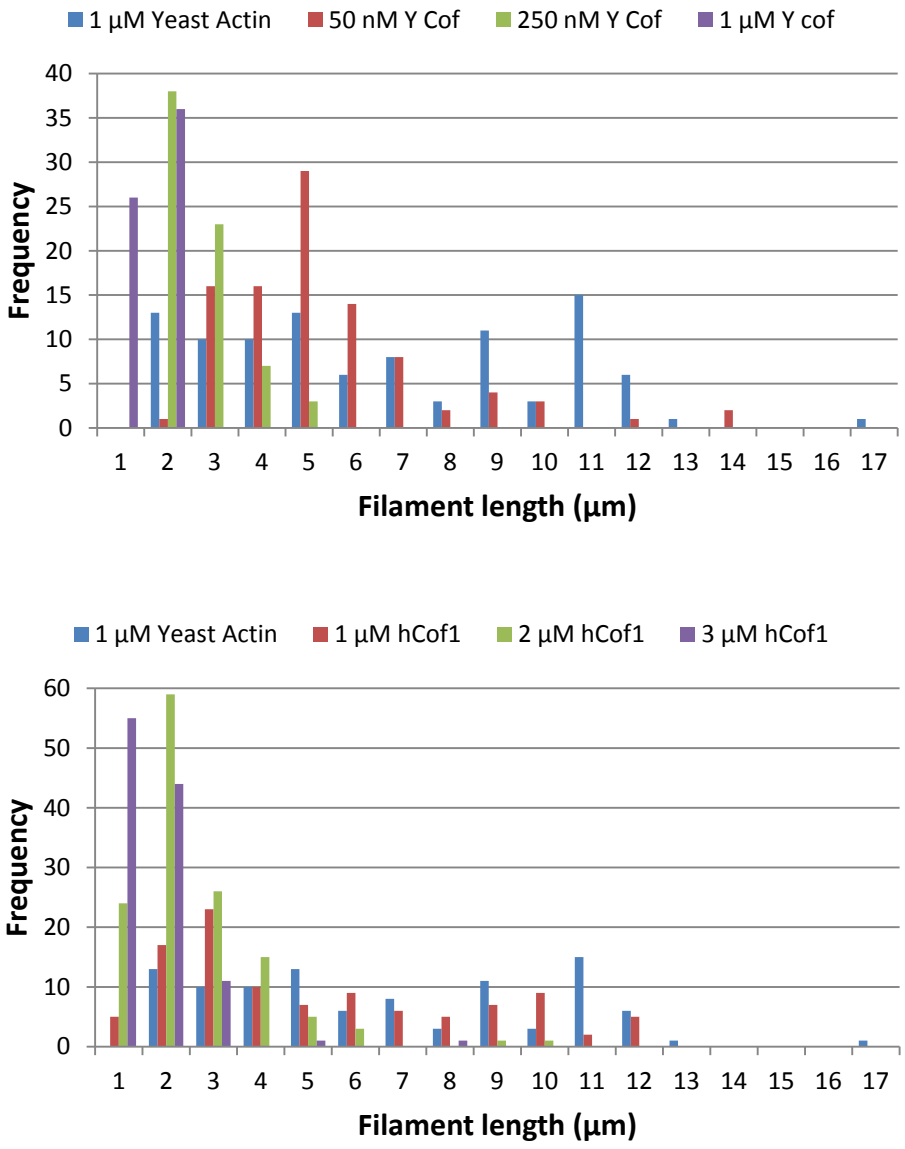

Figure S3. Filament length distributions for yeast actin incubated at different concentrations with either yeast cofilin or human cofilin1 (hCof1). A. The frequency of filaments shorter than 6 µm is evident with incubation of 50 nM yeast cofilin. Filaments are shorter than 3 µm after incubation with 1 µM yeast cofilin. B. The number of short filaments increases upon incubation with 1 µM hCof1. Further shortening of yeast actin filaments occurs upon their incubation with 3 µM hCof1.

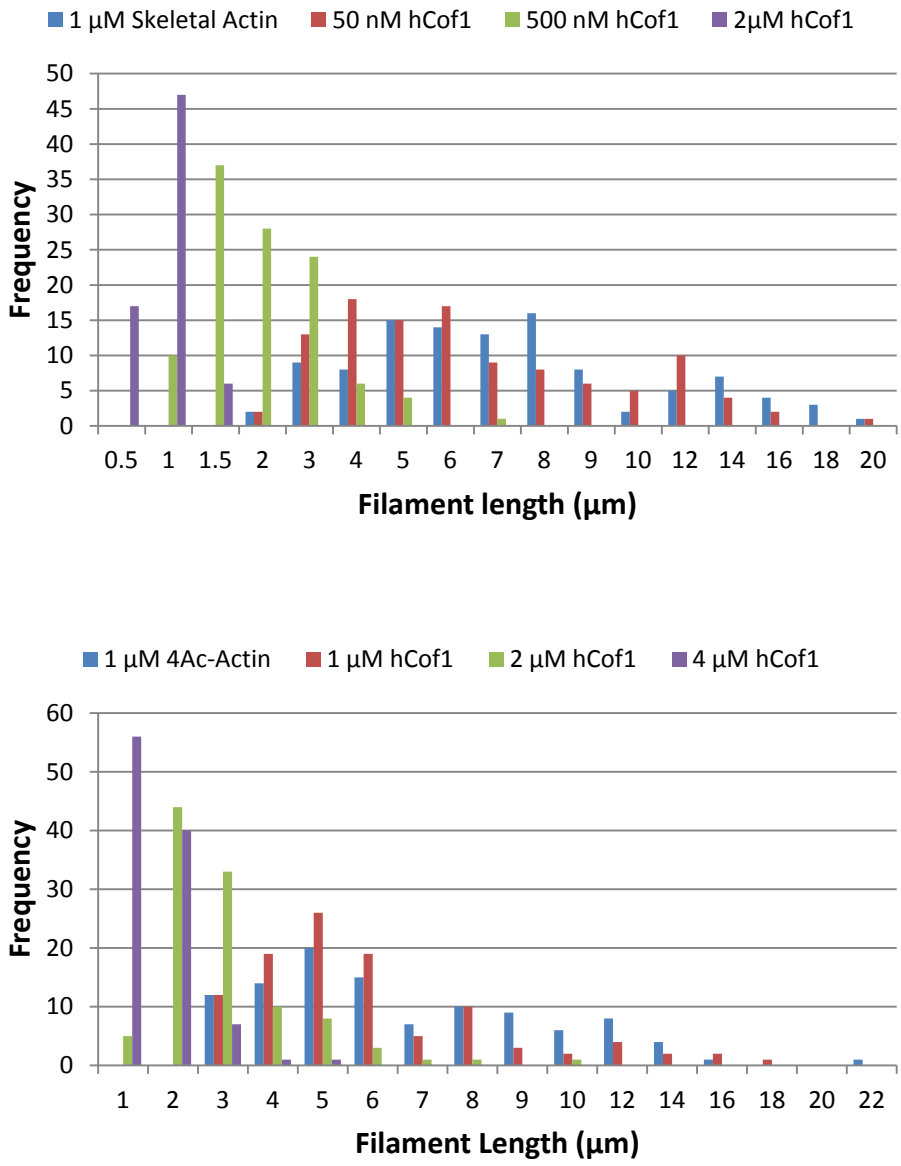

Figure S4. Filament length distributions for skeletal actin and the N-terminal acidic yeast actin mutant (4Ac-actin) incubated with increasing amounts of human cofilin1 (hCof1). A. The number of short filaments of skeletal actin increases with their incubation with 500 nM hCof1, and continues to increase upon incubation with 2 µM hCof1. B. The number of short 4Ac-actin filaments increases with their incubation with 2 µM hCof1 and 4 µM hCof1.

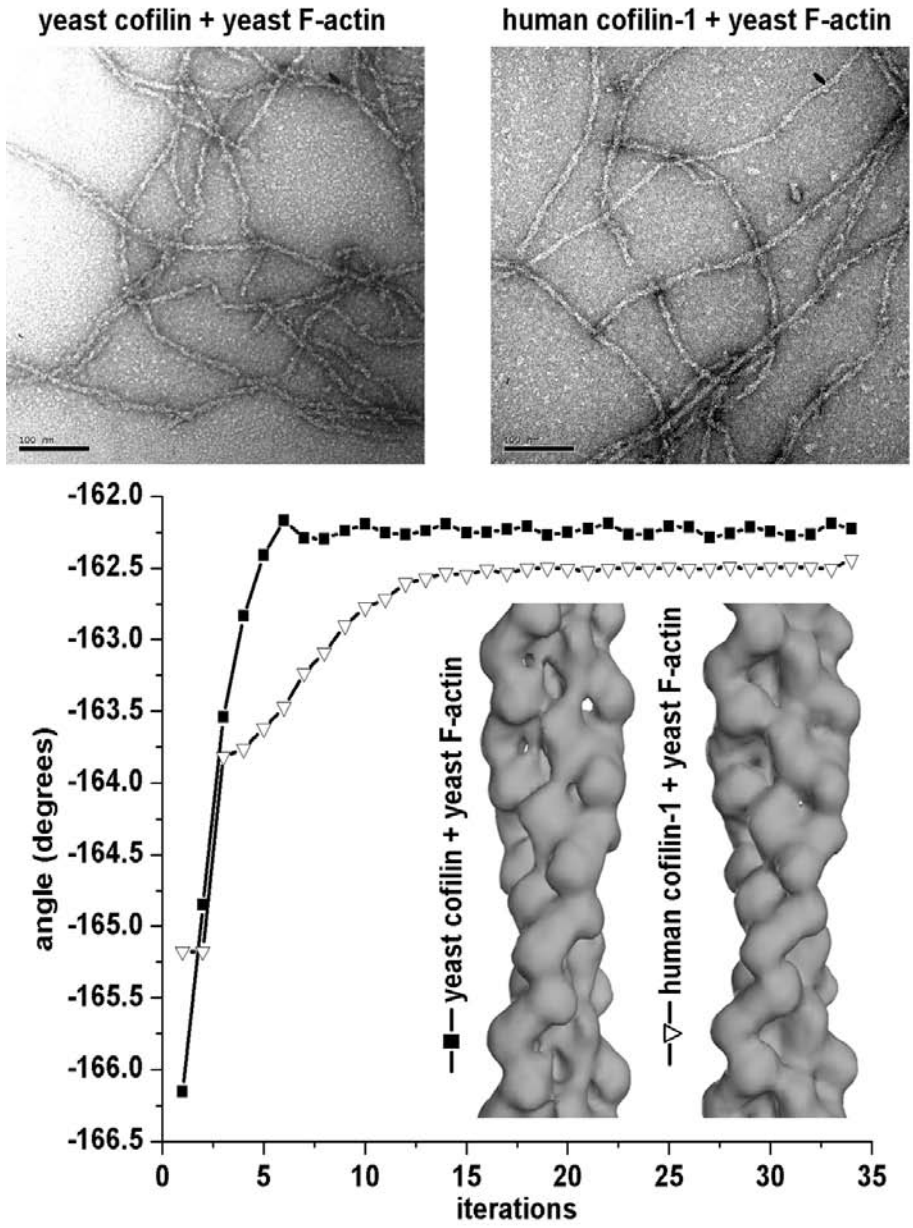

Figure S5. Comparison of F-actin twist in the presence of either yeast cofilin or human cofilin-1. A. Representative EM images of F-actin decorated with either yeast cofilin or human cofilin-1 are shown. B. Stereo views of the 3D reconstructions of F-actin decorated with either yeast cofilin or human cofilin-1 are shown. The twist in F-actin in the presence of both cofilins is close to -162°.

structural changes in yeast actin. If hCof1 can sever filaments, exhibit similar binding affinities to yeast cofilin on yeast F-actin, and induce a similar twist change in F-actin, then why is yeast cofilin a more efficient severer of yeast actin at lower ratios? Initial results with human cofilin 2 (hCof2), the major form in muscle, suggest that hCof2 is a more efficient severer than hCof1 at lower ratios (not shown). Sequence alignment of the two hCof isoforms indicates their ~80% identity. Most of the unconserved amino acid substitutions reside in the C-terminus of the sequences. Although none of the substitutions have been implicated to be critical in F-actin binding (10), the C-terminus of cofilin is involved in critical contacts with subdomain 3 in F-actin. Ono et al (11) also showed the importance of the C-terminus in cofilin to the interaction with F-actin using UNC-60B, the nematode isoform of ADF/cofilin. In their studies, they found the C-terminus to be in close proximity to subdomain 2 of actin. Thus, it would be interesting to mutate residues in the C-terminus of hCof1 and test for alterations in its severing rates.

Our initial results also contradict previous data of severing occurring mainly at subsaturating concentrations of cofilin (2), which leads us to question what other factors that are involved in the ability of hCof1 to sever filaments. We have observed that a change in twist correlates with severing, consistent with previous data (12). Cooperativity effects also contribute to severing (3). Can filaments still break in regions where cofilin is bound? Pavlov et al (1) showed that the maximum severing rate occurs at a 1:2 cofilin to actin molar ratio, suggesting that severing occurs at a site neighboring cofilin-bound actin. They also proposed that multiple tethering sites on a glass surface cannot dissipate strain induced by cofilin binding, thus promoting severing. Although we cannot completely eliminate tethering to a glass surface as a contributing factor to severing, our results showing severing at high concentrations of cofilin merit consideration of alternative mechanisms of severing. Real-time fluorescence assays with

labeled cofilin and actin should provide further insight into this apparent contradiction between the severing of yeast actin filaments by hCof1 and yeast cofilin. In addition, mutations in the additional loops seen in human cofilin that are not present in yeast cofilin may also shed some conclusions on the differences in severing activity.

REFERENCES

1. Pavlov, D.; Muhlrad, A.; Cooper, J.; Wear, M.; Reisler, E., *Journal of Molecular Biology* **2007,** 365, (5), 1350-1358.
2. Andrianantoandro, E.; Pollard, T. D., *Molecular Cell* **2006,** 24, (1), 13-23.
3. Bobkov, A. A.; Muhlrad, A.; Pavlov, D. A.; Kokabi, K.; Yilmaz, A.; Reisler, E., *Journal of Molecular Biology* **2006,** 356, (2), 325-334.
4. De La Cruz, E. M., *Journal of Molecular Biology* **2005,** 346, (2), 557-564.
5. Moseley, J. B.; Okada, K.; Balcer, H. I.; Kovar, D. R.; Pollard, T. D.; Goode, B. L., *Journal of Cell Science* **2006,** 119, (8), 1547-1557.
6. Pavlov, D.; Muhlrad, A.; Cooper, J.; Wear, M.; Reisler, E., *Cell Motility and the Cytoskeleton* **2006,** 63, (9), 533-542.
7. Galkin, V. E.; Orlova, A.; Kudryashov, D. S.; Solodukhin, A.; Reisler, E.; SchrÃ¶der, G. F.; Egelman, E. H., *Proceedings of the National Academy of Sciences* **2011,** 108, (51), 20568-20572.
8. Cook, R. K.; Blake, W. T.; Rubenstein, P. A., *Journal of Biological Chemistry* **1992,** 267, (13), 9430-9436.
9. Mannherz, H. G.; Ballweber, E.; Galla, M.; Villard, S.; Granier, C.; Steegborn, C.; Schmidtmann, A.; Jaquet, K.; Pope, B.; Weeds, A. G., *Journal of Molecular Biology* **2007,** 366, (3), 745-755.
10. Wong, D. Y.; Sept, D., *Journal of Molecular Biology* **2011,** 413, (1), 97-105.
11. Ono, S.; McGough, A.; Pope, B. J.; Tolbert, V. T.; Bui, A.; Pohl, J.; Benian, G. M.; Gernert, K. M.; Weeds, A. G., *Journal of Biological Chemistry* **2001,** 276, (8), 5952-5958.

12. McGough, A.; Pope, B.; Chiu, W.; Weeds, A., *The Journal of Cell Biology* **1997,** 138, (4), 771-781.

Chapter 5

Cofilin induced changes in F-actin mapped by cross-linking with benzophenone-4-maleimide

ABSTRACT

Cofilin belongs to the actin depolymerizing factor (ADF)/cofilin family and plays a key role in actin dynamics by promoting disassembly and assembly of actin filaments. Cofilin has been shown to decorate the side of actin filaments (F-actin) and promote the displacement and disordering of subdomain 2 of actin. Here, we show evidence of cofilin binding to F-actin and promoting a structural change in the actin filament, thus causing a switch in cross-linking sites. Benzophenone-4-maleimide, which normally promotes intramolecular cross-linking in F-actin, cross-links F-actin intermolecularly upon cofilin binding. We mapped the cross-linking sites and found that in the absence of cofilin, intramolecular cross-linking occurs between residues Cys374 and Asp11. In contrast, the presence of cofilin causes intermolecular cross-linking between residues Cys374, located within subdomain 1 of the upper protomer, and Met44, located in subdomain 2 of the lower protomer. Finally, we measured the dissociation rates of cofilin from both uncross-linked and cross-linked actin and find that cofilin dissociates from cross-linked actin significantly slower than from uncross-linked actins, suggesting a lack of filament flexibility and increased cofilin-actin interactions.

INTRODUCTION

Rapid remodeling of the actin cytoskeleton is essential for many cellular processes in eukaryotic organisms including cell motility, differentiation, and division. Proteins belonging to the actin-depolymerizing factor (ADF)/cofilin family play a key role in regulating actin dynamics (1). As the name implies, ADF/cofilin is able to enhance actin treadmilling by binding to ADP-actin with high affinity and promoting disassembly of actin filaments (F-actin) from the pointed-end. Cofilin is also able to bind to the side of F-actin, promoting severing and thus, creating more ends for depolymerization or polymerization (2, 3). Because cofilin plays a complex role in actin dynamics, cofilin is a ubiquitous protein and can associate, for example, with the entire lamellipodium. A detailed understanding of the global and local effects on F-actin by cofilin is still lacking due to cofilin's nucleation activity. Therefore, it is interesting to study cofilin's interaction with F-actin at a structural level.

Prior to the most recent ~9 Å resolution model of cofilin bound to F-actin (4), several groups have mapped the binding sites of cofilin onto both G and F-actin via mutagenesis, fluorescence probing, and chemical cross-linking in an effort to understand cofilin's functions (5-9). Grintsevich et al. (5) concluded that cofilin binds to the hydrophobic cleft between subdomains 1 and 3 on G-actin, which coincides with previous models (10-11). The atomic structure of the C-terminal ADF homology domain of twinfilin in complex with G-actin also supports binding between subdomains 1 and 3 of G-actin. The ADF homology domain inserts an alpha-helix into the hydrophobic cleft in a similar manner to gelsolin and WH2 domain proteins (12). The structure of cofilin-G-actin provides insight into the mechanism for ADF depolymerization of actin through the weakening of intrafilament interactions. EM reconstructions, chemical cross-linking, and molecular dynamic (MD) simulations also lead to a

model of the cofilin/F-actin complex (10, 13-16). Galkin et al. (4) showed that cofilin binding displaces substantially the subdomain 2 of actin and results in its disordering, thus disrupting interprotomer contacts. The disordering of subdomain 2 caused by cofilin binding leads to a four-fold increase in F-actin flexibility (17).

Here, we provide experimental evidence derived from actin cross-linking by benzophenone-4-maleimide (BPM) for two types of structural transitions in actin: one associated with actin polymerization into filaments, and the other coupled to coflin binding to F-actin. Although cross-linking captures changes that normally reflect contact-induced modification of specific sites, it is believed that actin polymerization prompts intramolecular changes as well.

Previous results from Tao et al. (18) showed little or no cross-linking in G-actin after Cys374 labeling with BPM. However, intramolecular BPM cross-linking was detected after G-actin polymerization into F-actin. We confirm here this observation and map the intramolecular cross-link in F-actin to Cys374 and Asp11. Binding of cofilin to F-actin replaces this intramolecular cross-link with an intermolecular cross-link from Cys374 to Met44. We also report differences in dissociation of cofilin from cross-linked and uncross-linked F-actin indicative of the need for filament flexibility in cofilin dissociation. Cofilin induced conformational changes may help elucidate the local and global changes that occur in F-actin and destabilize certain interprotomer contacts.

METHODS

Materials

Benzophenone-4-maleimide and acrylodan were obtained from Molecular Probes (Eugene, OR). Millipore-filtered water and analytical-grade reagents were used in all experiments.

Protein purification and labeling

Actin was purified from acetone powder of rabbit skeletal muscle as described previously (19). Recombinant *S. cerevisiae* wild type and cofilin-1 mutant (G1C and C62S) in pBAT4 vector were expressed and purified as described (5) with slight modifications. Cofilin-1 was labeled with acrylodan by first passing cofilin-1 through a Zeba Desalt Spin Column (Pierce) equilibrated with 10 mM Tris pH 8.0. Cofilin-1 was labeled at 1 mg/mL with a three time molar excess of acrylodan and incubated on ice for 2 hours. The reaction was stopped with 1 mM DTT and the protein was dialyzed overnight in 5 mM Hepes pH 7.5 and 1 mM DTT to remove excess label. Labeling efficiency was characterized by using an adjusted extinction coefficient determined as before (20) with slight modifications. The absorbance of acrylodan was measured first in methanol (ε = 20000 M^{-1} cm^{-1}, λ_{max} = 391 nm) (Molecular Probes, The Handbook) and then under denaturing conditions with 6 M guanidine-HCl (λ_{max} = 411 nm). The absorbance ratio [A_{max}(methanol)/A_{max}(Gu-HCl)=1.5] was used to correct the extinction coefficient determined in methanol for denaturing conditions (20000 M^{-1} cm^{-1}/1.5 = 13333 M^{-1} cm^{-1}). Cofilin-1 concentration was measured by the Bradford assay using wild-type cofilin as a standard.

BPM and ANP cross-linking

BPM and ANP cross-linking were performed as described previously (20, 21) with a few modifications. For BPM cross-linking, DTT was removed from G-actin with a PD-10 column (GE Healthcare) equilibrated with G-buffer (5 mM Tris pH 8.0, 0.2 mM $CaCl_2$, 0.4 mM ATP). BPM and actin (at 2:1 ratio) were incubated overnight at 4°C. Labeled G-actin was passed through a PD-10 column equilibrated with G-buffer (5 mM Hepes pH 7.5, 0.2 mM $CaCl_2$, 0.2 mM ATP) to remove excess label. Labeled actin was polymerized with 2 mM $MgCl_2$ and 50 mM KCl for 30 minutes at room temperature. Cofilin-1 was passed through Zeba Desalt Spin Columns equilibrated with G-buffer. Labeled actin was incubated with and without DTT-free cofilin and cross-linked under UV light (365 nm) for up to 90 minutes. The reaction was stopped with DTT.

BPM cross-linked dimers were further purified over a Sephacryl S200 HR gel filtration column (GE Healthcare) equilibrated with G-buffer and eluted at a rate of 0.2 mL/min.

Electron microscopy

For actin filament visualization, all samples were diluted to 2 µM in F-buffer (10 mM Tris pH 8.0, 2 mM $MgCl_2$, 100 mM KCl, 0.2 mM ATP) and deposited on 400-mesh carbon-coated copper grids coated with formvar film (Ted Pella Inc., CA). Samples were allowed to adsorb for 60 seconds and then negatively stained with 1% uranyl acetate (w/v) for 45 seconds. Grids were observed with a JEM-1200EX (JEOL) electron microscope operated at 80 kV and magnification in the 80,000-100,000× range. The images were analyzed using IMAGE J software.

Mass spectrometry

After tryptic in-gel proteolysis, online peptide sequencing was accomplished by liquid chromatography-tandem mass spectrometry (LC-MS/MS) on a quadrupole time-of-flight Applied Biosystems (Foster City, CA) QSTAR XL (QqTOF) mass spectrometer. The nano-LC was equipped with an LC Packings PepMap C18 precolumn (300 µm × 5 mm) and an LC Packings PepMap C18 column (75 µm × 150 mm). The eluents used for the LC were (A) 5% acetonitrile (ACN)/water containing 0.1% formic acid (FA) and 0.01% trifluoroacetic acid (TFA) and (B) 95% ACN/water acid containing 0.1% FA and 0.01% TFA. The flow rate was 200 nL/min, and the following gradient was used: 5% B to 35% B in 15 min then 35% B to 80% B in 4 min, and then maintained at 80% B for 9 min. The column was re-equilibrated with 5% B for 14 min before the next run. For online MS and MS/MS analyses, a New Objective (Woburn, MA) Pico Tip (i.d. 8 µm) was used for spraying with the voltage set at 2 kV. The MS/MS fragmentation spectrum of cross-linked peptides was analyzed using the MS2Assign Automatic Structure Assignment Program (ASAP) (22).

Co-sedimentation Assays

Actin was polymerized in F-buffer (pH 6.8). Actin and cofilin were mixed at equimolar ratios. Reactions were incubated for at least 30 minutes. Reactions were pelleted in an OPTIMA-TLX120 ultracentrifuge at 300,000 × g for 30 minutes, at 4°C. The pellet and supernatant were separated and run on SDS-PAGE for analysis. Scion imager was used to quantify the Coomassie-stained bands on the gel.

Analysis of Binding

Transient kinetic measurements were made at 25(±0.1)°C with an Applied Photophysics (Surrey, U.K.) SX.18MV stopped-flow apparatus. The excitation wavelength was set to 390 nm and the emission was monitored at 90° through a 435 nm long-pass colored glass filter. Time-courses of non-contiguous binding were measured by mixing acrylodan cofilin (1-5 μM) with 10 μM of actin filaments in F-buffer (pH 6.8). Time-courses of cofilin dissociation were measured by mixing an equilibrated mixture of acrylodan cofilin and actin filaments (5 μM) with 50 μM unlabelled cofilin. The indicated concentrations are final concentrations after mixing. Time-courses of fluorescence change were fitted to single exponentials by non-linear least squares fitting using software provided with the instrument. Standard errors in the fits are reported.

Dissociation rates from cross-linked actins were measured through an Alphascan fluorimeter (Photon Technology International). The excitation wavelength was set to 390 nm and emission detected at 505 nm. Conditions were the same as the control above. Fluorescence changes were fitted to single exponentials using SigmaPlot software.

RESULTS

Actin crosslinking by BPM changes in the presence of cofilin

Previous results from Tao et al. (18) showed site-specific photocrosslinking of F-actin with benzophenone-4-maleimide (BPM). In the presence of BPM, G-actin displays only slight intrasubunit crosslinking. In contrast, F-actin forms intrasubunit as well as some intersubunit crosslinking upon photoactivation. The maleimide moiety on BPM reacts efficiently with Cys374 on actin while its benzophenone (BP) moiety photoreacts with amino acids nonselectively, but with high yield. We thus can monitor the change and extent of F-actin crosslinking upon binding by various actin binding proteins.

F-actin was labeled with BPM and exposed to an equimolar concentration of yeast cofilin. The F-actin control formed intrasubunit cross-linking as previously shown (Figure 1). After photoactivation in the presence of cofilin, F-actin formed extensive intermolecular cross-links and virtually no intramolecular cross-links as compared with F-actin alone. A cofilin-induced switch from intramolecular to intermolecular cross-links in F-actin suggests a modification of the F-actin structure that allows for its extensive cross-linking.

Actin filaments formed from BPM crosslinked dimers are normal

To ensure that the BPM cross-linked dimers could be properly incorporated into a filament, we first purified BPM cross-linked dimers formed in the presence of cofilin via gel filtration. We then polymerized the cross-linked dimers in F-buffer. EM images comparing incorporation of cross-linked dimers and uncross-linked actin into a filament show little

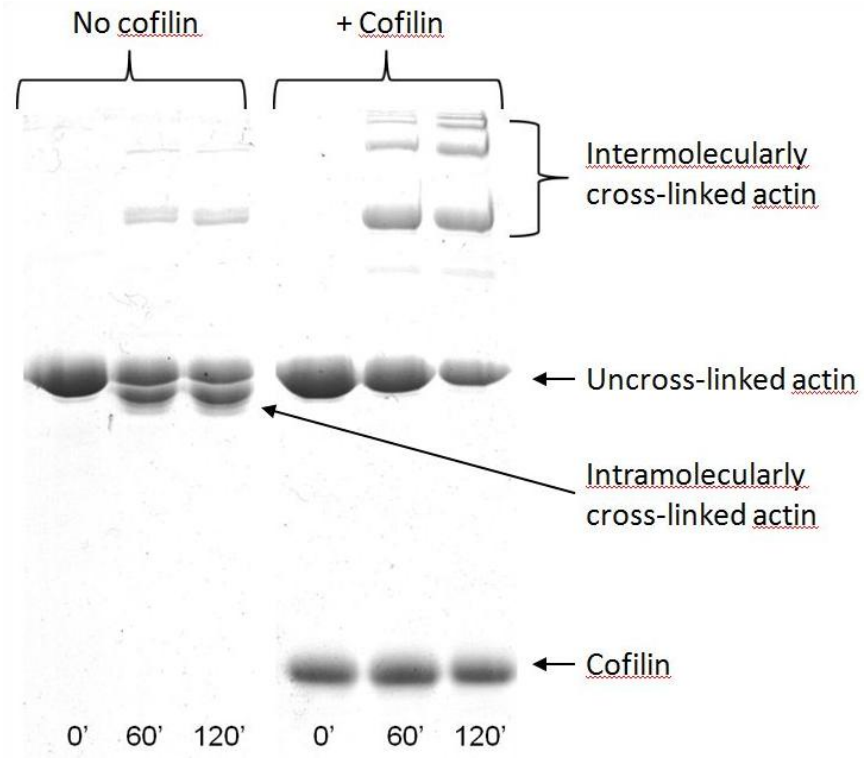

Figure 1. Cofilin causes a switch from intramolecular to intermolecular cross-linking by BPM (benzophenone maleimide) in F-actin. Cross-linking products are shown at time points of 0, 60 and 120 minutes after photoactivation of BPM. Cross-linking reaches maximum in 120 minutes.

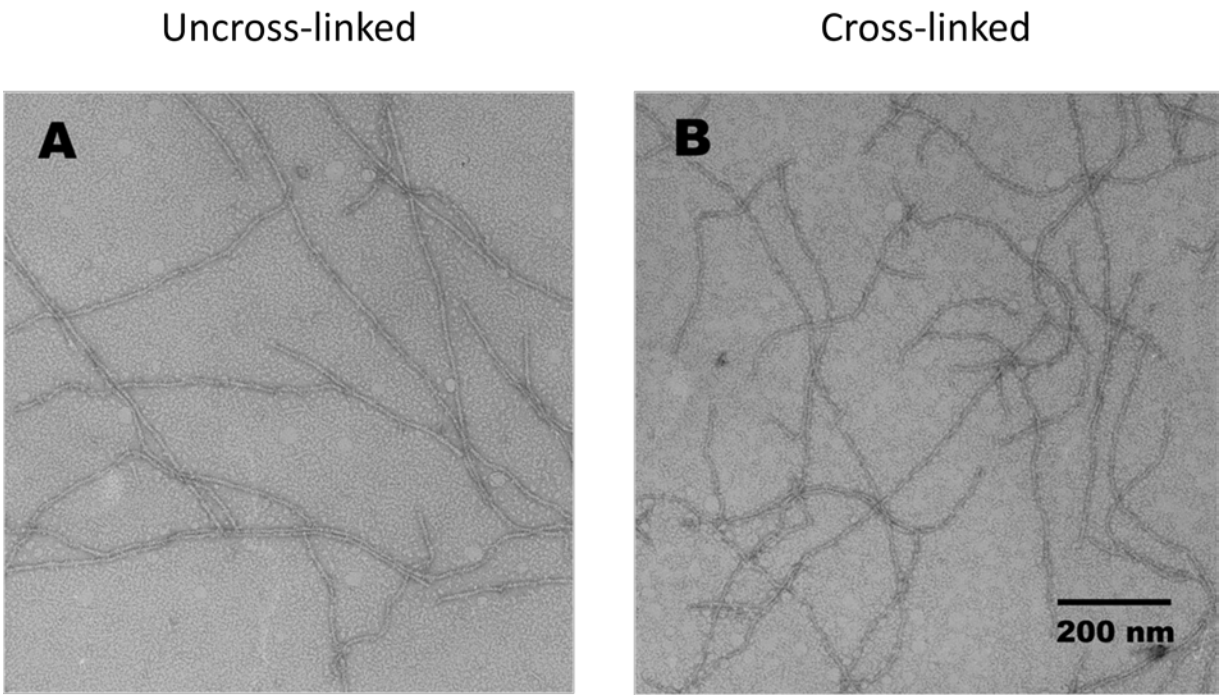

Figure 2. EM images of F-actin formed from BPM cross-linked dimers are similar to those of uncross-linked actin. BPM cross-linked dimers were purified by gel filtration and then polymerized into F-actin.

difference (Figure 2). Thus, we conclude that BPM cross-linked dimers capture a normal, filament-like arrangement of actins protomers.

Mapping of sites on actin for the BP intermolecular and intramolecular crosslinks

An F-actin model depicting the positions of cross-linked amino acids is shown (Figure 3). Because the BP moiety photoreacts nonselectively with amino acids, we used LC-MS/MS to determine the amino acid that is cross-linked in the absence and in the presence of cofilin (Figure 4). The maleimide moiety almost always labels the reactive Cys374 on actin, which allowed us to search for cross-linked fragments that had the peptide fragment, KCF or CF, attached to it. For the intramolecular cross-link, we were able to observe a unique peptide at 2639.14 Da. This mass corresponds to the additive mass of fragment Ac-DEDETTALVCDNGSGLVK (residues 1-18, 1906.85 Da, monoisotopic mass), the KCF peptide (396.18 Da), an attached BPM cross-linker (277.07 Da), and cysteine alkylation of the 1-18 peptide (57 Da). We were then able to map the cross-linked residue. Because product ion up to y_7 from the C-terminus and up to b_{10} from the N-terminus were detected, we concluded that the cross-link is to residue Asp11.

We used a similar method to determine the residue for the intermolecular cross-link. We assumed that the CF peptide remained attached, and we found a unique peptide at 1734.89 Da. This mass corresponds to the additive mass of fragment HQGVMVGMGQK (residues 40-50, 1170.57 Da), a CF peptide (268.09 Da), and the BPM cross-linker (277.07 Da). The BP moiety exhibits interesting characteristics when applied to MS/MS collisions. The maleimide ring of BPM can open by hydrolysis, increasing the MW by 18 Da. An abundant product ion at m/z 675.8 is the 2+-charged ion representing the loss of the CF dipeptide plus the maleimide ring from cleavage between the benzophenone and maleimide rings. Because product ions up to b_4

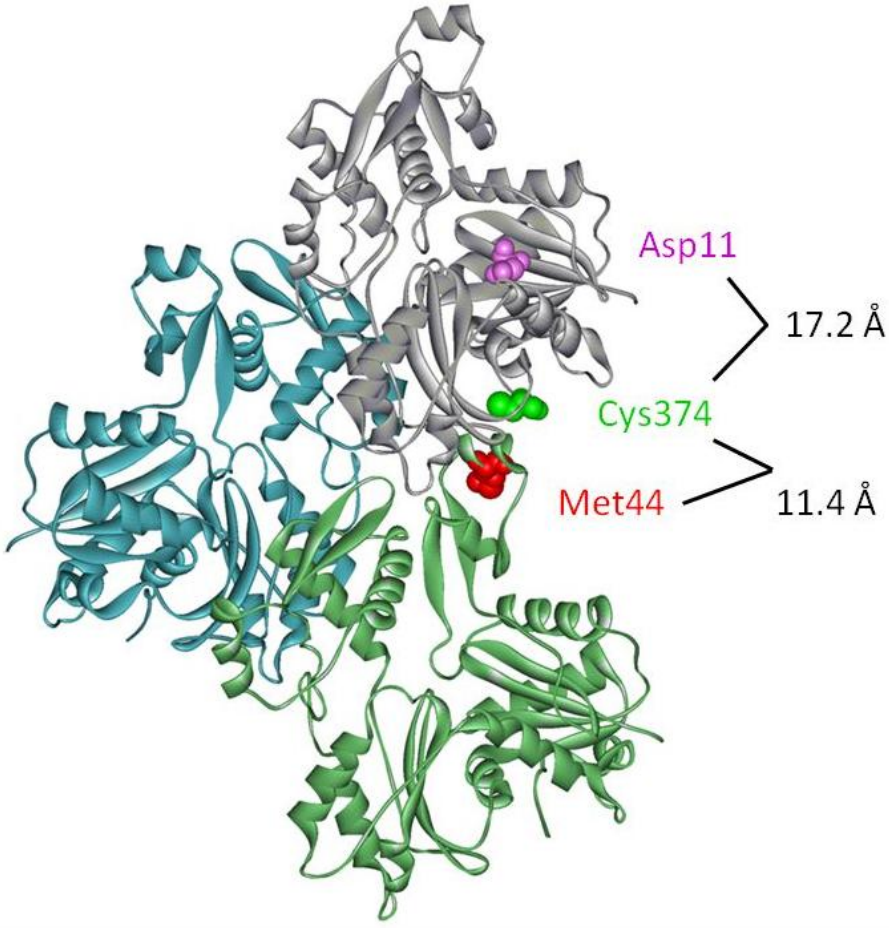

Figure 3. Mapping actin sites involved in intermolecular and intramolecular cross-linking by BPM. The amino acids on actin protomers cross-linked by BPM in the presence and absence of cofilin, and the distances between these residues are identified on the model of three actin protomers in F-actin. In the absence of cofilin, BPM cross-links actin intramolecularly between residues Asp11 and Cys 374. In the presence of cofilin, BPM cross-links two actins longitudinally, between residues Met44 and Cys374.

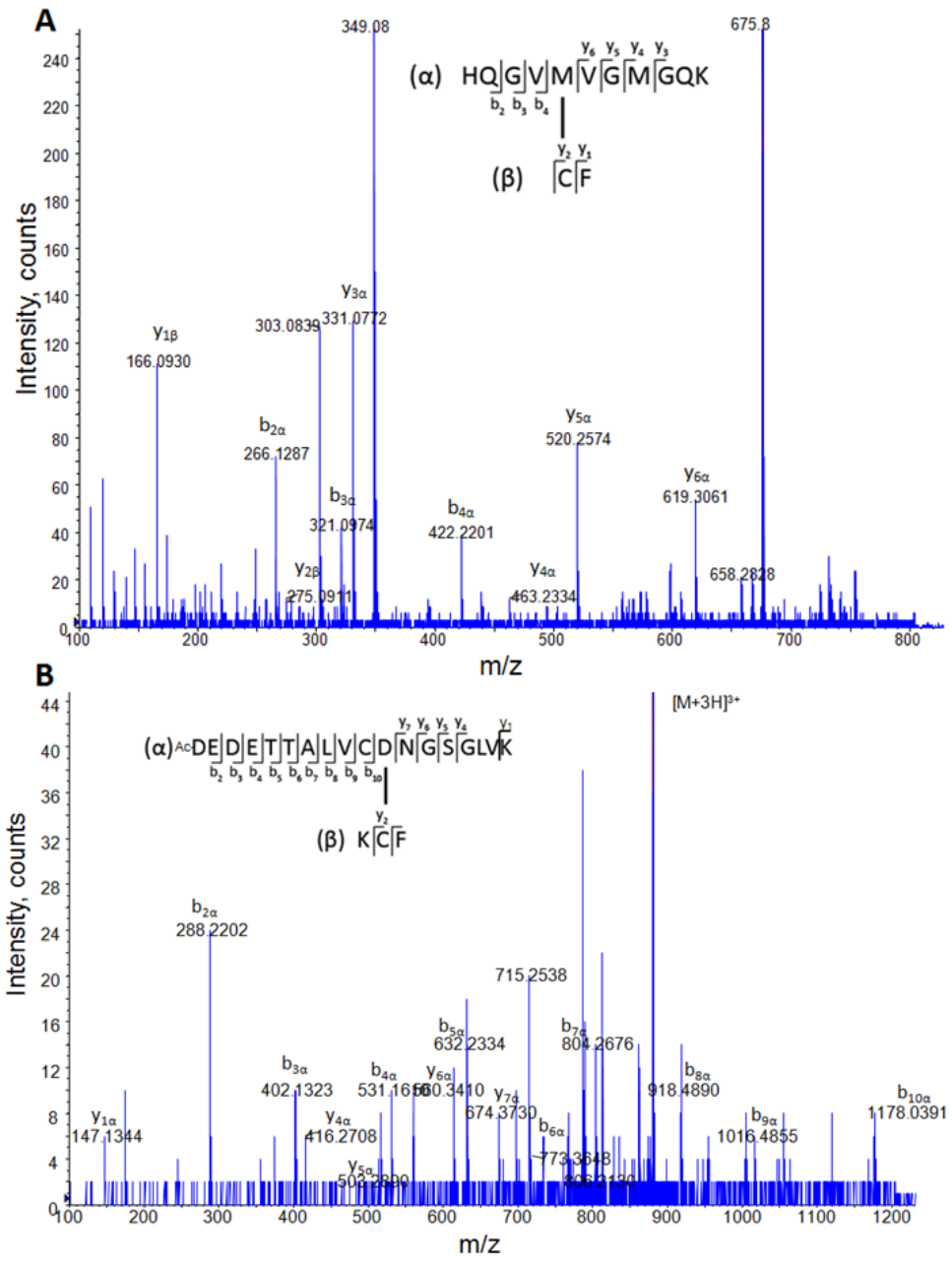

Figure 4. MS sequencing of the BP cross-linked actin to actin peptides. A. MS/MS spectrum of the $[M+3H]^{3+}$ of the BP cross-linked tryptic peptides at *m/z* 578.9 in the presence of cofilin. Peptides (α) and (*β*) are from the same G-actin. Singly and doubly-charged *y*-type product ions were generated from dissociation of the 3+-charged precursor ion. (Peptide fragments were denoted following the nomenclature for fragmentation of cross-linked oligopeptides. Subscripts are used to denote the residue position, counting from the N terminus for a_n, b_n, *and* c_n ions and from the C terminus for x_n, y_n, *and* z_n products. B. MS/MS spectrum of the $[M+3H]^{3+}$ of the BP cross-linked tryptic peptides at *m/z* 880.4 in the absence of cofilin. The representation is the same as in (A).

from the N-terminus and up to y_6 from the C-terminus were detected, we concluded that the cross-linking is to Met44 and cross-linking to Met47 is excluded.

Cofilin remains associated with cross-linked actin at high salt concentrations

Because bound cofilin causes a shift from intramolecular cross-linking to intermolecular cross-linking in F-actin, we tested the nature of cofilin binding to the cross-linked filaments. We also compared BPM cross-linked actin with ANP cross-linked actin due to their similarity in the extent and sites of cross-linking (Figure 5a). ANP forms an intermolecular cross-link between Cys374 and Gln 41 in the DNaseI loop of actin (23), the same subdomains that BPM forms cross-links in the presence of cofilin. As we increase the amount of salt in all cases, the amount of cofilin in the supernatant increases (Figure 5b). After the addition of 1 M KCl, the amount of cofilin in the supernatant in the reaction with uncross-linked F-actin increases to ~90% resulting in almost complete dissociation of cofilin from F-actin. In contrast, the addition of 1 M KCl results in the supernatant containing ~20% of cofilin in the reaction containing BPM-crosslinked actin and ~40% of cofilin in the reaction containing ANP-crosslinked actin suggesting that cofilin remains bound to cross-linked actin even at high salt concentrations.

Because high salt was needed to dissociate a fraction of cofilin from both cross-linked actins in the co-sedimentation assay, we measured the rates of cofilin association and dissociation using stopped-flow apparatus and normal fluorimetric analysis. ANP cross-linked actin was useful in the analysis of association rates because BPM cross-linked actin only forms in the presence of cofilin, making the calculation of binding rates difficult. Because ANP cross-linked actin exhibits the same degree of cross-linking as BPM-actin and shows similar affinities for cofilin by co-sedimentation, we assumed that ANP cross-linked actin would behave similarly

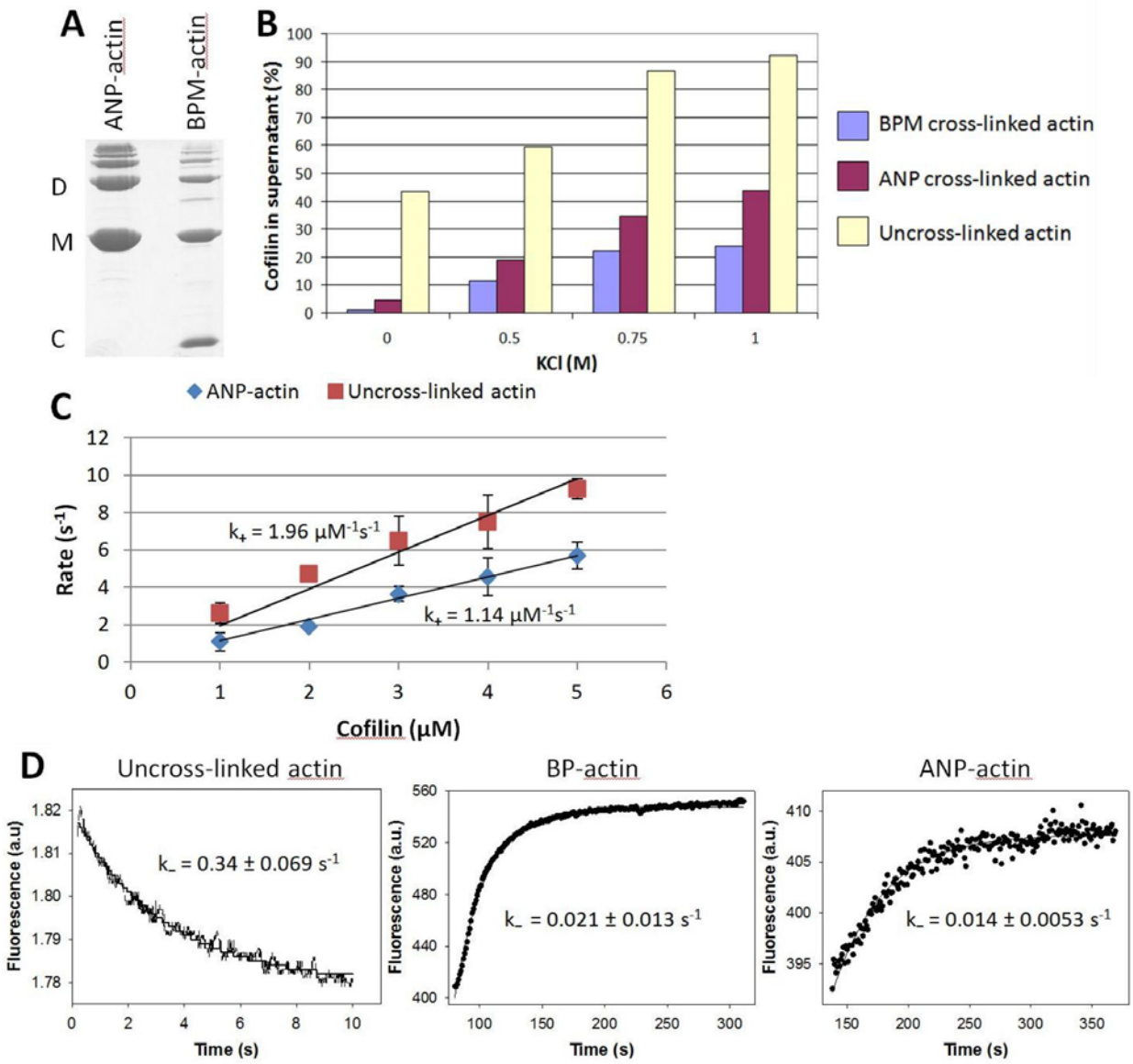

Figure 5. Cofilin remains associated with cross-linked actin at high salt concentrations. A. SDS-PAGE shows the extent of cross-linking in the ANP cross-linked and BPM cross-linked actin. Both show similar extents of cross-linking. M, D, and C refer to actin monomers, actin dimers, and cofilin. Bands above D on the gel represent higher actin oligomers. B. The bar graph shows the percentage of cofilin remaining in the supernatant after cosedimentation with F-actin in the presence of increasing amounts of salt. Very little cofilin is bound to and co-sediments with control F-actin in the presence of 1M KCl. In both ANP and BPM cross-linked actins, more than 50% of the cofilin remains bound to actin in the presence of 1 M KCl. C. Cofilin binds to uncross-linked actin (□) at a faster rate than to ANP cross-linked (◊) actin. D. Rates of cofilin dissociation from uncross-linked, BPM cross-linked, and ANP cross-linked actins are shown. The rates represent an average from 5-10 runs. A representative curve is shown for each rate. Cofilin bound to BPM and ANP cross-linked actins shows almost 15-fold slower rates of dissociation than from uncross-linked actin.

to BPM cross-linked actin in the binding assays. The binding rates for both ANP cross-linked and uncross-linked actins were similar, with the on rates slightly slower for ANP cross-linked actin (Figure 5c). However, a major difference is seen in the dissociation rates. Cofilin dissociation rates from uncross-linked actin were measured by stopped-flow methods over the course of 10 seconds, while for both ANP and BPM cross-linked actins these measurements were done with a fluorimeter, over the course of minutes. The rates of cofilin dissociation from ANP and BPM cross-linked actins are almost 15 times slower than those from uncross-linked actin (Figure 5d), suggesting that the less flexible cross-linked actin “locks” cofilin onto F-actin.

DISCUSSION

Chemical cross-linking has emerged as a useful tool in probing protein-protein interactions. Previous papers have shown the value of this technique and mapped the sites where cofilin binds to both G and F-actin (5, 6, 8). In combination with MS/MS analysis, we identified the BPM cross-linked residues in the presence and absence of cofilin. The cross-link switches from an intramolecular cross-link to an intermolecular cross-link upon cofilin binding. The model of F-actin shows that the distance between residues Cys374 and Asp11 is greater than the distance between Cys374 and Met44 (Figure 3). Why would the BP moiety have a preference to cross-link Asp11 instead of Met44? BPM is a relatively rigid cross-linker. The maleimide moiety of BPM labels the available cysteine while the BP moiety captures any amino acid within ~10 Å (24). The DNaseI loop is known to be a flexible region that is rarely seen in the atomic structure of G-actin. Although the most recent high resolution F-actin model predicts the loop to be within 12 Å from the C-terminus (25), other lines of evidence support the need for plasticity in the DNaseI loop for the stability of F-actin (26). The most recent F-actin model also supports the involvement of Met44 in important actin-actin contacts (25). The combined effect of Met44 protection via interprotomer contacts and/or the orientation/position of BPM attached to Cys374 relative to Asp11 may yield preferential BPM cross-linking to Asp11 in the filaments.

The binding of cofilin causes intermolecular cross-linking of F-actin, which leads us to consider the structural perturbations that occur upon its binding. Does the position of cofilin allow movement of the DNaseI loop into a more accessible and ideal position for cross-linking? Based on the current F-actin model, the DNaseI loop is already in a better position than Asp11, which may be the reason we observe some intermolecular cross-linking in the absence of cofilin (Figure 1). In the most recent high resolution model of cofilin binding to F-actin (4), the distance

between Asp11 and Cys374 is 19.8 Å, suggesting some intramolecular changes. This distance is beyond the upper limit of BPM cross-linking range, favoring the cross-linking to Met44. Binding of cofilin may also affect the space between Cys374 and Asp11, adding to the BP preference for Met44. Galkin et al (4) also concluded that the twist caused by cofilin binding causes a substantial displacement of subdomain 2 in actin, resulting in its disordering. The disordering of subdomain 2 caused by cofilin binding leads to a four-fold increase in F-actin flexibility and disruption of interprotomer contacts (17), which without cofilin involves probably the Met44 residue. If subdomain 2 is disordered upon cofilin binding, BPM may be able to "capture" an available amino acid. We allow the reaction to proceed to completion for 90 minutes, which would be enough time for the BP moiety to capture even an infrequent approach of Met44 to Cys374.

The C-terminus of actin is another region that is affected by cofilin binding. Because the C-terminus of actin is a highly flexible region, cofilin binding may cause intramolecular changes in the orientation/position of the C-termnius that allow for its cross-linking to Met44 and decrease the probability of Asp11 cross-linking. The flexibility of the C-terminus is proven in various fluorescence assays probing the change from monomer to filament. For example, filament growth can be tracked by labeling Cys374 with pyrene. In contrast, a non-polymerizable form of actin is created when Cys374 is labeled with tetramethylrhodamine-5-maleimide (27). Previous data supports fluorescence quenching of actin filaments fully labeled on Cys374 with pyrene to monitor the binding of cofilin (28-30). The fluorescence change is directly proportional to binding, suggesting a perturbation of that region. Thus, cofilin binding most likely alters the position of the C-terminus to favor its cross-linking to Met44.

Our binding data suggests that the dissociation rate of cofilin from actin is greatly reduced by its cross-linking. The breathing motions of filaments are generally restricted upon cross-linking. It appears that such motions are needed for “unlocking” the bound cofilin even after its affinity for actin is reduced by high ionic strength conditions. Cross-linking may also cause increased surface area of ionic interactions and enhanced salt bridges. In the most recent analysis of interactions between cofilin and F-actin, predictions from MD simulations of human cofilin on F-actin show that residues K22/S23/K31, which correspond to temperature-sensitive mutations K23A/K24A/Y25A on yeast cofilin, exhibit intermittent salt bridges with residues in subdomain 1 of actin (31). These salt bridges may be further enhanced by cross-linking but should be further tested with mutations.

In conclusion, our study shows the ability to track structural changes of F-actin, both intramolecularly and intermolecularly, through BPM cross-linking. We observe a significant structural change upon cofilin binding that is consistent with changes observed in the filament dynamics. This method may be useful in studying other F-actin binding proteins to provide evidence for structural transitions in the filament.

REFERENCES

1. Bamburg, J. R., *Annual Review of Cell and Developmental Biology* **1999,** 15, (1), 185-230.
2. Bamburg, J. R.; McGough, A.; Ono, S., *Trends in Cell Biology* **1999,** 9, (9), 364-370.
3. Du, J.; Frieden, C., *Biochemistry* **1998,** 37, (38), 13276-13284.
4. Galkin, V. E.; Orlova, A.; Kudryashov, D. S.; Solodukhin, A.; Reisler, E.; Schroder, G. F.; Egelman, E. H., *Proceedings of the National Academy of Sciences USA* **2011,** 108, (51), 20568-20572.
5. Grintsevich, E. E.; Benchaar, S. A.; Warshaviak, D.; Boontheung, P.; Halgand, F.; Whitelegge, J. P.; Faull, K. F.; Ogorzalek Loo, R. R.; Sept, D.; Loo, J. A.; Reisler, E., *Journal of Molecular Biology* **2008,** 377, (2), 395-409.
6. Mannherz, H. G.; Ballweber, E.; Galla, M.; Villard, S.; Granier, C.; Steegborn, C.; Schmidtmann, A.; Jaquet, K.; Pope, B.; Weeds, A. G., *Journal of Molecular Biology* **2007,** 366, (3), 745-755.
7. Lappalainen, P.; Fedorov, E. V.; Fedorov, A. A.; Almo, S. C.; Drubin, D. G., *EMBO J* **1997,** 16, (18), 5520-5530.
8. Benchaar, S. A.; Xie, Y.; Phillips, M.; Loo, R. R. O.; Galkin, V. E.; Orlova, A.; Thevis, M.; Muhlrad, A.; Almo, S. C.; Loo, J. A.; Egelman, E. H.; Reisler, E., *Biochemistry* **2006,** 46, (1), 225-233.
9. Pope, B. J.; Zierler-Gould, K. M.; Kühne, R.; Weeds, A. G.; Ball, L. J., *Journal of Biological Chemistry* **2004,** 279, (6), 4840-4848.
10. Wriggers, W.; Tang, J. X.; Azuma, T.; Marks, P. W.; Janmey, P. A., *Journal of Molecular Biology* **1998,** 282, (5), 921-932.

11. Dominguez, R., *Trends in Biochemical Sciences* **2004**, 29, 572-578.

12. Paavilainen, V. O.; Oksanen, E.; Goldman, A.; Lappalainen, P., *The Journal of Cell Biology* **2008,** 182, (1), 51-59.

13. McGough, A.; Pope, B.; Chiu, W.; Weeds, A., *The Journal of Cell Biology* **1997,** 138, (4), 771-781.

14. Galkin, V. E.; Orlova, A.; Lukoyanova, N.; Wriggers, W.; Egelman, E. H., *The Journal of Cell Biology* **2001,** 153, (1), 75-86.

15. Kudryashov, D. S.; Galkin, V. E.; Orlova, A.; Phan, M.; Egelman, E. H.; Reisler, E., *Journal of Molecular Biology* **2006,** 358, (3), 785-797.

16. Pfaendtner, J.; De La Cruz, E. M.; Voth, G. A., *Proceedings of the National Academy of Sciences USA* **2010,** 107, (16), 7299-7304.

17. Galkin, V. E.; Orlova, A.; VanLoock, M. S.; Shvetsov, A.; Reisler, E.; Egelman, E. H., *The Journal of Cell Biology* **2003,** 163, (5), 1057-1066.

18. Tao, T.; Lamkin, M.; Scheiner, C. J., *Archives of Biochemistry and Biophysics* **1985,** 240, (2), 627-634.

19. Spudich, J. A.; Watt, S., *Journal of Biological Chemistry* **1971,** 246, (15), 4866-4871.

20. Grintsevich, E. E.; Phillips, M.; Pavlov, D.; Phan, M.; Reisler, E.; Muhlrad, A., *Biochemistry* **2010**, 49, (18), 3919-3927.

21. Kudryashov, D. S.; Sawaya, M. R.; Adisetiyo, H.; Norcross, T.; Hegyi, G. r.; Reisler, E.; Yeates, T. O., *Proceedings of the National Academy of Sciences USA* **2005,** 102, (37), 13105-13110.

22. Schilling, B; Row R.H.; Gibson B.W.; Guo X.; Young M.M., *Journal of the American Society for Mass Spectrometry* **2003,** 14, (8), 834-850.

23. Hegyi, G.; Mák M., Kim, E.; Elzinga, M.; Muhlrad, A.; Reisler, E., *Biochemistry* **1998,** 37, (51), 17784-92.

24. Luo, Y.; Wu, J.-L.; Li, B.; Langsetmo, K.; Gergely, J.; Tao, T., *Journal of Molecular Biology* **2000,** 296, (3), 899-910.

25. Fujii, T.; Iwane, A. H.; Yanagida, T.; Namba, K., *Nature* **2010,** 467, (7316), 724-728.

26. Oztug Durer, Z. A.; Diraviyam, K.; Sept, D.; Kudryashov, D. S.; Reisler, E., *Journal of Molecular Biology* **2010,** 395, (3), 544-557.

27. Otterbein, L.R., Graceffa, P., Dominguez, R., *Science* **2001,** 293, (5530), 708-11.

28. Blanchoin, L.; Pollard, T. D., *Journal of Biological Chemistry* **1999,** 274, (22), 15538-15546.

29. Carlier, M.F.; Laurent, V. R.; Santolini, J. r. m.; Melki, R.; Didry, D.; Xia, G.-X.; Hong, Y.; Chua, N.-H.; Pantaloni, D., *The Journal of Cell Biology* **1997,** 136, (6), 1307-1322.

30. De La Cruz, E. M., *Journal of Molecular Biology* **2005,** 346, (2), 557-564.

31. Wong, D. Y.; Sept, D., *Journal of Molecular Biology* **2011,** 413, (1), 97-105.

Chapter 6

Conclusions

The goal of this dissertation was to study the effects of both Spir and cofilin on actin dynamics and its functional states *in vitro*. Although Spir and cofilin overlap in some functional respects, including the ability to sever, nucleate, and depolymerize filaments, they differ in the mechanisms of their action. Nevertheless, the techniques used in this study could be utilized to investigate the interaction of both proteins with actin. TIRF microscopy was especially useful in analyzing the dynamics of filaments in real-time while other fluoroscence measurements (e.g. pyrene assays) informed on actin assembly in bulk assays. EM, x-ray crystallography, mass spectrometry and analytical ultracentrifugation provided insight into structural changes in actin and actin complexes with Spir and cofilin.

Because current models of Spir's interaction with actin contradict each other (1-4), we re-examined Spir's association with actin monomers and filaments. Our results, showed that Spir is both a weak nucleator and a weak severer of actin filaments *in vitro*. Filaments exhibit rapid depolymerization in the presence of high concentrations of Spir, which we attribute to its weak severing activity as well as its ability to sequester monomers. We showed also that Spir-actin seeds can either nucleate filaments or impede their formation depending on their ratio to actin monomers added to the reaction. We obtained evidence for the formation of both longitudinal and lateral contacts in a Spir-actin nucleus, but the formation of these contacts varies between Spir-ABCD and Spir-CD. Incomplete occupancy of all Spir WH2 domains by actin and the heterogeneity of Spir-actin species suggest that individual WH2 domains have different affinities for actin, which may affect how actin monomers assemble into a proper nucleus. Weak nucleation activity could be attributed to the formation of an improperly aligned nucleus. We obtained two forms of crystallized Spir-D-actin complex, but Spir-C and the linker between them remained disordered in both crystal structures, providing additional evidence for different

binding affinities of C and D domains for actin monomers. Together, these data implicate Spir as a multifunctional protein (*in vitro)* that nucleates filaments in a more complex fashion than originally believed.

In contrast to Spir's weak severing and nucleation activities, cofilin is a strong severer and nucleator *in vitro*. Although cofilin's severing activity has been extensively studied (5-8), we examined the effects of cofilin isoforms on the dynamics of actin isoforms in an effort to explain differences in their severing activities. We studied the change in persistence length of both vertebrate and yeast F-actin upon binding of vertebrate and yeast cofilin. We observed that human cofilin-1 (hCof1) binds to yeast actin filaments but neither increases filament flexibility nor severs them. In contrast, yeast cofilin is able to increase filament flexibility of both skeletal and yeast actin while efficiently severing them, thereby allowing us to correlate the two effects. We also observe that severing events are associated with local bending - when deformations reach a critical angle - leading us to propose a cofilin-severing mechanism whereby mechanical asymmetry promotes local stress accumulation at boundaries between bare and decorated filaments. Contradicting previous observations that severing occurs mainly under subsaturating conditions (9), we further observe that yeast cofilin is an effective severer of yeast actin at low ratios of cofilin to actin, but continues to sever even at high ratios. In contrast, hCof1 is not an effective severer of yeast actin at low ratios but is able to sever filaments when added in excess. The same hCof1 severs much better skeletal actin filaments, allowing us to conclude that severing is both cofilin and actin isoform-dependent and that it involves specific actin-cofilin contacts.

Lastly, we examine the structural perturbations that occur upon cofilin binding. Using benzophenone-4-maleimide, we mapped an intramolecular cross-link in F-actin from Cys374 to

Asp11. Upon cofilin binding this is shifted to an intermolecular cross-link in F-actin, from Cys374 to Met44. We also report a slower rate of cofilin dissociation from cross-linked F-actin, indicative of the role of filament dynamics in cofilin dissociation. The conformational changes observed upon cofilin binding help elucidate the local and global changes that occur in F-actin that affect interprotomer contacts.

Future Directions

The question about the need for Spir multifunctionality in the cell remains open. There is little evidence to indicate the need for Spir severing or sequestration *in vivo*, in contrast to the evidence establishing the need for its weak nucleation activity in early oogenesis (10, 11). The concentrations of Spir required for severing and sequestration far exceed its local concentrations in the cell, posing questions about the *in vivo* significance of these *in vitro* observations. More in-depth analysis of various Spir activities is needed, perhaps via mutagenesis to determine the sequences necessary for contributing to nucleation, severing, and sequestration. Additional sequences, such as the MBL domain of Spir, may aid in its nucleation ability. Cappuccino (Capu) has also been implicated in boosting Spir's nucleation ability by binding two molecules of Spir (12). Although we did not observe Capu enhancement of Spir-based depolymerization and lateral cross-linking, other factors may be involved if Spir exhibits these activities *in vivo*.

Further examination of the different binding modes of the WH2 domains and their different affinities for actin monomers is also needed to understand the nucleation mechanism of Spir. Other WH2 domain constructs of Spir could be used in the mutant yeast actin fluorescence assays to that end. Current models of the Spir-actin nucleus depict a longitudinal arrangement of

actin monomers, but our data suggests that a lateral configuration - which would improve the nucleation of filaments - is possible. The linkers between the WH2 domains are vital to Spir's nucleation activity and most likely play an important role in its ability to form either longitudinal or lateral contacts. Future higher resolution models are needed to map the linkers between WH2 domains and to map the actual configuration of actin monomers that form a proper Spir-actin nucleus.

A natural progression of the work with cofilin is to further examine the interactions between different cofilin isoforms with different actin isoforms. Preliminary results obtained with human cofilin-2 establish possible variations in severing activity from hCof1. Mutations on the C-terminus of cofilin may provide some insight into the variability of severing between the two species. Mutations on the additional loops in hCof1 that are absent in yeast cofilin may also provide evidence for differences in severing. Because we also observe severing events above saturating conditions, contradicting previous results, further investigations into the mechanism of severing under these conditions are needed. Future TIRF microscopy analysis of F-actin severing with labeled cofilins may shed real-time information on whether filaments sever exclusively in regions nearby a bound cofilin or can sever also in areas where cofilin is bound.

The work in this dissertation clarifies the main effects of Spir and cofilin on actin dynamics. Future work should seek further mechanistic explanations of the different activities of these proteins.

REFERENCES

1. Quinlan, M. E.; Heuser, J. E.; Kerkhoff, E.; Dyche Mullins, R., *Nature* **2005,** 433, (7024), 382-388.
2. Bosch, M.; Le, K. H. D.; Bugyi, B.; Correia, J. J.; Renault, L.; Carlier, M.-F., *Molecular Cell* **2007,** 28, (4), 555-568.
3. Rebowski, G.; Boczkowska, M.; Hayes, D. B.; Guo, L.; Irving, T. C.; Dominguez, R., *Proceedings of the National Academy of Sciences* **2008,** 105, (31), 10785-10790.
4. Ducka, A. M.; Joel, P.; Popowicz, G. M.; Trybus, K. M.; Schleicher, M.; Noegel, A. A.; Huber, R.; Holak, T. A.; Sitar, T., *Proceedings of the National Academy of Sciences* **2010,** 107, (26), 11757-11762.
5. Pavlov, D.; Muhlrad, A.; Cooper, J.; Wear, M.; Reisler, E., *Journal of Molecular Biology* **2007,** 365, (5), 1350-1358.
6. De La Cruz, E. M., *Biophysical Review* **2009,** 1, (2), 51-59.
7. McCullough, B. R.; Blanchoin, L.; Martiel, J.-L.; De La Cruz, E. M., *Journal of Molecular Biology* **2008,** 381, (3), 550-558.
8. Pavlov, D.; Muhlrad, A.; Cooper, J.; Wear, M.; Reisler, E., *Cell Motility and the Cytoskeleton* **2006,** 63, (9), 533-542.
9. Andrianantoandro, E.; Pollard, T. D., *Molecular Cell* **2006,** 24, (1), 13-23.
10. Manseau, L. J.; Schupbach, T., *Genes & Development* **1989,** 3, (9), 1437-1452.
11. Pfender, S.; Kuznetsov, V.; Pleiser, S.; Kerkhoff, E.; Schuh, M., *Current biology : CB* **2011,** 21, (11), 955-960.
12. Quinlan, M. E.; Hilgert, S.; Bedrossian, A.; Mullins, R. D.; Kerkhoff, E., *The Journal of Cell Biology* **2007,** 179, (1), 117-128.